

the guideline for crack length measurement by potential drop method (PDM), basic specifications of test equipment and environmental precrack introduction, are specified in the appendices of the standard. This paper presents an outline of the standard.

2. TERMS AND DEFINITIONS

The main terms and definitions used in this standard are indicated below as well as in JIS Z0103.

K_I = stress intensity factor (mode I)

E_{corr} = corrosion potential

T = specified temperature measured at the position close to a specimen installed inside the pressure vessel

\dot{m} = circulating water flow (value of the pressure vessel capacity divided by the circulating flow per hour)

$a_{p1/4}$ = precrack length at the position of $1/4B$

$a_{p2/4}$ = precrack length at the position of $2/4B$

$a_{p3/4}$ = precrack length at the position of $3/4B$

a_{p0} = average precrack length of $a_{p1/4}$, $a_{p2/4}$ and $a_{p3/4}$

a_{p0s} = average of surface precrack lengths

a_0 = initial crack length (distance from loading point to fatigue precrack tip)

a_f = final crack length (distance from loading point to final crack tip in test environment)

W = specimen width

b = specimen ligament (= $W-a$)

σ_{yT} = yield stress at testing temperature

$\sigma_{\text{flow}T}$ = flow stress at testing temperature (= $([\sigma_{yT} + \sigma_{UT}] / 2)$)

A_1 = average crack length ([SCC area / specimen thickness] or equal divided method)

A_2 = average crack length in crack engagement area (SCC area / engaged crack width)

C = maximum crack length

D = fatigue precrack length

$[da/dt]_Q$ = provisional crack growth rate (interim crack growth rate calculated using the standard test method described herein)

$da/dt = [da/dt]_Q$ in a case where all validity criteria are met

B_e = effective specimen thickness (= $(B \cdot B_N)^{1/2}$)

where B is the distance between the sides of the specimen and B_N is the distance between the roots of the side groove notches. If no side groove is adopted, $B_e = B$.

3. SCOPE OF THE STANDARD

This standard applies to austenitic steels and alloys (including weld metals, heat-affected zones, cold-worked materials and precipitation-hardening steels and alloys), which are considered to be important for SCC issues in light water reactor (LWR) primary coolant systems. Since local deformation of the crack tip of irradiated materials differs from that of unirradiated materials and a smaller specimen is generally used for irradiated materials, irradiated materials are excluded from the application of the standard.

The standard provides a test method for determining SCC growth rate using compact tension (CT) specimens in simulated light water reactor environmental conditions (primary water) in a nuclear power plant.

4. PRINCIPLE OF TEST

Stress corrosion cracking is a phenomenon in which a crack initiates in an environment when stress is applied to a material susceptible to SCC. Thus, SCC is influenced by three factors: material, stress and environment. If SCC grows beyond a certain extent, subsequent crack growth behavior is considered to be influenced by the stress field at the crack tip. Therefore, the SCC growth rate is related to the stress intensity factor, K_I , which is the parameter expressing stress distribution at the crack tip. SCC growth rate, da/dt , is defined as the temporal differentiation of crack length. By applying a load to the specimen in an environment and measuring the crack length (a) continuously using PDM, the crack growth rate (da/dt) is calculated in which K_I can be determined from the crack length (a) and the applied load. The average K_I is determined by the average of the stress intensity factors calculated from the crack length at the start point for the evaluation and the final crack length (the crack length at the final point of the term for the evaluation). This standard specifies the preparation of specimens, adjustment of testing environment, method for applying load, and crack growth calculation method required to measure the crack growth rate using the fracture mechanics specimen in the simulated water environment of light water reactors.

5. SPECIMEN FOR TEST

5.1 Specimen Position and Direction

The position and direction of the specimen from the test sample is shown in Figure 1, which is basically determined from ISO 7539-6. Identification of the specimen position and direction is expressed using the letters L, T, S, R and C, defined as follows. In this notation, the first and second letters indicate the direction of the loading axis and crack growth, respectively.

(1) Plate material

L: long direction (final rolling direction, main forging direction)

T: width direction

S: thickness direction

(2) Round bar and hollow circular cylinder

L: axis direction

R: radial direction

C: circumferential direction

5.2 Specimen Geometry

The geometry of the specimen is the CT type as shown in Figure 2, which is similar to that of other standards, e.g., ISO 7539-6, ASTM E399, ASTM E647, and E1820. A narrow notch (2) can be formed at the tip of the straight notch (1). The specimen thickness, B , shall be equal to or greater than 25.4×10^{-3} m. However, it can be set to between 12.5×10^{-3} m and 25.4×10^{-3} m based on discussions. The specimen width, W , shall be equal to or greater than two times the specimen thickness (B). Side grooves can be prepared on both sides of the specimen. Taking into consideration existing related standards, e.g. ISO 7539-6, the depth of the side groove is 5% of the specimen thickness in general. This can be omitted based on discussions.

5.3 Size Requirement of Specimen

Following the existing fracture mechanics test standards using CT specimens, this standard prescribes the size requirement of the specimen in terms of the size of the plastic zone and small-scale yielding. Specimen thickness Be and ligament b shall satisfy the following formulas (1) and (2). The factor β has been derived by analyzing existing SCC growth data and the test conditions including specimen size, stress intensity factor, etc. However, these formulas can be changed depending on the test objects based on discussions. The technical basis of the specimen size requirement will be presented in another paper at this conference [1].

$$Be > \beta (K_I / \sigma_{yT})^2 \quad (1)$$

$$b > 4/\pi (K_I / \sigma_{yT})^2 \quad (2)$$

where

Be : effective specimen thickness (m)

b : ligament (m)

K_I : stress intensity factor ($\text{MPa}\sqrt{\text{m}}$)

β : factor relating to specimen thickness. Normally, $\beta = 0.5$. In the case of cold-worked materials, and precipitation-hardening materials and alloys, $\beta = 2.5$ is appropriate.

σ_{yT} : yield stress at testing temperature (MPa)

$\sigma_{\text{flow}T}$: flow stress at testing temperature (MPa)

However, in formula (2), when (ultimate tensile strength σ_{uT})/(yield stress σ_{yT}) > 1.3 is satisfied, $\sigma_{\text{flow}T}$ can be used instead of σ_{yT} .

5.4 Specimen Finish and Dimensional Measurement

The surface of the specimen is mechanically finished in order to remove the working layers and residual stress, and the surface roughness is as shown in Figure 2. Prior to testing, the dimensions of the specimen are measured and confirmed to be within the fabrication tolerance as shown in Figure 2.

5.5 Stress Intensity Factor K_I

The stress intensity factor, K_I , is defined as follows, which is the same as that in ISO 7539-6 and ASTM E399.

$$K_I = \frac{P}{B_e \sqrt{W}} \frac{(2+\alpha)}{(1-\alpha)^{3/2}} (0.886 + 4.64\alpha - 13.32\alpha^2 + 14.72\alpha^3 - 5.6\alpha^4) \quad (3)$$

where

K_I : stress intensity factor ($\text{MPa}\sqrt{\text{m}}$)

P : load (MN)

α : a/W , a is crack length (m), W is specimen width (m)

Be : effective specimen thickness (m)

Note: The accuracy of formula (3) is $\pm 0.5\%$ and the effective range is $0.2 \leq \alpha \leq 1.0$. K_I may be obtained by methods other than formula (3) based on discussions.

5.6 Precrack Introduction

A fatigue precrack is introduced at the tip of the machined notch of the specimen in the atmosphere as well as the fracture toughness test and fatigue crack growth test, e.g. ASTM E813 and ASTM E647. The conditions for introducing the precrack into the specimen have been determined as follows, taking into consideration existing related standards and experimental data. The fatigue precrack shall not be less than $0.05B$ or 1.0×10^{-3} m. The geometries of the notch and fatigue precrack should be within the required envelope shown in Figure 3. The final maximum load during precracking shall not exceed the initial load of the SCC growth test in the water environment, preferably less than 80%. The crack length (a_{0s}) after precrack introduction is measured at both sides of the front and back faces of the specimen and recorded. The loading condition during precracking is recorded for reference.

6. TEST EQUIPMENT

The test equipment consists of a high-temperature high-pressure water circulation system that can simulate the water chemistry environment in light water reactors, and a pressure vessel (autoclave) with the loading machine connected to the high-temperature high-pressure part. Figure 4 shows an example schematic diagram of the test equipment. The test equipment includes a continuous measuring device for the crack length of the specimen and a measuring device for the corrosion potential (the corrosion potential may not be measured in the test in the simulated PWR environment). The basic specifications of the test equipment simulating BWR and PWR water environments are shown in the appendix in the standard.

7. TEST METHOD

7.1 Installation of Specimen, Terminals for Crack Length Measurement, and Electrodes for Corrosion Potential Measurement

The specimen with the introduced precrack described earlier is set on the loading axis and the terminals for crack length measurement by PDM are installed. The indicated value of the crack length means the crack length obtained from the output of this method.

Two types of terminals are installed on the specimen; one is for supplying DC or AC current to the specimen and the other is for measuring the electrical potential drop across the crack. The locations of the terminals are set with reference to literatures (e.g. [2]). To prevent electric conduction between the terminals except through the specimen, the specimen is sufficiently isolated from the fixtures.

In the simulated BWR environment test, a sample electrode and a reference electrode are installed close to the CT specimen in the pressure vessel to measure the corrosion potential (E_{corr}) of the material tested. The sample electrode is the CT specimen itself or a coupon specimen made of the same material as the CT specimen. The sample electrode and the reference electrode are installed to face each other. In the PWR simulated environment test, E_{corr} is not measured in principle, but it is measured for any objects if necessary.

7.2 Adjustment of Test Water Chemistry

By adjusting test water in the water chemistry controlled tank and circulating the test water at a high-temperature and high-pressure condition through the pressure vessel containing the specimen, the water chemistries at the inlet and the outlet of the pressure vessel are set as the target test conditions. The test conditions are set to meet the test purposes. The simulated BWR environment includes normal water chemistry (NWC) and hydrogen water chemistry (HWC). Typical water chemistry of the simulated BWR environment test under NWC conditions is shown in Table 1 as an example. Typical water chemistry of the simulated PWR environment test is shown in Table 2. Temperatures A, B and C for the PWR test provide the temperature at the outlet of the pressure vessel, the outlet of the steam generator and the

typical temperature acceleration condition, respectively. Environment I for the PWR test provides the initial water chemistry condition considering the extension of the running cycle. Environment II for the PWR test provides the typical average water chemistry.

In the case of the test in the water chemistry simulated BWR environment as shown in Table 1, test water from the pressure vessel should go through the ion exchange resin to eliminate impurity ions. Then, the test water is circulated from the water chemistry controlled tank to the pressure vessel. On the other hand, in the simulated PWR environment, if the test water contains boric acid or lithium ion as shown in Table 2, the test water from the pressure vessel flows through the bypass line, not the ion exchange resin, to the water chemistry controlled tank and is circulated to the pressure vessel.

When E_{corr} is measured during the test, measurement begins after the test water chemistry is adjusted to the target condition. E_{corr} is monitored continuously by measuring the potential difference between the sample electrode and the reference electrode using a high input impedance electrometer.

The measurement items during the test are shown in Table 3. There are differences in some of the measured items for the BWR test and the PWR test due to the difference in water chemistry for the tests.

7.3 Introduction of Environmental Precrack

In the case of the SCC growth test using materials with low SCC susceptibility (e.g., low carbon stainless steels), an intergranular SCC crack generally does not occur from the tip of a transgranular fatigue precrack and/or an SCC crack front becomes uneven. Also, in the case of the SCC growth test using Ni base weld metal, it is known that the crack front of the specimen has an uncracked ligament and takes on an uneven form. This situation is considered to result in low-quality data. From this viewpoint, in the case of a test using such materials, the environmental precrack introduction before the constant load test can be adopted so that an intergranular SCC crack can easily occur from the tip of the fatigue precrack at the beginning of the test. This process will shorten the incubation time and result in the uniform SCC crack front. For this purpose, cyclic loading with the combination of a high stress ratio ($R = \text{min. stress}/\text{max. stress}$) and a low frequency, constant loading with periodical unloading, etc., are used for the environmental precrack introduction. In this standard, it is prescribed that a precrack may be introduced at the front face of the fatigue precrack in the atmosphere by applying cyclic loading to the specimen in the test environment.

Based on the results of literature survey concerning this issue, examples of recommended loading conditions for environmental precracking introduction are indicated in this standard.

As for low carbon stainless steels, the loading condition of high R (e.g., 0.9) and low frequency (e.g., 0.0001 Hz) was applied to intergranular precrack introduction for SCC crack growth test in a simulated BWR environment [3], [4]. For nickel based alloy weld metal, the method for regular environmental intergranular crack through the CT specimen thickness was investigated in a simulated BWR reactor water environment [5]. The test was conducted under various cyclic loading conditions, the shape of the crack, and the morphology of the extended crack in the environment were investigated. The test results revealed that intergranular precrack on the fracture surface through the entire thickness of the specimen could be obtained using gentle load cycling with $R = 0.9$ and $f = 0.01\text{--}0.0001$ Hz for the materials. Thus, an intergranular precrack can be introduced in a test environment by using the adequate conditions combined with the R ratio and frequency.

Andresen [6] proposed the guideline for a test method to obtain a high-quality SCC crack growth rate from the viewpoint of intergranular precracking introduction. Several loading methods were applied for environmental crack introduction at the initial stage of the test as follows: after changing $R = 0.5 \rightarrow 0.6 \rightarrow 0.7$ in steps at $f = 1$ Hz, the frequency was decreased to 0.0001 Hz at $R = 0.7$ accompanied by periodic unloading with a hold time prior to final constant loading [7]. It was pointed out that the transition from transgranular morphology to intergranular morphology can be done by such loading mode at the initial

stage and that the loading mode change and resulting crack growth behavior should be closely monitored at this stage so that the appropriate load setting and change can be made in accordance with the crack behavior [8].

Crack growth tests have also been carried out using Ni-based alloys in a simulated PWR reactor water environment, and intergranular crack growth was observed under the loading conditions of $T_{\text{Hold}} = 0.3$ h, $R = 0.5$ or 0.7 [9] and [10]. Toloczko et al. applied several loading modes in steps at the initial stage of the SCC growth test in order to introduce intergranular precrack to specimens [11], [12]. In these tests, the strain rate at the crack tip gradually decreased by decreasing the frequency at $R = 0.5 \sim 0.7$ at the initial stage. Then, the loading condition just before the start of the final constant K condition was set to $f = 0.01$ Hz, $R = 0.5$, and $T_{\text{Hold}} = 2.5$ h, for example.

Based on the above information, examples of the recommended loading conditions for the combinations of material and environment where the introduction of environmental precrack is effective are shown in Table 4.

7.4 Test Load

7.4.1 Basic Procedure

The setup of a test load for the duration of the crack growth test is based on the measured crack length and the test load is calculated from formula (3) so that K_I at the crack tip becomes the target value. The test load is basically constant during the crack growth test.

7.4.2 Optional Procedures

(1) Periodic unloading operation

Under the condition that the stress corrosion crack growth rate is significantly slow, constant loading with periodic unloading operation can be applied during the test time in order to promote stable crack growth. In this case, in order to set the unloading conditions, it is necessary to consider fatigue crack growth because of cyclic loading during the loading and unloading operations. Therefore, the loading conditions (stress ratio, time spent for loading and unloading) shall be adequately set so that the amount of fatigue crack growth by cyclic operations of loading and unloading becomes negligibly small compared with the amount of stress corrosion crack growth.

The loading condition shall be established so that the amount of crack growth by fatigue by periodic unloading becomes 5% or less of the amount of stress corrosion crack growth. An example condition that has displayed good performance is shown in Table 5. The periodic unloading operation may be adopted based on discussions.

(2) Crack-tip activation operation

In a case where it is necessary to stop the SCC growth test, the crack-tip activation loading may be performed after restarting the test, where appropriate. When the SCC growth test is performed under the condition that continuous crack growth is difficult because of small test load, etc., crack growth may become very slow or may stop. In addition, long-time discontinuation of a test or a change in conditions during testing might influence the behavior of SCC growth. Therefore, in an SCC growth test, the promotion of crack growth by crack-tip activation and the mitigation of effects of long-time discontinuation and previous test conditions are possible by cyclic unloading of the test load, which is referred to as crack-tip activation loading.

Crack growth in the term for crack-tip activation loading includes fatigue crack growth because in crack-tip activation loading, cyclic unloading of the test load is performed. Therefore, the term for providing crack-tip activation loading is not included in the term for measurement in the SCC growth test.

An example of the loading conditions of crack-tip activation loading is shown in Table 6, where R is the stress ratio (minimum load/test load in periodic unloading), T_{Hold} is the interval of periodic unloading (duration of the test load), T_{Fall} is the time required for unloading from the test load to the minimum load, and T_{Rise} is the time required for loading from the minimum load to the test load.

7.5 Crack Growth Test

After the water chemistry is stabilized, the test load is applied to the specimen. Measurement of the crack length using PDM is started simultaneously with loading, and the behavior of the acquired data is monitored. In accordance with the planned test procedures and the situation after starting the test, the test shall be conducted as follows:

- (a) If an environmental precrack is introduced, the required cyclic load is applied after the water chemistry is stabilized. Measurement of the crack length is started simultaneously with applying the load. After the indicated value of the crack length shows the target value, which is set by the concerned persons, the test load is applied to the specimen.
- (b) When the water chemistry for introduction of the environmental precrack differs from that for the SCC growth testing, the required test load is applied to the specimen after the water chemistry is adjusted.
- (c) When the indicated value of the crack length shows no significant increase for the duration of the SCC growth testing, crack-tip activation loading as described in Section 7.4 may be performed by cyclic loading, as needed.
- (d) When the water chemistry is changed during the SCC growth testing, after adjusting the water chemistry, crack-tip activation loading as described in Section 7.4 may be performed, where appropriate.
- (e) When the test load is changed during the SCC growth testing, it can be changed only in the case of an increased load. After changing the test load, crack-tip activation loading as described in Section 7.4 may be performed, where appropriate.
- (f) When the water chemistry or the test load is changed during the SCC growth testing, the SCC crack growth rate is evaluated in the period when the conditions of the water chemistry and the test load are kept constant.

The test is completed after the increase in the indicated value of the crack length measured continuously during testing is judged to satisfy the average crack length specified in Section 8.4. However, even if the indicated value cannot be judged to satisfy the increase in average crack length, the completion time of the test can be determined based on discussions.

8. EVALUATION METHOD OF TEST RESULTS

After the test, the CT specimen is forced to fracture by fatigue in the atmosphere. The fatigue precrack and the SCC growth surface developed in the high-temperature and high-pressure water environment are determined by observing the crack tip at an identifiable magnification with an optical microscope and/or scanning electron microscope (SEM). The crack geometry, the area of growth region and the maximum growth length are recorded. The typical SCC growth surface of the crack growth region in the high-temperature and high-pressure water environment is observed with SEM, and is recorded. The test results are evaluated as follows.

8.1 Crack Length Measurement and Evaluation

The average crack lengths A_1 (average crack length), A_2 (average crack length in crack engagement area), C (maximum crack length), and D (precrack length) are determined from the SCC growth surface of the specimen. The methods for determining the crack lengths are shown in Figure 5 as an example. Then, the

precrack lengths at the positions of $1/4B$, $2/4B$ and $3/4B$ from the surface are measured and expressed as $a_{p1/4}$, $a_{p2/4}$, and $a_{p3/4}$, respectively.

The following check is performed for the precrack, which is similar to that of a Japanese test standard for elastic-plastic fracture toughness [13].

- Difference of each of $a_{p1/4}$, $a_{p2/4}$ and $a_{p3/4}$ is less than $0.1 a_{p0}$.
- a_{p0s} is greater than $0.9 a_{p0}$.

where

a_{p0} : average precrack length of $a_{p1/4}$, $a_{p2/4}$ and $a_{p3/4}$

a_{p0s} : average of surface precrack lengths

In order to establish a crack length versus test time curve, the initial crack length (a_0) and final crack length (a_f) are calculated by the following equations.

$$a_0 = D + (\text{distance from loading point to machined notch})$$

$$a_f = D + A_2 + (\text{distance from loading point to machined notch})$$

8.2 Crack Growth Rate Determination

The crack lengths measured at the starting point and at the end of the test by PDM are corrected so as to meet the initial crack length (a_0) and final crack length (a_f) calculated in Section 8.1, respectively. Based on the results, a figure showing the relationship between the crack length and the test time is prepared. When the crack length measured with PDM increases linearly with time in the evaluation period and shows a change beyond the fluctuation of PDM defined in the standard, the provisional crack growth rate $[da/dt]_Q$ is calculated. Examples of the conceptual figures for the method of estimating the provisional crack growth rate from the crack length versus test time curve are prepared as reference in the standard. However, the crack lengths in obtaining the provisional crack growth rate are determined based on discussions.

8.3 K_I Determination

The stress intensity factor K_I at the time of testing is determined from the crack length and the setting load by the method described in Section 5.5. The stress intensity factor is calculated by averaging the stress intensity factors calculated from the crack length at the start point and the final crack length at the final point of the term for evaluation.

8.4 Validity Criteria of Crack Growth Rate

The criteria for valid crack growth rate have been discussed in terms of crack shape and length, and are defined as follows in the standard. In a case where all the criteria are satisfied, $[da/dt]_Q = da/dt$.

- a) Crack engagement (ratio of SCC to the specimen thickness) is 50% or more.
- b) Ratio (C/A_1) of the maximum crack length C to the average crack length A_1 is three or less.
- c) Average crack length A_1 is 0.2×10^{-3} m or more.
- d) The requirement for the precrack length given in Section 8.1 is satisfied.
- e) Ligament b satisfies the requirements given in Section 5.3.

As for item c), the average crack length ($A_1 \geq 0.2 \times 10^{-3}$ m) has been set from the idea that more than one grain is necessary for intergranular crack growth. The average crack length A_1 includes precrack growth

area. More details of the technical basis for the criteria are described in an explanatory document in the standard.

9. OTHER ITEMS

The standard also includes several other items as appendices, such as the basic specifications of the test equipment, the procedures for determining the crack growth rate from a schematic diagram of crack length vs. time curve, guideline for crack length measurement by PDM, and so on, in the text.

The standard is accompanied by an explanatory document describing the background and technical basis, etc. Also included are several other items, such as the methods for measuring the water chemistry, method for measuring E_{corr} , the use of CDCB (contoured double cantilever beam) specimens for the SCC growth test, and so on.

CONCLUSIONS

The nuclear subcommittee of the JSCE has developed a standard of the test method for measuring SCC growth rate in high-temperature water that simulates the primary water environment of light water reactors (BWR and PWR). In the course of developing the standard, some items have been prescribed based on the test data analysis with technical discussion while related standards and guidelines have been referenced and accepted. Basic items such as test equipment, test procedures and evaluation method are specified in the appendices. Also, the standard is accompanied by an explanatory document describing the background and technical basis, etc. The standard is going to be published in the near future. This standard will be revised based on technological progress and improved knowledge.

This standard has been developed by the JSCE subcommittee for the SCC growth test method. The subcommittee consisted of experts from industry and academia as follows: Chubu Electric Power Co., Hitachi Ltd., Institute of Nuclear Safety System Inc., Kansai Electric Power Co., Japan Atomic Energy Agency, Japan Atomic Power Co., Mitsubishi Heavy Industries Ltd., Nippon Nuclear Fuel Development, Nippon Steel and Sumitomo Metal Corp., Nuclear Regulation Authority, Tokyo Electric Power Co., Toshiba Corp., and Tohoku University.

REFERENCES

- [1] Arai, T., Hirano, T., Aoike, S., and Terachi, T.: "Technical Basis of the JSCE Standard of the Method for Measuring SCC Growth Rate in High Temperature Water – Specimen Size Requirement," *Proc. 17th Inter. Conf. on Environmental Degradation of Materials in Nuclear Power Systems – Water Reactors*, CNS, August 10-13, 2015, Ottawa, Ontario, Canada.
- [2] Catlin, W.R., Lord, D.C., Prater, T.A. and Coffin, L.F.: "The Reversing D-C Electrical Potential Method," in "Automated Test Methods for Fracture and Fatigue Crack Growth," *ASTM STP-877*, pp. 67-85 (1985).
- [3] Itow, M., Itatani, M., Kikuchi, M., and Tanaka, N.: "Crack Growth Behaviors of Low Carbon 316 Stainless Steels in 288°C Pure Water," *Proc. 12th Inter. Conf. on Environmental Degradation of Materials in Nuclear Systems – Water Reactors*, Allen, T.R., King, P.J. and Nelson, L., eds., TMS, pp. 65-71 (2005).
- [4] Ando, M., Nakata, K., Itow, M., Tanaka, N., Koshiishi, M., Obata, R., Miwa, Y., Kaji, Y., and Hayakawa, M. "CGR Behavior of Low Carbon Stainless Steel of Hardened Heat Affected Zone in PLR Piping Weld Joints," *Proc. 13th Inter. Conf. on Environmental Degradation of Materials in Nuclear Systems – Water Reactors*, King, P.J., Allen, T.R., Busby, J., eds., Canadian Nuclear Soc., No. P0045 (2007).

- [5] Ozawa, M., Yamamoto, Y., Itow, M., Tanaka, N., Kasahara, S., and Kuniya, J.: “Interdendritic Crack Introduction before SCC Growth Tests in High-Temperature Water for Nickel-Based Weld Alloys,” *Proc. 2nd Inter. Conf. on Environmental-Induced Cracking of Metals (EICM-2)*, Vol. 2, p. 153 (2004).
- [6] Andresen, P.: “SCC Testing and Data Quality Consideration,” *Proc. 9th Inter. Symp. on Environmental Degradation of Materials in Nuclear Power Systems – Water Reactors*, S. Bruemmer, P. Ford, G. Was, eds., TMS, pp. 411-421 (1999).
- [7] Andresen, P., and Morra, M.: “SCC of Stainless Steels and Ni Alloys in High Temperature Water,” *Corrosion 2007*, NACE International, Paper No. 07612 (2007).
- [8] Andresen, P.: “Irradiation Effects on Reactor Internals: IASCC,” *International Boiling Water Reactor and Pressurized Water Reactor Materials Reliability Conference and Exhibition*, EPRI, Maryland USA, July 16-19 (2012).
- [9] Yamamoto, Y., Ozawa, M., Nakata, K., Yoshimoto, K., Toyoda, M., and Okuda, J.: “Evaluation of Crack Growth Rate for Alloy 600 Vessel Penetration in a Primary Water Environment,” *Proc. 12th Inter. Conf. on Environmental Degradation of Materials in Nuclear Systems – Water Reactors*, Allen, T.R., King, P.J., Nelson, L., eds., TMS, pp. 1019-1028 (2005).
- [10] Yamamoto, Y., Nakata, K., Ozawa, M., Yoshimoto, K., Kanasaki, H., Tomimatsu, M., and Okuda, J.: “Development of the Crack Growth Rate Curves for Stress Corrosion Cracking of Nickel Based Alloys in a Simulated Primary Water Environment,” *Fontevraud 6th*, Paper A061-T04 (2006).
- [11] Toloczko, M.B., Olszta, M. J., and Bruemmer, S.M.: “One Dimensional Cold Rolling Effects on Stress Corrosion Crack Growth in Alloy 690 Tubing and Plate Materials,” *Proc. 15th Inter. Conf. on Environmental Degradation of Materials in Nuclear Power Systems – Water Reactors*, TMS, pp. 91-106 (2011).
- [12] Toloczko, M.B., Olszta, M.J., and Bruemmer, S.M.: “Stress Corrosion Crack Growth of Alloy 52M in Simulated PWR Primary Water,” *Proc. 15th Inter. Conf. on Environmental Degradation of Materials in Nuclear Power Systems – Water Reactors*, TMS, pp. 225-243 (2011).
- [13] “Standard Method of Test for Elastic-Plastic Fracture Toughness J_{Ic} ,” *JSME S 001-1981*.

Table 1 Water chemistry for simulated BWR environment test (typical example)

| Analysis items | Controlled values for water chemistry |
|--|---------------------------------------|
| Temperature | 288±3°C |
| Conductivity (inlet) | ≤ 0.01 mS/m (at 25°C) |
| Conductivity (outlet) | ≤ 0.02 mS/m (at 25°C) |
| Dissolved oxygen concentration | 200 to >8000 ppb |
| Corrosion potential | 0.15±0.05 V vs. SHE |
| Sulfate ion (SO ₄ ²⁻) concentration | ≤ 5 ppb |
| Chloride ion (Cl ⁻) concentration | ≤ 5 ppb |

Table 2 Water chemistry for simulated PWR environment test (typical example)

| Analysis items | Controlled values for water chemistry | |
|--|---|-------------------------|
| Temperature | Temperature A | 325±3°C |
| | Temperature B | 290±3°C |
| | Temperature C | 360±3°C |
| Conductivity | Environment I | 3.5±0.3 mS/m (at 25°C) |
| | Environment II | 2.15±0.3 mS/m (at 25°C) |
| pH | Environment I | 6.25±0.15 (at 25°C) |
| | Environment II | 7±0.15 (at 25°C) |
| Boric acid concentration (As H ₃ BO ₃ is added) | Environment I | 1800±180 ppm (as B) |
| | Environment II | 500±50 ppm (as B) |
| Lithium ion concentration (As LiOH is added) | Environment I | 3.5±0.35 ppm |
| | Environment II | 2±0.2 ppm |
| Dissolved oxygen concentration | ≤ 5 ppb | |
| Dissolved hydrogen concentration | 30±5 cm ³ -STP/kg·H ₂ O * | |
| Sulfate ion (SO ₄ ²⁻) concentration | ≤ 50 ppb | |
| Fluoride ion (F ⁻) concentration | ≤ 50 ppb | |
| Chloride ion (Cl ⁻) concentration | ≤ 50 ppb | |

* cm³-STP/kg·H₂O = 0.0893 ppm

Table 3 Measurement items in test

| Measured items | Simulated BWR condition | Simulated PWR condition |
|--|-------------------------|-------------------------|
| Conductivity (inlet) | ○ | ○ |
| Conductivity (outlet) | ○ | △ |
| DO concentration (inlet) | ○ | △ |
| DO concentration (outlet) | ○ | △ |
| DH concentration (inlet) | Note 1) | △ |
| DH concentration (outlet) | | △ |
| Specified temperature | ○ | ○ |
| E_{corr} | ○ | Note 1) |
| Boric acid concentration | — | △ |
| Lithium acid concentration | — | △ |
| Sulfate ion (SO_4^{2-}) concentration | □ | △ |
| Chloride ion (Cl^-) concentration | □ | △ |
| Fluoride ion (F^-) concentration | Note 1) | △ |
| pH | Note 1) | △ |
| ○: continuously measured items △: items measured at the beginning of the test □: items measured one or more times during the test Note 1) Measured, if needed | | |

Table 4 Examples of conditions of environmental precrack introduction

| Loading condition | Test environment | Material |
|--|---------------------------|--|
| - Maximum load: test load - Stress ratio (R) = 0.9 - Frequency = 0.0001 Hz - Load waveform is triangular wave | Simulated BWR environment | Stainless steel |
| - Maximum load: test load - Stepwise load mode change Step 1: Frequency = 0.1 Hz, $R = 0.3 \rightarrow 0.5 \rightarrow 0.7$ Step 2: $R = 0.7$, Frequency = 0.01 Hz \rightarrow 0.001 Hz Step 3: Frequency = 0.01 Hz, $R = 0.7$, Maximum load hold time = 9000 s - Load waveform is triangular wave | Simulated BWR environment | Stainless steel Ni-based alloy base metal or weld metal |
| | Simulated PWR environment | Ni-based alloy base metal or weld metal |
| - Maximum load: test load - $R = 0.9$ - Frequency = 0.01 – 0.0001 Hz - Load waveform is triangular wave | Simulated BWR environment | Ni-based alloy base metal or weld metal |
| - Maximum load: test load - $R = 0.5$ or 0.7 - Maximum load hold time = 0.3 h - Load waveform is triangular wave | Simulated PWR environment | Ni-based alloy base metal or weld metal |

Table 5 Example of periodic unloading condition

| Item | Condition |
|-------------------|--------------|
| R | 0.7 or more |
| T_{Hold} | 9000 (s) |
| T_{Fall} | About 10 (s) |
| T_{Rise} | 150 (s) |

Table 6 Example of crack-tip activation loading condition

| Item | Condition |
|-------------------|-------------|
| R | 0.7 or more |
| T_{Hold} | 9000 (s) |
| T_{Fall} | 500 (s) |
| T_{Rise} | 500 (s) |
| Duration | 100 (h) |

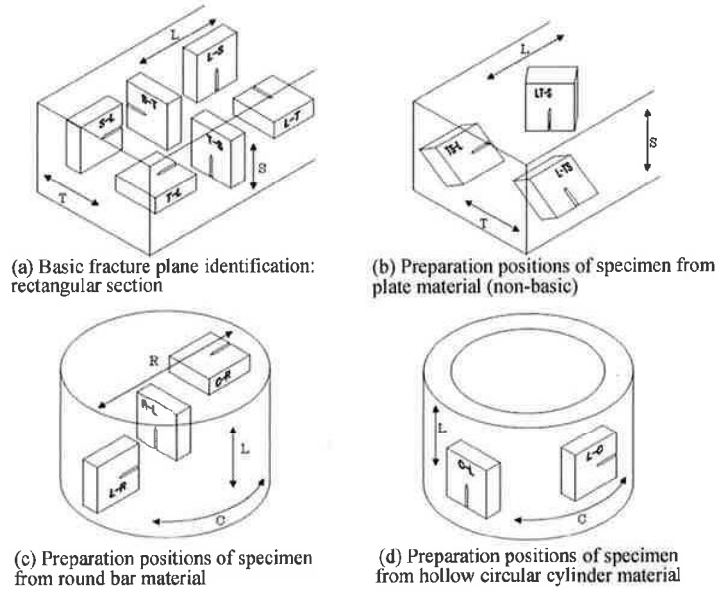
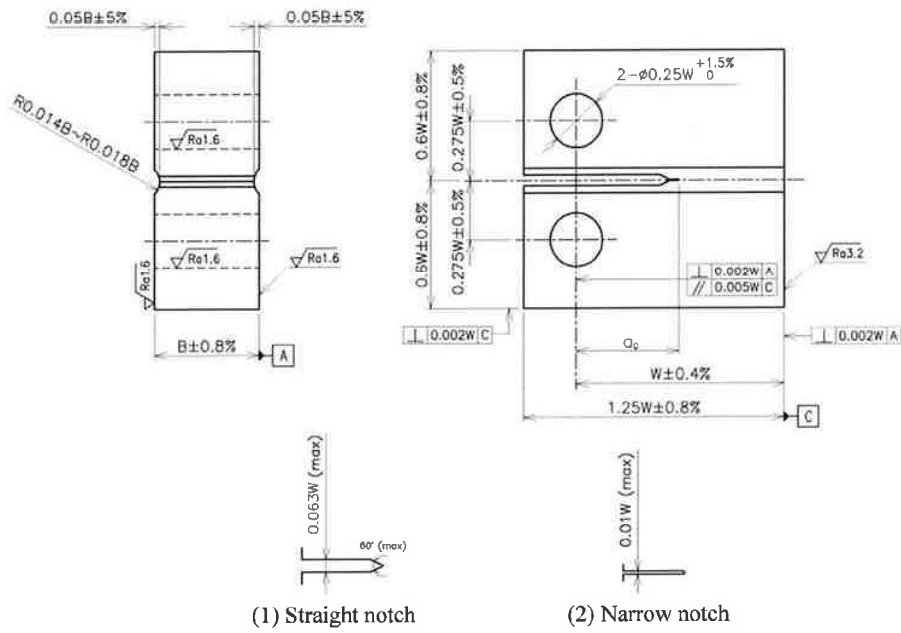


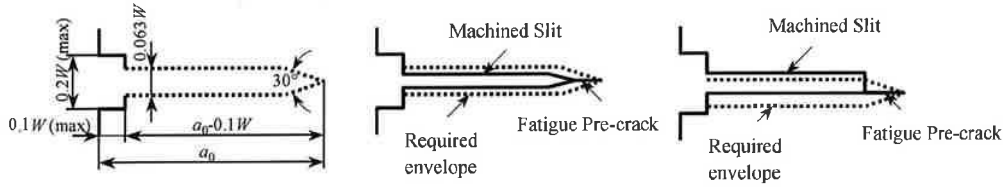
Figure 1 Specimen position and direction



Note: 1) $a_0 > 0.45W$

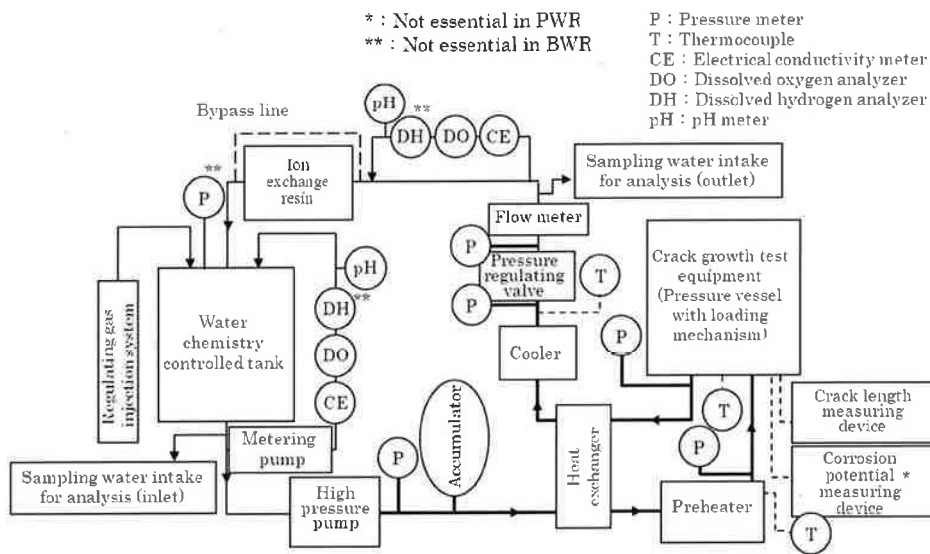
2) Radius of notch tip is less than 0.25 mm

Figure 2 Geometry of CT specimen



(1) Required envelope (2) Example of acceptable notch (3) Example of unacceptable notch

Figure 3 Required envelope for fatigue precrack and notch



※Bold line means high pressure part.
 ※Dashed line means electrical instrumentation cable.

Figure 4 Schematic diagram of test equipment

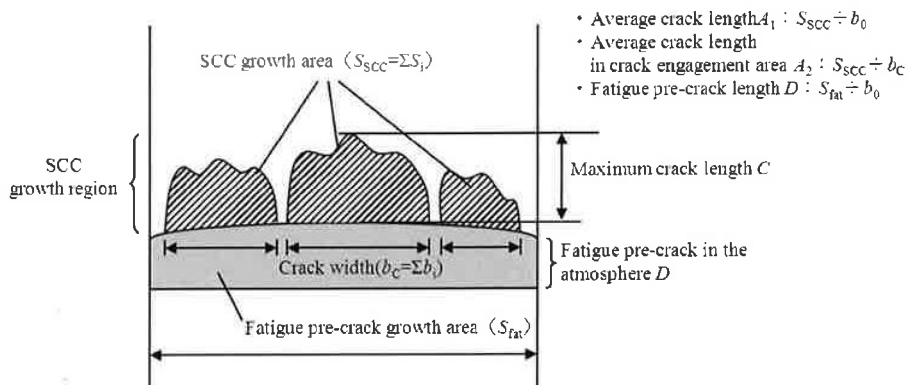


Figure 5 Method for obtaining crack lengths on the specimen fracture surface [Area method]

H21年度 電共研「強加工 SCC 懸念部位差別化のためのデータ拡充研究」最終報告書 要約版(1/3)

1. はじめに

沸騰水型軽水炉 (BWR) プラントでは、冷間加工されたオーステナイト系ステンレス鋼の応力腐食割れ (SCC) が顕在化し、対策が進められている。一方、加圧水型軽水炉 (PWR) においても、特異事例である可能性も否定できないながら、平成 19 年 10 月に美浜 2 号機の蒸気発生器 (SG) 入口管台セーフエントにおいて境界き裂が発見された。美浜 2 号機事例の更なる原因究明研究及び冷間加工に起因する SCC (以降、強加工 SCC と称す) の知見拡充の結果から動向によっては、既設の機器・配管に対しても劣化緩和等の保全が必要となる可能性がある。BWR プラントのシミュラード・PIR 配管及び美浜 2 号機セーフエントの損傷事例が、いずれも溶接部近傍であったことを考えると、水平展開においては、特に溶接部近傍を重点的に考慮する必要があると考える。これは、溶接部近傍は溶金収縮・溶接線により板厚内部が硬化しており、溶接残留応力も重畳することで SCC き裂が進展する可能性が高いためである。特に、配管溶接部は物量が多く保全が必要な部位の差別化が必要であるが、差別化のためのデータは少なく精緻化が必要状況である。

2. 実施内容

本研究では、配管・管台溶接部のモックアップを製作し、溶接部近傍の硬さ調査、表層の残留応力測定を実施する。また、FEM による溶接後の応力分布解析及びモックアップの板厚内部の残留応力測定の結果より、溶接残留応力値の精緻化を図る。表 1 に試験マトリックスを示す。

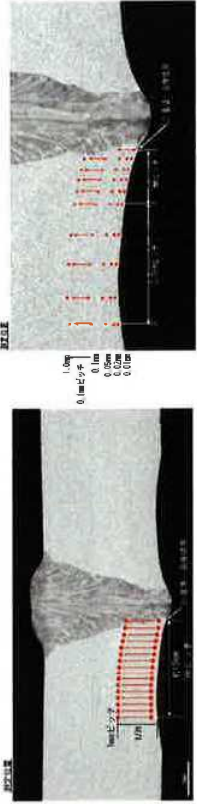
表 1 試験マトリックス

| 種類 | 硬さ・残留応力調査※1 | | | | | 応力解析 | | |
|----------------|-------------|-------|-----------|-------|-----------|------|-----------|-------|
| | 溶接手法 | TIG | TIG +SMAW | A-TIG | TIG +SMAW | TIG | TIG +SMAW | A-TIG |
| 3/4B | | O,△ | | | | | | |
| 1B | | O | | | | | | |
| 2B | | O | | O | | | | |
| 3B (BW※2) | | O,△ | | | | | | |
| 4B | | O | | | | | | |
| 6B | | O | | | | | | |
| 8B | | O,□,△ | | | | | | O |
| 14B | | O,□,△ | | | | | | O |
| 3/4B | | | O | | | | | |
| (SW※2) 2B | | | O | | | | | |
| 3/4B 管台 | | | O | | | | | O |
| 1 1/4B 管台 | | | O | | | | | O |
| MCP 管台 4B(切材) | | | O,△ | | | | | O |
| MCP 管台 14B(切材) | | | | | | | | O |
| MCP 管台 6B(切材) | | | | | | | | O |

※1: モックアップを製作し、硬さ・残留応力調査を実施。記号の意味は以下の通り。
 O: 硬さ調査
 △: 表層の残留応力調査 (ひずみゲージ)
 □: 板厚内部の残留応力調査 (計測 (ひずみゲージ))
 ※2: BW (突合せ溶接)、SW (ソケット溶接)

2.1 硬さ測定

板厚内部 (板厚の約 1/3 程度の深さ)、表層 (深さ 1mm まで) のビッカース硬さを測定した。図 1 に、一般配管突合せ溶接の硬さ測定位置の例を示す。



(b) 表層硬さマップ

(a) 板厚内部硬さマップ

図 1 硬さ調査位置 (一般配管突合せ溶接の例)

2.2 残留応力測定

2.3 項にて実施する FEM 解析の妥当性を示すために、ひずみゲージによる板厚部の残留応力測定を実施した。



図 3 残留応力測定状況例

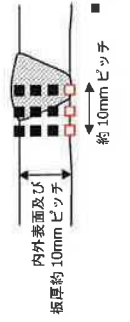
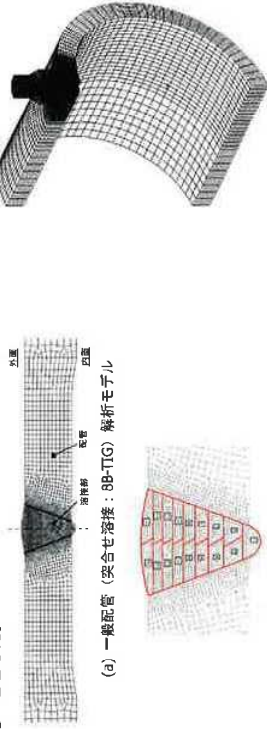


図 2 応力調査位置

2.3 残留応力解析

運転中応力を考慮した板厚内部の残留応力を求めるために、FEM により非定常熱伝導解析及び熱弾塑性解析機能を用いた残留応力解析を実施した。一般配管は軸対称モデル、管台は 3 次元モデルとした。なお、残留応力解析結果の妥当性については、2.2 項にて実施する板厚内部の残留応力測定結果により確認することとした。



(b) 溶接構図の例 (一般配管: 8B-TIG)

(c) MCP 管台 (4B) 解析モデル

図 4 解析モデルの例

3. 結果

3.1 硬さ測定結果

(1) 板厚内部の硬さ

各モックアップの硬さ結果を図5・表2に示す。また、各モックアップの板厚内部の硬さの傾向を表3に整理した。

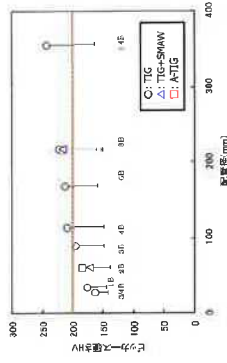


図5 一般配管 硬さまとめ

表2 ソケット溶接・配管管台・MCP管台硬さまとめ

| 種別 | 配管径 | 測定位置 | 硬さ(HVT) | | 溶接手法 | |
|-----------|--------|------|---------|---------|---------|------|
| | | | 0° 側 | 90° 側 | | |
| 一般配管 (SW) | 3/4B | ソケット | 144~182 | | TIG | |
| | 2B | ソケット | 129~186 | | | |
| 配管管台 | 3/4B | 母管 | 154~210 | 147~201 | TIG | |
| | 1-1/4B | 母管 | 149~206 | 143~204 | +SMAW | |
| MCP管台 | 4B | 母管 | 155~211 | 146~196 | TIG | |
| | 4B | 管台 | 147~204 | 143~206 | TIG | |
| | | 4B | 管台 | 148~204 | 152~225 | SMAW |

表3 板厚内部硬さ 結果概要

| 種別 | 板厚内部硬さ | 傾向 | 硬さ |
|------------|--------|---|---|
| 一般配管 (BW) | | <p>小 → 大</p> | <p>板厚が小さい場合には、200HV以下の硬さしか確認されない。</p> <p>板厚増加に伴い、溶接境界近傍の硬さ増加。溶接始端部から影影に硬化領域が広がる。</p> <p>4B以上で200HV以上の硬さが確認された。ただし最大で14BSch160</p> |
| 一般配管 (SW) | | (3/4B, 2Bのみ取得) | 硬化傾向は認められず、いずれも200HV以下 |
| 配管管台 MCP管台 | | <p><配管管台> 0°側では溶接境界近傍で200~220HVの領域が確認される。測定方向により同一径管台でも溶接近傍の硬さ傾向が異なる。</p> <p><MCP管台> MCP管台のみ、4Bのみ取得</p> | <p>板厚近傍は溶接後にリリルにて穴を加工しているため、内表面近傍で硬化傾向が認められる。</p> <p>硬化領域は内表面から0.1~0.3mm程度。</p> |

(2) 表層の硬さ

配管管台・MCP管台等、溶接後に機械加工するものについては、300HV0.01以上の硬さとなる領域があることを確認した。一方、溶接後に機械加工等を実施しない配管溶接部 (BW、SW) いずれも機械加工後に溶接) については、溶接境界から離れた位置では硬化傾向が確認されたが、溶接部近傍では表層硬度の低下が確認された。

表4 表層硬さ 測定結果概要

| 種別 | 板厚内部硬さ | 硬さ |
|------------|--------|---|
| 一般配管 (SW) | | <p>板厚の影響は小さく、内表面近傍の硬さは、200HV0.01程度</p> <p>溶接境界から離れた位置では、シンニング機械加工の影響が認められる場合があり、内表面から0.1mm程度まで200HV以上の硬化領域が認められる。</p> |
| 一般配管 (SW) | | <p>板厚の影響は小さく、内表面近傍の硬さは、200HV0.01程度</p> <p>ソケット側では内表面から0.1mm程度まで機械加工の影響による200HV以上の硬化領域が認められる。</p> |
| 配管管台 MCP管台 | | <p>内表面近傍は溶接後にリリルにて穴を加工しているため、内表面近傍で硬化傾向が認められる。</p> <p>硬化領域は内表面から0.1~0.3mm程度。</p> |

3.2 残留応力測定結果

一般配管の内面及び板厚内の応力分布の測定結果と、3.3 項に示す解析結果は概ね一致しており、解析による応力評価手法の妥当性が確認できた。なお、MCP 管台(4B)では計測と解析値では差が生じており、溶接後の機械加工の影響等も推測されるが、管台部の評価目的は板厚内の応力分布傾向の把握という位置付けであることから、本解析手法を用いた評価をそのまま適用することとする。

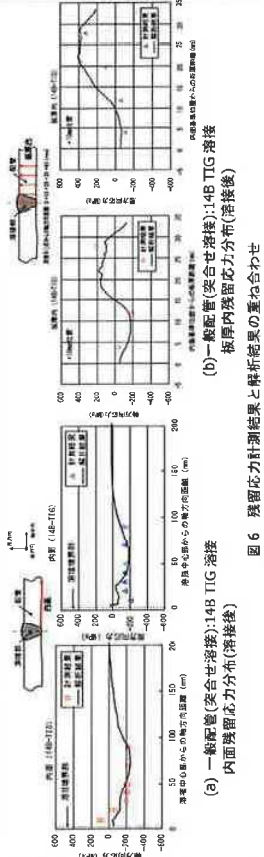


図6 残留応力計測結果と解析結果の重ね合わせ

3.3 残留応力解析結果

(1) 一般配管(突合せ溶接)

運転条件時の板厚内の応力分布より、全て配管モデルにおいて、板厚内の応力分布は軸方向、周方向応力とも引張であることが確認でき、き裂は停滞せず、進展する可能性があることと推定される。

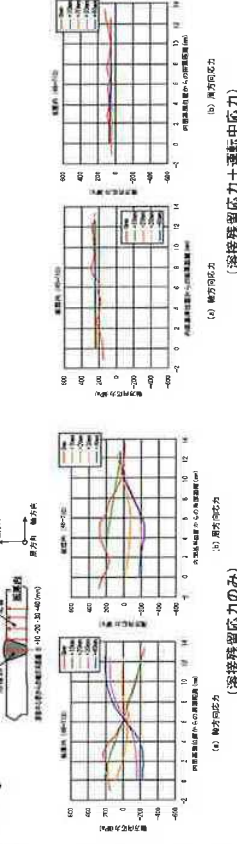


図7 応力解析結果(4B 配管)

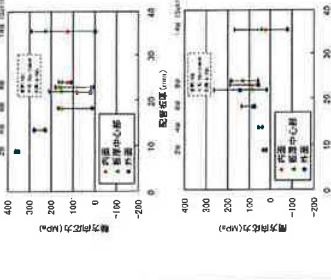


図8 配管残留応力解析結果のまとめ(運転中応力含む)(溶接中心から10mm位置)

| 解析ケース | 温度(°C) | 内圧(MPa) | 曲げ応力 ²⁾ (MPa) |
|---------|--------|---------|---------------------------------|
| 2B TIG | 343 | 18 | 300 |
| 一般配管 | 350 | 18 | 200 |
| 4B TIG | 360 | 18 | 100 |
| 6B TIG | 360 | 18 | 100 |
| 突合せ溶接 | 360 | 18 | 150 |
| 14B TIG | 360 | 18 | 150 |
| 配管管台 | 360 | 18 | X=0.05mm, Y=0.5mm ³⁾ |
| 1-1/4B | 360 | 18 | 考慮しない ⁴⁾ |
| 4B | 330 | 15.51 | 考慮しない ⁵⁾ |
| MCP 管台 | 330 | 15.51 | 考慮しない ⁵⁾ |
| 6B(セト) | 330 | 15.51 | 考慮しない ⁵⁾ |

*1: 工況・PALM 評価を参考に、各口部の配管・管台が圧に曝露されているラインの条件を仮定して設定した。
 *2: 曲げ応力は、配管側面にその応力値が偏在する様に仮定される。
 *3: 管台側面に負荷を負荷すること、曲げ応力を考慮(X: 母線方向、Y: 母線方向)
 *4: 1-1/4B 管台は、主に片持りのベント・ドレンラインの管台として使用されているため、母管と接合部の相対変位(相対移動)による曲げ応力は考慮しない。
 *5: MCP 管台に発生する曲げ応力は、通常運転時には該 MPa 程度と推定され、考慮の解析には運転中応力として考慮しない。

(2) 配管・MCP 管台
 表5に示す運転中応力も考慮した応力解析結果概要の一覧を表6に示す。内面側はほとんどの解析ケースで引張傾向であったが、MCP 管台(4B)では、周・軸方向いずれの応力も内面側で圧縮応力であった。

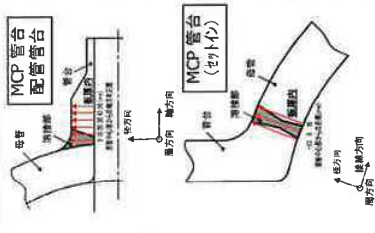


図9 管台解析の際の応力成分

| 応力成分 | MCP 管台 | | | 配管管台 | | |
|-----------|--------|---------|--------|------|--------|--------|
| | 4B | 6B (セト) | 1-1/4B | 3/4B | 1-1/4B | 1-1/4B |
| 軸方向(接線方向) | 内面 | + | + | + | + | + |
| | 外面 | + | + | + | + | + |
| 周方向 | 内面 | + | + | + | + | + |
| | 外面 | + | + | + | + | + |

+: 引張応力 - : 圧縮応力

3.4 計測結果をふまえた評価クライテリア例

これまでの PWR 環境での強加工 SCC のき裂進展速度の知見^{※1}より、200HV 以上ではき裂が進展すると仮定し、下記の図10のフローでは、200HV 以上の領域を抽出することとした。ただし、今後 200~250HV 間の硬さに関するき裂進展データが拡充された場合には、クライテリアが変更になる可能性がある。
 図10のフローによると、3B 以下の突合せ溶接配管、ソケット溶接については、強加工 SCC で進展せず、対策不要とすることができ^{※2}。

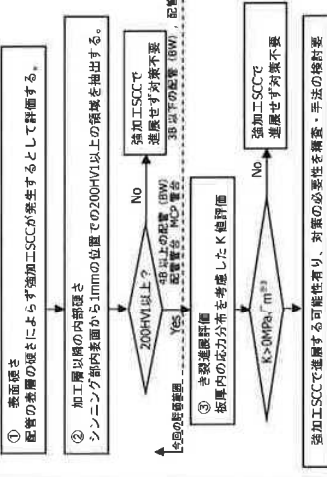


図10 評価フローと評価例

※1: 硬さデータは、ほとんどの厚肉等について今後精査化する必要がある。
 ※2: き裂進展の下限応力値が推定されていないため、ここでは $K > 0 \text{ MPa}\cdot\text{m}^{1/2}$ と設定した。

4. まとめ

配管・管台溶接部近傍の硬さ・残留応力のデータを収集し、保全部位の差別化に資するデータベースを構築した。主な成果は以下の通りである。
 1) SUS316 の配管・管台溶接部のモックアップを製作し、溶接部近傍の硬さ調査、表面の残留応力測定を実施した。
 2) 一般配管溶接部溶接の硬さ結果を基に、配管板厚と内表面 1mm 位置硬さの関係をjつて評価クライテリアを策定し、3B 以下の配管(BW)、配管(SW)については、強加工 SCC で進展せず、対策不要とする³⁾ことができる可能性が高くなった。
 3) FEM による溶接部の残留応力解析及びモックアップの板厚内部の残留応力測定の結果より、応力解析評価の妥当性を確認した。
 4) FEM による運転条件時の応力解析を行い、配管・管台溶接部近傍の板厚内の残留応力分布データを取得し、セットオンの MCP 管台については応力面で進展を否定できる可能性があることを確認した。

PWR 環境下の SCC 進展データの拡充に関する研究 (Step2) H24 年度報告書 要約版 (1/5)

試験内容

沸騰水型圧水炉 (BWR) プラントでは、シュラウドや原子炉再循環系配管等のオーステナイト系ステンレス鋼の非脱酸水材冷間加工部において応力腐食割れ (SCC) が顕在化したため、対策が進められている。また、環境条件は BWR 環境水と異なるものの、加圧水型軽水炉 (PWR) プラントにおいても機械加工・曲げ加工や溶接部の溶金収縮・溶接熱により、材料が硬化している部位が存在している。特異事例である可能性も否定できないながら、PWR プラントにおいても美浜 2 号機の蒸気発生器 (SG) の入口管台座・ブエント溶接部近傍に切削加工に起因しているとも推測される粒界割れが発見された。そこで本研究では、既往研究にて取得したデータに加えて温度、硬さ、応力拡大係数、鋼種などの条件をパラメータとしたオーステナイト系ステンレス鋼の非脱酸水材に対する SCC 進展データの拡充を目的として SCC 進展試験を実施した。

はじめに

沸騰水型圧水炉 (BWR) プラントでは、シュラウドや原子炉再循環系配管等のオーステナイト系ステンレス鋼の非脱酸水材冷間加工部において応力腐食割れ (SCC) が顕在化したため、対策が進められている。また、環境条件は BWR 環境水と異なるものの、加圧水型軽水炉 (PWR) プラントにおいても機械加工・曲げ加工や溶接部の溶金収縮・溶接熱により、材料が硬化している部位が存在している。特異事例である可能性も否定できないながら、PWR プラントにおいても美浜 2 号機の蒸気発生器 (SG) の入口管台座・ブエント溶接部近傍に切削加工に起因しているとも推測される粒界割れが発見された。そこで本研究では、既往研究にて取得したデータに加えて温度、硬さ、応力拡大係数、鋼種などの条件をパラメータとしたオーステナイト系ステンレス鋼の非脱酸水材に対する SCC 進展データの拡充を目的として SCC 進展試験を実施した。

試験内容

強加工材のき裂進展試験環境は、PWR 一次系機械水に溶存酸素を添加した環境 (高 DO 環境) 及び PWR 一次系純水環境 (低 DO 環境) とする。
 高 DO 環境条件下での試験マトリクスを表 1 に示す。Step1 研究にて、290°C/140HV にてき裂進展が確認されている。したがって、当該データの妥当性確認、及び高 DO 環境の低硬度範囲 (160~180HV、3/4B~2B 配管溶接部等) の保全範囲検証のための試験マトリクスを、250°C 及び 290°C での進展速度データを得ることをとした。

表 1 試験マトリクス (高 DO 環境条件)

| 材料 | 試験温度 | | | | | 備考 |
|---------------------|-----------------------|-------|-------|-------|------|-----------------------------|
| | 290°C | 250°C | 200°C | 150°C | 90°C | |
| SUS316 ラボ 溶接材 | 300HV (15, 25, 35) | ▲ | ▲ | ▲ | ● | 高 DO 環境条件下での低硬度での進展速度データの取得 |
| | 250HV | ▲ | ● | ● | — | |
| | 200HV | ▲ | ● | ● | — | |
| | 180HV | ○ | ○ | — | — | |
| SUS304 ラボ 溶接材 | 160HV | ○ | ○ | — | — | |
| | 140HV | ● | — | — | — | |
| | 300HV | ▲ | — | — | — | |
| | 250HV | ● | — | — | ● | |
| 200HV | ● | — | — | — | — | |

▲: H15~H17 特許法研究で実施済, ●: Step1 研究で実施済み, ○: 本研究で実施 (特記なき場合は 25MPa√m)
 <試験水質>
 溶存酸素濃度: 8ppm, ほう酸濃度: 500ppm, リチウム濃度: 2ppm

表 2 試験マトリクス (低 DO 環境条件)

| 材料 | 試験温度 | | | | | 備考 | |
|---------------|------------------------------------|-------|-------|---|-------|----|---|
| | 345°C | 320°C | 290°C | 250°C | 200°C | | 150°C |
| ラボ 溶接材 | 300HV | ▲ | ● | ▲(15, 25, 35) ●(6.5×2, 10×2, 25) ○(8)×2 | ▲ | ○ | 硬さ・K値の測定 しきい値の算定 ・硬度が異なる 場合の硬度依存 性の確認 ・低温脆性度 しきい値の明確化 |
| | 250HV | ○ | ○ | ▲(25) ○(8, 10, 15, 25) | ○ | ▲ | |
| | 225-250HV 程度 | | | ○(10, 15, 25) | | | |
| | 200-225HV 程度 | | | ○(10, 15, 25) | | | |
| SUS316 製造材 | 200HV | ▲ | | ▲ | ○ | | C 量による硬度 依存性の影響の取 得 |
| | 250HV | | | ● | ● | | |
| | C 量 依存性 | | | ○×4 LN 材 | | | |
| | | | | C 量: 0.04%/0.06%/0.07% | | | |
| 溶接 継手 | 200HV 相当 点 HV 粗い (230~250HV) | ● | | ● | | ● | 溶接継手 (溶接 により硬化した 部位) の SCC 進 展データの取得 |
| | 溶接金属 新製 | | | ○ | | | |
| | As weld | | | ○ | | | |
| | 280HV | | | ● | | | |
| ラボ 溶接材 | 300HV | ○ | ○ | ○(6.5, 8, 10, 15, 25) | ○ | ○ | 低 DO 環境条件下 における SUS304 の進展 速度の硬さ・K 値・温度依存性 の整備 |
| | 250HV | | | ●(25) ○(10, 15) | | | |
| | 225-250HV 程度 | | | ○(10, 15, 25) | | | |
| | 200-225HV 程度 | | | ●(25) ○(10, 15) | | | |
| SUS304 製造材 | 250HV | | | ○ | ○ | | 溶接継手 (溶接 により硬化した 部位) の SCC 進 展データの取得 |
| | C 量 依存性 | | | ○×4 LN 材 | | | |
| | | | | C 量: 0.04%/0.06%/0.07% | | | |
| | 250HV 程度 継手 | | | ○ | ○ | | |

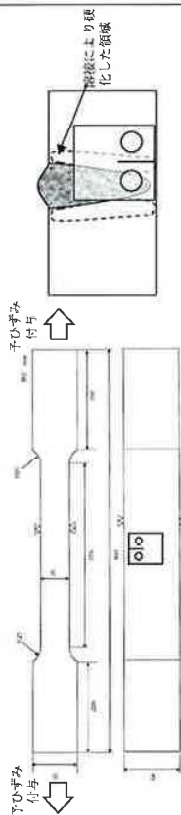
▲: H15~H17 特許法研究で実施済, ●: Step1 研究で実施済み, ○: 本研究で実施 (特記なき場合は 25MPa√m)
 <試験水質>
 溶存酸素濃度: <5ppb, 溶存水素濃度: 30cc・STP/kg・H₂O, ほう酸濃度: 500ppm, リチウム濃度: 2ppm

供試材及び試験片

(1) 供試材

- SCC 進展試験には以下の供試材を用いた。
 - ① SUS316/SUS304 (ラボ溶解材) の冷間加工材 (高 DO : 160HW ~ 180HW, 低 DO : 200HW ~ 300HW)
 - ② SUS316/SUS304 (ラボ溶解材) の C 量変化材及び LN 材
 - ③ SUS316/SUS304 (ラボ溶解材) の熱影響部
 - ④ SUS304 (鍛造材)

なお、高 DO 環境条件での試験には①のみを用い、低 DO 環境条件での試験には①~④を用いた。冷間加工は、供試材から大型引張試験片を加工し、これに引張りひずみを付与する方法で行った。硬さについては、表 1 及び表 2 に示す目標硬さとなっていることを確認するため、試験前に試験片表面で測定するとともに、試験後に試験片の中央断面におけるき裂近傍でも測定を行った。大型引張試験片 (予ひずみ付与) 及び溶接継手熱影響部からの試験片採取要領を図 1 に示す。



(a) 大型引張試験片からの試験片採取

(b) 溶接継手からの試験片採取

図 1 試験片の採取要領

(2) 試験片

SCC 進展試験には、試験装置の荷重負荷能力及び試験時の最大応力条件を考慮し、図 2 に示す 0.7 インチ厚さ (0.7T : 17.8mm) の CT 試験片を用いた。実機配管におけるき裂は、蒸管の圧延方向 (配管の長さ方向) に対して垂直方向に進展するため、図 3 に示すように圧延方向と垂直方向とが垂直になる L-S 方向にて試験片を採取した。

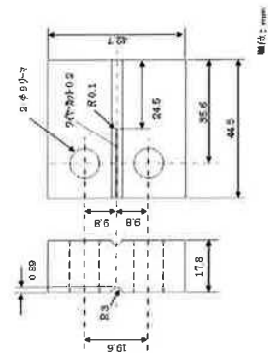


図 2 0.7TCT 試験片の形状及び寸法

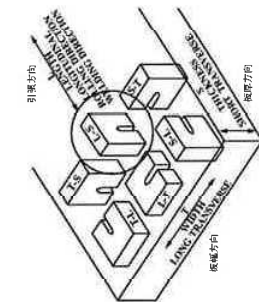


図 3 試験片の採取方向

試験方法及びき裂進展速度評価方法

(1) 試験方法

高 DO 環境条件での試験については、CT 試験片に大気中で疲労予き裂を導入後、定荷重で試験を実施した。低 DO 環境条件での試験では、SCC 進展が生じにくいことが想定されたため、大気中で疲労予き裂導入後に試験環境にて、図 4 に示す負荷上下降時間 30s、保持時間 0.3h、応力比 R=0.7 の条件で環境中予き裂導入を行った。環境中予き裂導入時の K 値は、SCC 進展試験時の K 値と同じ値に設定した。SCC 進展試験の試験水質条件を表 3 に、試験装置の概略を図 5 に示す。

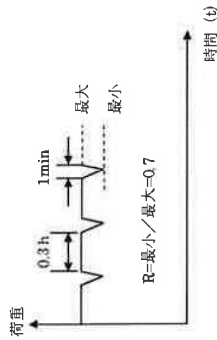
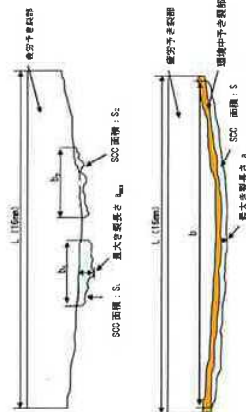


図 4 環境中予き裂導入条件の概要

表 3 SCC 進展試験の水質条件

| 項目 | 高 DO 環境条件 | 低 DO 環境条件 |
|----------------|-----------|---------------------------------|
| 試験温度 (°C) | 250, 290 | 150, 200, 250, 290, 320, 345 |
| 溶存酸素濃度 (DO) | 8 ppm | < 5 ppb |
| 溶存水素濃度 (DH) | — | 30 cc/kg H ₂ O · STP |
| ほう酸濃度 (as B) | 500 ppm | — |
| リチウム濃度 (as Li) | 2 ppm | — |

図 5 試験装置及び系統の概略図



- 最大き裂進展速度: 最大き裂長さ (l_{max}) / 進展速度評価時間 (E)
- 平均き裂進展速度: 平均き裂長さ / 進展速度評価時間 (E)
- 平均き裂長さは: SCC 面積 (ΣS) / CT 試験片幅 (L)
- 平均き裂進展速度: 平均き裂長さ / 進展速度評価時間 (E)
- 平均き裂長さは: SCC 面積 (ΣS) / SCC 発生幅 (Σb)
- SCC 発生端: Σb = b₁ + b₂ + ...

図 6 最大、平均、平均き裂長さの定義

試験結果及び考察

(1) 高 D0 環境条件の試験結果
高 D0 環境条件における試験結果の概要を、既往研究の結果も含めて表 4 に示す。

① SCC 進展に対するしきい値

SCC 進展に対する硬さのしきい値に関しては、温度が 200°C 以下であれば 200HV 程度であるが、高温例 (250°C 及び 290°C) では今回の 160HV 及び 180HV の結果も含めて、低硬度条件でも SCC 進展が認められている。温度に関しては、150°C 以下であれば進展が認められていない。

代表的な試験条件に対する試験後の破面観察結果を図 7 に示す。定荷重試験の SCC 進展破面は粒界破面となっていることを確認した。

表 4 高 D0 環境条件の試験結果の概要

| 材料 | 硬さ | 290°C | 250°C | 200°C | 150°C | 90°C |
|----------------------|-------|-------|-------|-------|-------|------|
| SUS316 フラボ 溶解材 | 300HV | ★ | ● | ● | ● | ○ |
| | 250HV | ● | ● | ● | ● | ○ |
| | 200HV | ● | ● | ● | ○ | ○ |
| | 180HV | ● | ● | ● | ○ | ○ |
| SUS304 フラボ 溶解材 | 160HV | ● | ● | ● | ○ | ○ |
| | 140HV | ● | ● | ● | ○ | ○ |
| | 300HV | ● | ● | ● | ○ | ○ |
| | 250HV | ● | ● | ● | ○ | ○ |

注) 表中の記号は以下のとおり。
白抜きは進展なし、黒りつぶしは進展ありを示す。
黒色は平成 17 年度持荷重試験データ①、青色は Step1 研究データ①、
赤色は本研究データを示す。
★: K=35MPa√m
●: K=25MPa√m
○: K=15MPa√m

② SCC 進展速度の K 値、硬さ、温度に対する依存性
300HV、290°C における SUS316 及び SUS304 の平均②き裂進展速度の K 値依存性を図 8 に示す。K 値の増加に伴ってき裂進展速度も増加する傾向が認められた。

K 値と平均②き裂進展速度の関係を近似した結果、次式 (1) が得られた。

$$da/dt = 1.04 \times 10^{-30} \times K^{1.79} \quad (\text{mm/s}) \quad (1)$$

$$15\text{MPa}\sqrt{m} \leq K \leq 35\text{MPa}\sqrt{m}$$

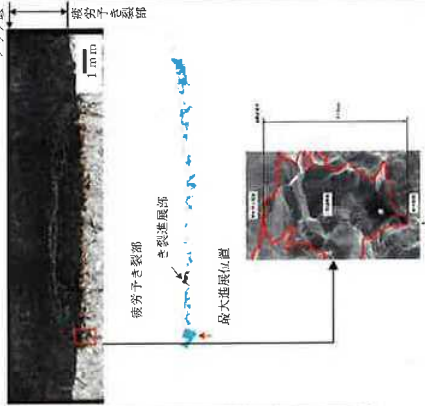


図 7 試験後の破面観察結果の例 (SUS316 フラボ溶解材, 180HV, 250°C, K=25MPa√m)

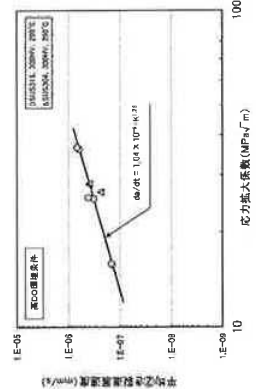


図 8 き裂進展速度の K 値依存性 (高 D0 環境条件)

290°C, K=25MPa√m の条件に対する SUS316 及び SUS304 の平均②き裂進展速度の硬さ依存性を図 9 に示す。K 値依存性と同様、硬さの増加に伴ってき裂進展速度も増加する傾向が認められた。硬さと平均②き裂進展速度の関係を近似した結果、次式 (2) が得られた。

$$da/dt = 4.71 \times 10^{-13} \times \text{HV}^{2.32} \quad (\text{mm/s}) \quad (2)$$

$$145\text{HV} \leq \text{HV} \leq 360\text{HV}$$

300HV, K=25MPa√m の条件に対する SUS316 及び SUS304 の平均②き裂進展速度の温度依存性を図 10 に示す。温度の上昇に伴ってき裂進展速度も増加する傾向が認められた。温度と平均②き裂進展速度の関係を近似した結果、次式 (3) が得られた。

$$da/dt = 5.30 \times 10^{-16} \times T^{7.22} \quad (\text{mm/s}) \quad (3)$$

$$200^\circ\text{C} \leq T \leq 290^\circ\text{C}$$

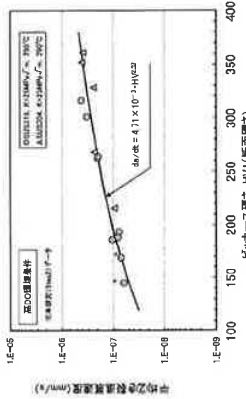


図 9 き裂進展速度の硬さ依存性 (高 D0 環境条件)

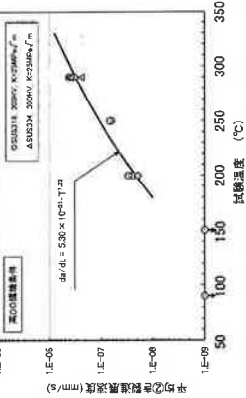


図 10 き裂進展速度の温度依存性 (高 D0 環境条件)

③ SCC 進展速度式の検討

本研究を含めてこれまで得られた SCC 進展速度データを基に、SCC 進展速度式を作成した。進展速度式の検討は、手法 1 (パラメータごとに近似式を求めて算出する方法) 及び手法 2 (重回帰分析を用いる方法) の 2 通りに行っている。検討の結果、得られた SCC 進展速度式を次式 (4) (5) に示す。また、SCC 進展速度式による進展速度の予測結果を図 11 及び図 12 に示す。

・手法 1: $da/dt (K, HV, T) = 2.09 \times 10^{-30} \times K^{1.79} \times \text{HV}^{2.32} \times T^{7.22} \quad (\text{mm/s}) \quad (4)$

・手法 2: $da/dt (K, HV, T) = 2.62 \times 10^{-30} \times K^{1.01} \times \text{HV}^{2.61} \times T^{7.10} \quad (\text{mm/s}) \quad (5)$

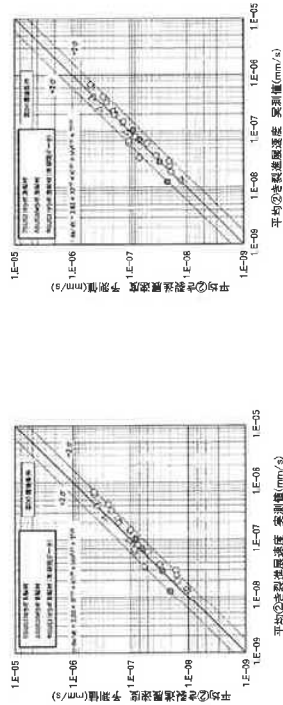


図 11 き裂進展速度の予測結果 (高 D0 環境条件, 手法 1) 図 12 き裂進展速度の予測結果 (高 D0 環境条件, 手法 2)

試験結果及び考察

(2) 低 D0 環境条件の試験結果
 低 D0 環境条件における試験結果の概要を、既往研究の結果も含めて表 5 に示す。
 ① SCC 進展に対するしきい値
 K 値のしきい値については、本研究での試験結果から、8MPa√m 以下となる領域では、ほとんどを進展
 展が認められていないことから、しきい値としては 8MPa√m 程度と考えられる。しかしながら、Step1
 研究において 300HV、290°C、K=6.5MPa√m の試験で一部の試験片のき裂先端部に粒界破面が観察されてお
 り、SCC によるき裂進展が否定できないことから、K 値のしきい値については 6.5MPa√m とする。
 一方、硬さについては、SUS316 及び SUS304 のいずれも、200HV、290°C、K=25MPa√m の試験において、
 破面観察の結果、き裂先端部に粒界破面がわずかながら観察された。これは 200HV 以下の硬さにおいて
 もき裂進展が生じうることを示唆するものであるが、次のような理由から、硬さについても、これまで
 と同様 200HV をしきい値とすることとする。

表 5 低 D0 環境条件の試験結果の概要

| 材料 | 硬さ | 345°C | 320°C | 300°C | 290°C | 250°C | 200°C | 150°C |
|---------------------|-------|-------|-------|-------|-----------------------|-------|-------|-------|
| SUS316 ラボ 溶融材 | 300HV | ●●●●● | ● | — | ★ ● ▲ ◆ □ | ●●● | ●● | ○ |
| | 250HV | ● | — | — | ● ▲ ◆ □ | ●● | — | — |
| | 235HV | — | — | — | ● ▲ ◆ □ | — | — | — |
| | 215HV | — | — | — | ● ▲ ◆ □ | — | — | — |
| | 200HV | ○ | ○ | ○ | ○ ○ | ○ | ○ | ○ |
| SUS304 ラボ 溶融材 | 250HV | — | — | — | ● ▲ ◆ □ | — | — | — |
| | 235HV | — | — | — | ● ▲ ◆ □ | — | — | — |
| | 215HV | — | — | — | ● ▲ ◆ □ | — | — | — |
| | — | — | — | — | ● ▲ ◆ □ | — | — | — |
| | 200HV | — | — | — | ● ▲ ◆ □ | — | — | — |

注) 表中の記号は以下のとおり。
 記号の白抜きは進展なし、塗りつぶしは進展ありを示す。
 黒点は平成 17 年度溶融材研究データ、白点は Step1 研究データ、赤色は本研究データを示す。
 丸：K=35MPa√m、○：K=25MPa√m、△：K=15MPa√m、◇：K=10MPa√m、▽：K=8MPa√m、□：K=6.5MPa√m

＜硬さのしきい値を 200HV とする理由＞

- ・本研究の 200HV の試験片で観察された粒界破面はごくわずかな領域 (図 13 参照) であり、定荷重条件で進展した破面と判断することが難しい。
 - ・定荷重条件の前に環境中予き裂を導入したことによる影響の可能性があるが、環境中予き裂を導入することは必ずしも実機の状態を適切に評価することにならない。
 - ・平成 17 年度溶融材研究の結果では、200HV の条件でき裂進展が認められておらず、また、200HV ではき裂が進展しないことが他の研究者によっても報告されている。
- また、温度に関しては、SUS316 では 150°C 以下、SUS304 では 200°C 以下の温度条件で、それぞれき裂進展が認められなかったことから、低 D0 環境条件での SCC 進展に対する温度のしきい値は 150~200°C 程度と考えられる。
- 低 D0 環境条件の代表的な試験条件に対する試験後の破面観察結果を図 13 に示す。

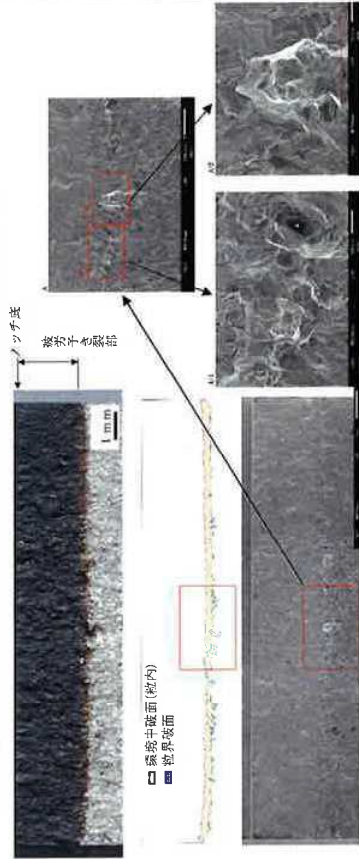


図 13 試験後の破面観察結果の例 (SUS316 ラボ溶融材, 200HV, 290°C, K=25MPa√m)

- ② SCC 進展速度の K 値、硬さ、温度に対する依存性、及び材質による差
 300HV、290°C における SUS316 及び SUS304 の平均のき裂進展速度の K 値依存性を図 14 に示す。K 値の増加に伴ってき裂進展速度は増加する傾向が認められた。K 値と平均のき裂進展速度の関係を近似した結果、次式が得られた。

$$da/dt = 1.01 \times 10^{-10} \times K^{6.6} \quad (\text{mm/s}) \quad (6)$$

$$10\text{MPa}\sqrt{\text{m}} \leq K \leq 35\text{MPa}\sqrt{\text{m}}$$

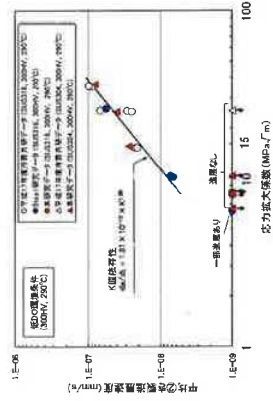


図 14 き裂進展速度の K 値依存性 (低 D0 環境条件)

試験結果及び考察

290°C, K=25MPa \sqrt{m} の条件に対する SUS316 及び SUS304 の平均②き裂進展速度の硬さ依存性を図 15 に示す。硬さの増加に伴ってき裂進展速度も増加する傾向が認められた。硬さと平均②き裂進展速度の関係を近似した結果, 次式が得られた。

$$da/dt = 1.93 \times 10^{-15} \times HV^{2.69} \quad (7)$$

300HV, K=25MPa \sqrt{m} の条件に対する SUS316 及び SUS304 の平均②き裂進展速度の温度依存性を図 16 に示す。低 DO 環境条件においては, 250°C 以上の温度領域においてはき裂進展速度の温度依存性が明確に認められなかったことから, 250°C~345°C の温度範囲ではき裂進展速度を以下のとおり一定とみなした。

$$da/dt = 3.76 \times 10^{-4} \quad (mm/s) \quad 250^\circ\text{C} \leq T \leq 345^\circ\text{C} \quad (8)$$

250HV, 290°C, K=25MPa \sqrt{m} の条件における平均②き裂進展速度の材質間での比較結果を図 17 に示す。Step1 研究で試験を実施した SUS316 高 C 材, 316 鋼溶接金属, SCS14A 鋳鋼の 3 材料については, 明確なき裂進展が認められなかったが, この 3 材料以外の材料のき裂進展速度はほぼ同程度であった。

290°C, K=25MPa \sqrt{m} の条件において, 溶接熱影響部のき裂進展速度と SUS316 及び SUS304 ラゾ溶解材の冷間加工材に対するき裂進展速度との比較を図 18 に示す。SUS316 及び SUS304 のいずれも, 熱影響部と同等の硬さを有する冷間加工材のき裂進展速度に比べて, 熱影響部のき裂進展速度は同等以下となっていることから, 熱影響部のき裂進展速度は, 硬化部の硬さを考慮すれば, 冷間加工材のき裂進展速度で代表可能と評価される。

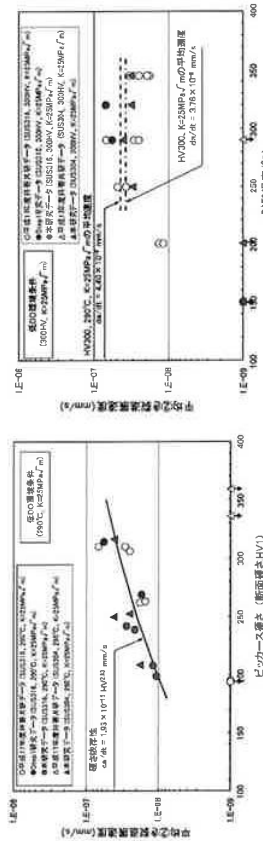


図 15 き裂進展速度の硬さ依存性 (低 DO 環境条件)

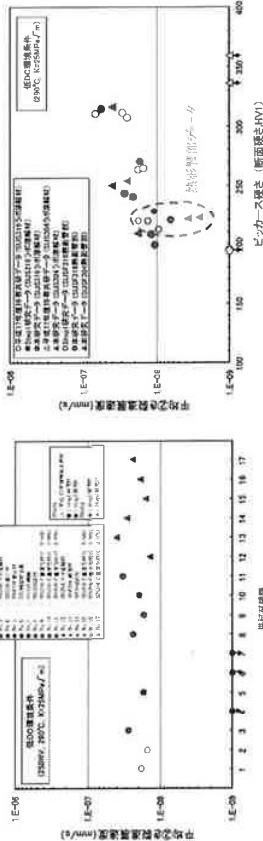


図 16 き裂進展速度の温度依存性 (低 DO 環境条件)

図 17 き裂進展速度の材質間比較 (低 DO 環境条件)

図 18 溶接熱影響部のき裂進展速度 (低 DO 環境条件)

③ SCC 進展速度式の検討

本研究を含めてこれまでに得られた SCC 進展速度データを基に, SCC 進展速度式を作成した。進展速度式の検討は, 手法 1 (ノイズデータごとに近似式を求めて算出する方法) 及び手法 2 (重回帰分析を用いる方法) の 2 通りについて行った。検討の結果, 得られた SCC 進展速度式を次式 (9) (10) に示す。また, SCC 進展速度式による進展速度の予測結果を図 19 及び図 20 に示す。

$$\text{手法 1: } da/dt(K, HV) = 3.79 \times 10^{-18} \times K^{1.69} \times HV^{2.33} \quad (9)$$

$$\text{手法 2: } da/dt(K, HV) = 1.88 \times 10^{-14} \times K^{1.10} \times HV^{1.98} \quad (10)$$

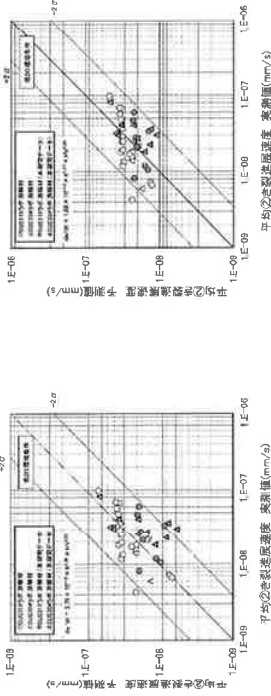


図 19 き裂進展速度の予測結果 (低 DO 環境条件, 手法 1) 図 20 き裂進展速度の予測結果 (低 DO 環境条件, 手法 2)

まとめ

本研究により得られた主な成果は以下のとおりである。

- 1) 高 DO 環境条件では, 主として SUS316 を用いた高温・低硬度領域 (250°C 及び 290°C, 200HV 以下) を対象とした進展試験を行い, SCC 進展速度データを取得した。この結果, K 値・硬さの増加及び温度の上昇に伴ってき裂進展速度が単調に増加する傾向が認められ, 既往研究と整合する試験結果が得られた。得られた試験結果に基づき, K 値, 硬さに対する依存性を考慮したき裂進展速度式を提案した。
 - 2) 低 DO 環境条件では, 主として SUS316 及び SUS304 の低硬度・低 K 値領域を対象とした進展試験を行い, SCC 進展速度データを取得した。この結果, K 値・硬さの増加に伴ってき裂進展速度が増加する傾向が認められたが, 温度に対しては 200°C 以上の温度領域では明確な依存性が認められなかった。得られた試験結果に基づき, K 値, 硬さに対する依存性を考慮したき裂進展速度式を提案した。
 - 3) 低 DO 環境条件で実施した SUS316 と SUS304 の LN 材, C 量変化材の代表条件でのき裂進展試験の結果, き裂進展速度は SUS316 と SUS304 のラゾ溶解材とほとんど差が認められず, 材質の影響は小さいと評価される。また, 熱影響部に対する試験の結果, 熱影響部のき裂進展速度は熱影響部と同等の硬さを有する冷間加工材のき裂進展速度と同等以下であったことから, 冷間加工材のき裂進展速度で代表できることを確認した。
- なお, 2013 年 2 月の時点において, 非酸化化オーステナイト系ステンレス鋼の冷間加工 SCC に起因した損傷事例は実機 PWR プラントではほとんど報告されていないが, 今後は, 本研究で得られたデータを基に, 維持規格への反映等, 実機保全に向けて検討を行っていく必要があると思われる。



SCC growth behaviors of austenitic stainless steels in simulated PWR primary water

T. Terachi^{a,*}, T. Yamada^b, T. Miyamoto^b, K. Arioka^b

^aRadiological Management Group, The Kansai Electric Power Co, Inc., Japan

^bInstitute of Nuclear Safety System, Inc., 64 Sata, Mihama-cho, Mikata-gun, Fukui 919-1205, Japan

article info

Article history:
Received 12 July 2011
Accepted 6 March 2012
Available online 16 March 2012

abstract

The rates of SCC growth were measured under simulated PWR primary water conditions (600 ppm B + 2 ppm Li + 30 cm³/kg-H₂O-STP D₂H₂) using cold worked 316SS and 304SS. The direct current potential drop method was applied to measure the crack growth rates for 53 specimens. Dependence of the major engineering factors, such as yield strength, temperature and stress intensity was systematically examined. The rates of crack growth were proportional to the 2.9 power of yield strength, and directly proportional to the apparent yield strength. The estimated apparent activation energy was 84 kJ/mol. No significant differences in the SCC growth rates and behaviors were identified between 316SS and 304SS. Based on the measured results, an empirical equation for crack growth rate was proposed for engineering applications. Although there were deviations, 92.8% of the measured crack growth rates did not exceed twice the value calculated by the empirical equation.

© 2012 Elsevier B.V. All rights reserved.

1. Introduction

Stress corrosion cracking (SCC) is an important degradation issue, especially for keeping reliability of pressurized water reactors (PWRs). In nickel-based alloys such as Alloy 600 and their weld metals, SCC has been reported since the 1980s in steam generator tubing, and since the 1990s in the nozzles of pressure vessels and steam generators [1,2]. In comparison with nickel-based alloys, SCC incidence of austenitic stainless steels has not been reported except in some particular cases such as for irradiated materials [3] or in oxygenated environments [4]. However, in recent years, limited examples of SCC were reported in high strain hardened areas or in heat affected zones of stainless steels in PWR primary systems [5,6].

Studies have been done on the SCC behaviors of austenitic stainless steels in simulated environments of light water reactors [7–20]. Cold work (CW) significantly enhanced SCC growth in both BWRs and PWRs. One explanation for the acceleration was reported as due to the reduced plastic zone size at a given stress intensity which produced steeper strain gradients at the crack tip [21–24]. A similar effect of CW on SCC growth was observed in various alloys and environments [24]. Furthermore, formation of vacancies and deformation structures in materials might have some role in the acceleration effect from CW [25]. Arioka et al. [25] reported that the diffusion of vacancies at the grain boundary might be an important process because some similarities were observed between intergranular (IG) creep and SCC in high temperature water. In addition,

nickel enrichment was observed ahead of the crack tips at the grain boundary which suggested that grain boundary diffusion did occur before crack advancement. Alternatively, Lozano-Pérez et al. [26] pointed out that the length of the localized oxidation region at deformation bands increased with decreasing chromium content in the alloy. Since the deformation bands were formed by CW, the oxidation at crack tips seemed to have some role in the SCC growth process.

Rolling direction of CW also affected the crack growth rate (CGR). Using 316 stainless steel (316SS), Arioka et al. [27] found that much faster CGRs were observed in the T–L orientation than in the T–S orientation; a schematic drawing showing definitions of the orientations is given in Fig. 1. Moshier and Brown [20] reported that CGRs were 10 times more rapid in the S–T orientation compared to the L–T orientation of Alloy 600. The effect of the CW orientation is not well clarified, except that S–L, S–T and T–L orientations provide aggressive cracking compare to T–S and L–S orientations [20,27,28]. In considering an actual component with elbow structures, for example, while the bending method is not simple rolling, the crack direction for penetration might correspond to T–S or L–S orientations. In the present paper, T–S orientation specimens were used to estimate CGRs for 316SS and 304SS specimens.

Elucidating the temperature dependence on SCC is of great importance not only for a mechanistic viewpoint, but also for the prediction of CGRs of each system at operating power plants. The reported activation energies of SCC in CW stainless steels under PWR conditions range from 56 kJ/mol to 107 kJ/mol [25,29,30]. Several factors including chemical reaction, diffusion at a grain boundary and mechanical properties have some potential to change the apparent activation energy of cracking [31]. If the

* Corresponding author. Tel: +81 770 32 3650.
E-mail address: terachi.takumi@a4.kepcoco.jp (T. Terachi).

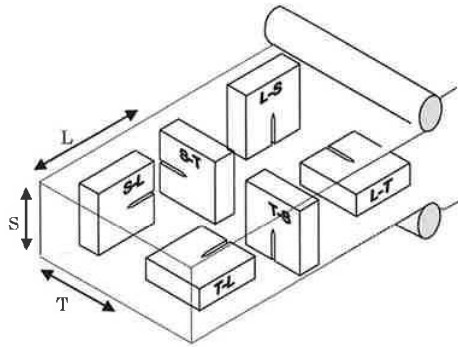


Fig. 1. Schematic of rolling orientation in relation to the longitudinal (L), thickness (T) and short transverse (S) directions.

surface reaction at a metal–water interface controls the thermal activation process, activation energy will be affected by the water chemistry conditions. From this perspective, obtaining systematic CGRs is important to get accurate activation energies and elucidate the SCC mechanism.

The objective of this study is to quantify systematically the rate of SCC growth of CW 316SS and 304SS in PWR primary water conditions. The influences of yield strength, temperature dependence and stress intensity factors were examined using 53 0.5T compact tension (CT) specimens.

2. Experimental

2.1. Materials

Specimens of 316SS and 304SS were used to determine the CGRs of SCC in hydrogenated high temperature water. The elemental components and material properties are listed in Tables 1 and 2, respectively. The materials were solution-treated at 1060–1080 °C for 10 min then water quenched. To examine the influence of CW, materials were cold-rolled in one dimension to produce 5%, 10%, 15% and 20% reductions in thickness at room temperature (RT).

The yield strengths of specimens at the test temperature were required to confirm the validity of the SCC test, and they were estimated from the measured data at RT and 320 °C using the trend of reported temperature dependence as shown in Fig. 2 [32]. The estimated values are listed in Table 3.

2.2. Specimen preparation

Specimen morphology was as shown in Fig. 3. The CT specimens were extracted from the CW plate. Prior to the CGR measurement, each specimen was pre-cracked in air by fatigue stress by applying a symmetrical triangle wave equal to or less than 10 Hz. The stress intensity factor of pre-cracking was controlled so that it did not exceed 80% of the stress intensity factor of the initial CGR measurement. However due to the difficulty of pre-cracking under quite a small stress condition, the minimum stress intensity factor for

Table 1
Compositions of alloys (mass%).

| | C | S | Mn | P | S | Ni | Cr | Mo |
|-------|-------|------|------|-------|-------|------|-------|------|
| 316SS | 0.047 | 0.45 | 1.42 | 0.024 | 0.001 | 11 | 16.45 | 2.07 |
| 304SS | 0.04 | 0.31 | 1.59 | 0.031 | 0.001 | 9.21 | 18.34 | 0.37 |

Heat treatment: 316SS, 1080 °C; 304SS, 1060 °C, water quenched.

Table 2
Mechanical properties of alloys.

| | Cold work (%) | Yield strength (N/mm ²) (320 °C) | Tensile strength (N/mm ²) (320 °C) | Elongation (%) (320 °C) | HV (1 kg) |
|-------|---------------|--|--|-------------------------|-----------|
| 316SS | 5 | 248 | 458 | 36 | 184 |
| | 10 | 345 | 495 | 29 | 219 |
| | 15 | 495 | 565 | 15 | 254 |
| | 20 | 572 | 607 | 10 | 270 |
| 304SS | 5 | 270 | 434 | 38 | 205 |
| | 10 | 365 | 466 | 32 | 214 |
| | 15 | 436 | 503 | 24 | 243 |
| | 20 | 498 | 564 | 16 | 267 |

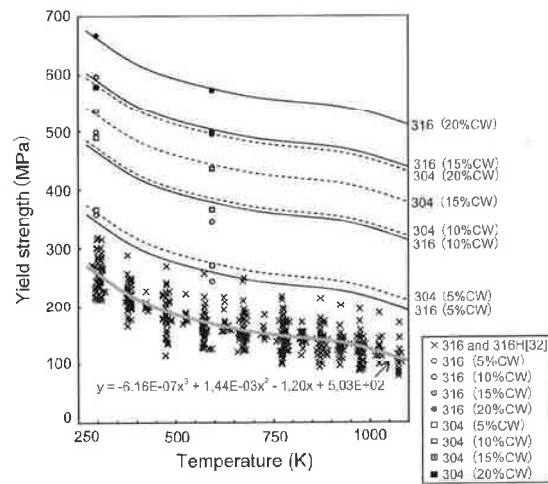


Fig. 2. Yield strength as a function of temperature [32]. Prediction curves for CW alloys are roughly parallel to the reference data.

pre-cracking was fixed to 10 MPa√m. Target length of a pre-crack was set to 2–2.5 mm and actual length was assessed after the SCC test.

2.3. Crack growth rate measurements

All CGR measurements were carried out using water circulation type autoclaves. An example of the SCC test facility set-up is shown in Fig. 4. Specimens were immersed in simulated PWR primary water that contained 500 ppm boron as boric acid, 2 ppm lithium as LiOH and 30 cm³-STP/kg-H₂O of dissolved hydrogen (DH). Dissolved oxygen in the water was continuously monitored at the inlet of the autoclave and controlled not to exceed 5 ppb. CGR trends of most specimens were monitored by the direct current potential drop method (PDM) described in ASIM standard B47-11[33]. Applied reversing direct current was 0.8–5 A and potential drop signals were detected by a high precision nano-voltmeter. Electric noise was reduced by analog and digital filtering, and noise possibly derived from temperature fluctuation of the water (less than ±1 °C) was eliminated by a smoothing technique. Calculated CGR resolution from PDM signal was roughly 10–50 l/m. RT which would also affect the entire monitoring system was maintained 25 ± 2 °C.

Example CGR measurement results are shown in Fig. 5. A trapezoidal wave loading with R=0.7, x = 0.017 s⁻¹ was applied every 4 h for 10–20 days to initiate crack growth through a grain

Table 3
Estimated yield strength at high temperature (N/mm²).

| Temperature (°C) | 316SS | | | | 304SS | | | |
|------------------|-------|-------|-------|-------|-------|-------|-------|-------|
| | 5%CW | 10%CW | 15%CW | 20%CW | 5%CW | 10%CW | 15%CW | 20%CW |
| 250 | 268 | 389 | 513 | 587 | 285 | 395 | 453 | 506 |
| 270 | 264 | 385 | 509 | 583 | 281 | 391 | 449 | 502 |
| 280 | 262 | 383 | 507 | 581 | 279 | 389 | 447 | 500 |
| 290 | 260 | 382 | 506 | 580 | 278 | 388 | 446 | 499 |
| 300 | 259 | 380 | 504 | 578 | 276 | 386 | 444 | 497 |
| 310 | 257 | 379 | 502 | 576 | 275 | 385 | 443 | 496 |
| 320 | 256 | 377 | 501 | 575 | 273 | 383 | 441 | 494 |
| 330 | 254 | 376 | 500 | 574 | 272 | 382 | 440 | 493 |
| 340 | 253 | 374 | 498 | 572 | 270 | 380 | 438 | 491 |
| 350 | 252 | 373 | 497 | 571 | 269 | 379 | 437 | 490 |
| 360 | 251 | 372 | 496 | 570 | 268 | 378 | 436 | 489 |

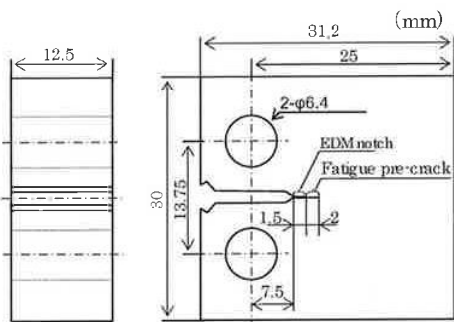


Fig. 3. Example of compact tension specimen morphology.

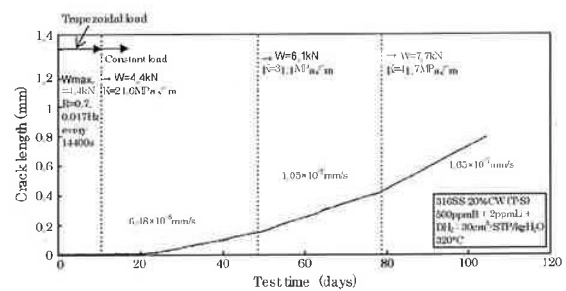


Fig. 5. Potential drop measurement of 316SS (20%CW, T-S Specimen No. SSC2E) under simulated PWR primary water conditions.

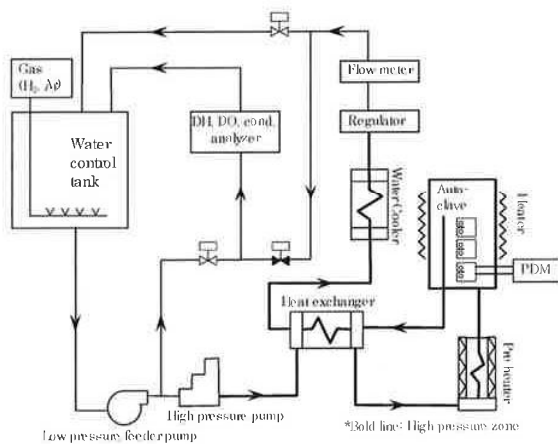


Fig. 4. Example of SCC test equipment set-up.

boundary. After the trapezoidal wave loading, the stress condition was kept constant to measure the CGR data. Several CGR data were obtained from a specimen by changing the test conditions such as applied stress, as shown in Fig. 5, or the temperature condition. After the test, the specimens were fractured by fatigue stress in air, and the crack length was measured using a scanning electron microscope (SEM). The PDM signals for the CGR were corrected by means of the average crack length that was measured by SEM fracture surface observation. However, on account of the difficulty for maintaining electrical insulation in high temperature water, the PDM technique was not applied for tests above 330 °C. This is because the present system used polytetrafluoroethylene for insular

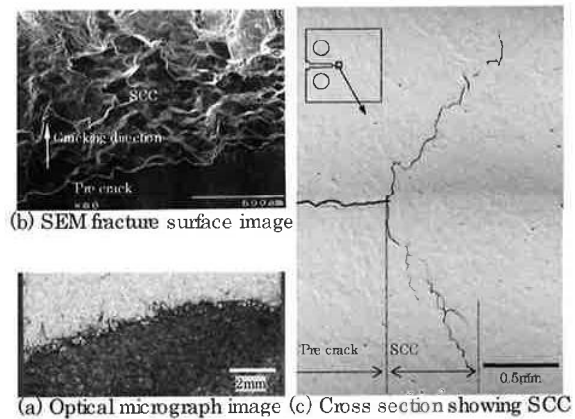


Fig. 6. Example of fracture surface and cross-sectional observation of 316SS (20%CW, T-S Specimen No. SSC2E), tested under simulated PWR primary water conditions (500 ppm B + 2 ppm Li + DH₂; 30 cm³-STP/kg H₂O, 320 °C).

tion. In the case of no PDM signal, trapezoidal wave loading was not applied as a starter due as it was not possible to eliminate the effect of fatigue loading.

3. Results

3.1. Crack growth rate measurements

Fig. 6 shows an example of a fracture surface and a cross-sectional observation of a tested 316SS (20%CW) specimen

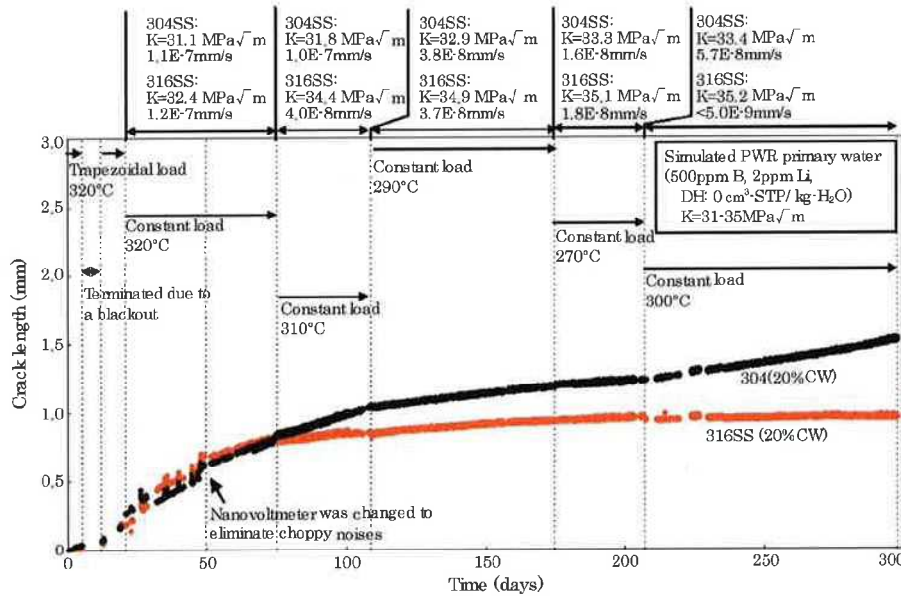
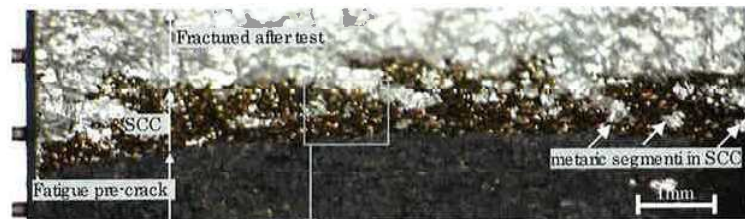
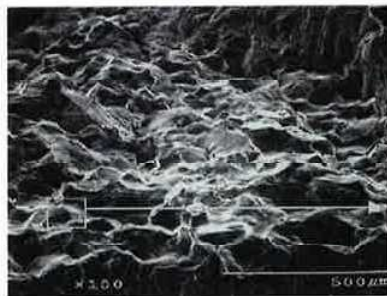


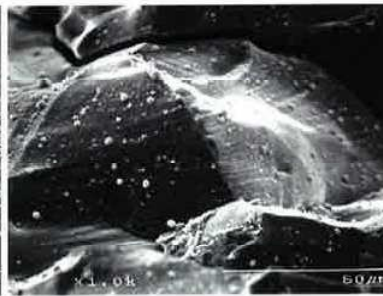
Fig. 7. Crack growth rate measurement of 316SS (20% CW, T-S Specimen No. G316A8) and 304SS (20% CW, T-S Specimen No. G304B9) under simulated PWR primary water conditions.



(a) Optical microscope image of fracture surface



(b) SEM image in low magnification



(c) SEM image in high magnification

Fig. 8. Fracture surface of 316SS (20% CW, T-S Specimen No. G316A8), tested under simulated PWR primary water conditions for 6650 h (500 ppm B + 2 ppm Li + DH: 30 cm³-STP/kg H₂O, 270–320 °C).

revealing that the SCC propagated through the grain boundary. The cross-sectional image showed the crack deviated in two directions, approximately 60° from normal cracking. This kind of splitting was reported on T-S orientation CW specimens [27]. Even though the mechanism is not clear, the important crack orientation for operating plants is propagation in the wall thickness direction; therefore in the paper, the crack length was defined as the measured length

observed from the loading direction using an SEM image. Theoretically branching also affects the calculation of stress intensity factor, because the stress to open the crack mouth decreases and shear stress increases [34]. However it is difficult to determine the branched angle for the entire thickness especially in specimens with short cracks, so from a practical viewpoint, apparent stress intensity factor was calculated using the ASTM E399-09 [35] code

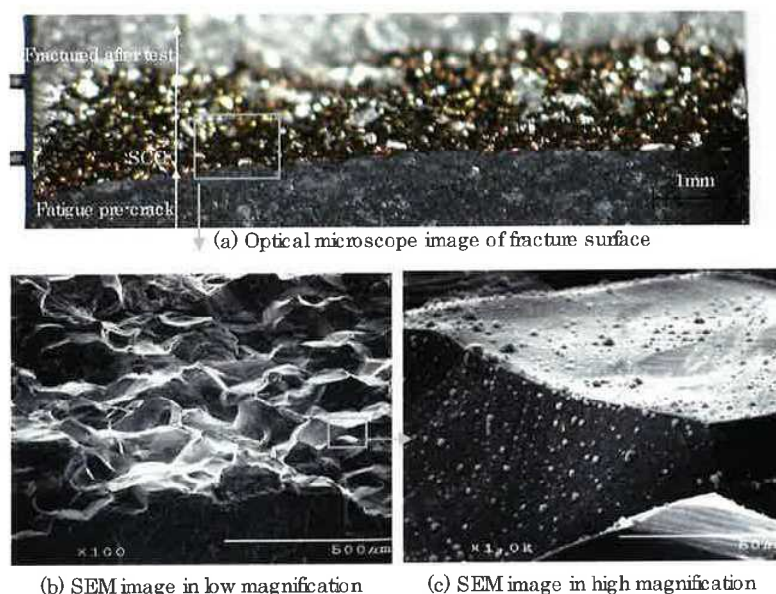


Fig. 9. Fracture surface of 304SS (20%CW, T-S Specimen No. G304B9), tested under simulated PWR primary water conditions for 6650 h (500 ppm B+ 2 ppm Li +DH₂: 30 cm³-SiH/kg H₂O, 270–320 °C).

Table 4
SCC growth rates of 316SS (5–10%CW, T-S).

| Specimen no. | Cold work (%) | Temperature (°C) | Test time (days) | Apparent stress intensity factor (MPa√m) | Average crack length increment (mm) | Average crack growth rate (mm/s) |
|--------------|---------------|------------------|------------------|--|-------------------------------------|----------------------------------|
| S6C5A | 5 | 290 | 31 | 34.1 | 0.02 | 6.3E-09 |
| | 5 | 300 | 55 | 34.0 | 0.02 | 4.2E-09 |
| | 5 | 320 | 42 | 26.1 | 0.02 | 5.5E-09 |
| | 5 | 320 | 36 | 33.9 | 0.05 | 1.5E-08 |
| GC S6C5 C | 5 | 320 | 182 | 31.9 | 0.27 | 1.7E-08 |
| S6C10A | 10 | 320 | 26 | 20.3 | <0.01 | <5.0E-09 |
| | 10 | 320 | 32 | 27.9 | 0.05 | 1.8E-08 |
| | 10 | 320 | 28 | 34.6 | 0.11 | 4.4E-08 |
| S6C10B | 10 | 290 | 60 | 30.2 | <0.01 | <5.0E-09 |
| | 10 | 270 | 35 | 30.2 | <0.01 | <5.0E-09 |
| | 10 | 310 | 25 | 30.2 | 0.02 | 9.6E-09 |
| S6C10D | 10 | 300 | 71 | 30.9 | 0.04 | 5.8E-09 |
| S6C10C | 10 | 290 | 71 | 30.0 | <0.01 | <5.0E-09 |
| S6C10E | 10 | 290 | 27 | 26.1 | 0.01 | <5.0E-09 |
| | 10 | 290 | 15 | 40.2 | 0.03 | 2.3E-08 |
| | 10 | 320 | 47 | 25.8 | 0.15 | 3.6E-08 |
| S6C10-2 | 10 | 320 | 55 | 28.0 | <0.01 | <5.0E-09 |
| | 10 | 310 | 39 | 22.9 | <0.01 | <5.0E-09 |
| | 10 | 290 | 49 | 28.0 | <0.01 | <5.0E-09 |
| | 10 | 270 | 17 | 28.0 | <0.01 | <5.0E-09 |
| | 10 | 300 | 98 | 28.0 | <0.01 | <5.0E-09 |
| GS6C10-4 | 10 | 320 | 41 | 28.2 | 0.166 | 4.7E-08 |
| G316-10-TS-1 | 10 | 360 | 20 | 30.9 | <0.01 | <5.0E-09 |
| G316-10-TS-2 | 10 | 340 | 34 | 31.7 | <0.01 | <5.0E-09 |
| G316-10-TS-3 | 10 | 330 | 61 | 31.7 | 0.07 | 1.3E-08 |

for non-branched cracks. The apparent stress intensity factors in this paper were the averaged values during crack propagation.

Crack propagation curves of 316SS (20%CW) and 304SS (20%CW) below 320 °C are shown in Fig. 7. Initially a trapezoidal wave load was applied for IG cracking, and then it was switched to a constant load for a SCC test. The crack growth rates of 316SS

(20%CW) and 304 (20%CW) at 320 °C were estimated from the PDM trend as 1.2×10^{-7} mm/s and 1.1×10^{-7} mm/s, respectively. While similar CGRs were obtained at 320 °C, slower CGRs in 316SS (20%CW) were observed at 310 °C. During the test at 290 °C and 270 °C similar CGRs trend were observed in both steel types, and they decreased with decreasing temperature conditions. When

Table 5
SCC growth rates of 316SS (15%CW, T-S).

| Specimen no. | Cold work (%) | Temperature (°C) | Test time (days) | Apparent stress intensity factor (MPa \sqrt{m}) | Average crack length increment (mm) | Average crack growth rate (mm/s) |
|--------------|---------------|------------------|------------------|--|-------------------------------------|----------------------------------|
| S6C15A | 15 | 320 | 26 | 20.8 | 0.10 | 4.4E-08 |
| | 15 | 320 | 32 | 29.1 | 0.19 | 6.9E-08 |
| | 15 | 320 | 28 | 36.9 | 0.28 | 1.2E-07 |
| S6C15B | 15 | 270 | 35 | 30.8 | 0.02 | 6.1E-09 |
| | 15 | 290 | 60 | 30.7 | 0.07 | 1.3E-08 |
| | 15 | 310 | 25 | 30.4 | 0.04 | 1.7E-08 |
| S6C15C | 15 | 290 | 71 | 30.0 | 0.01 | <5.0E-09 |
| S6C15D | 15 | 300 | 71 | 30.1 | 0.21 | 3.4E-08 |
| S6C15E | 15 | 290 | 15 | 25.7 | 0.02 | 1.4E-08 |
| | 15 | 290 | 27 | 25.7 | 0.04 | 1.6E-08 |
| | 15 | 290 | 15 | 39.7 | 0.07 | 5.0E-08 |
| | 15 | 320 | 47 | 25.3 | 0.18 | 4.5E-08 |
| S6C15-4 | 15 | 320 | 27 | 8.5 | <0.01 | <5.0E-09 |
| | 15 | 290 | 34 | 13.0 | 0.04 | 5.6E-09 |
| | 15 | 320 | 34 | 13.0 | 0.03 | 4.1E-09 |
| S6C15-5 | 15 | 290 | 56 | 13.5 | 0.10 | 2.0E-08 |
| | 15 | 290 | 21 | 17.3 | 0.04 | 2.2E-08 |
| | 15 | 290 | 63 | 17.9 | 0.01 | <5.0E-09 |
| | 15 | 290 | 48 | 21.8 | 0.01 | <5.0E-09 |
| | 15 | 290 | 50 | 21.9 | 0.09 | 2.0E-08 |
| | 15 | 290 | 35 | 26.1 | <0.01 | <5.0E-09 |
| G316-15-TS-1 | 15 | 360 | 30 | 31.7 | <0.01 | <5.0E-09 |
| G316-15-TS-2 | 15 | 340 | 34 | 31.6 | <0.01 | <5.0E-09 |
| G316-15-TS-5 | 15 | 330 | 61 | 30.9 | 0.11 | 2.1E-08 |
| G316-15-TS-3 | 15 | 250 | 409 | 30.1 | 0.08 | 2.3E-09 |

Table 6
SCC growth rates of 316SS (20%CW, T-S).

| Specimen no. | Cold work (%) | Temperature (°C) | Test time (days) | Apparent stress intensity factor (MPa \sqrt{m}) | Average crack length increment (mm) | Average crack growth rate (mm/s) |
|--------------|---------------|------------------|------------------|--|-------------------------------------|----------------------------------|
| S6C2E | 20 | 250 | 75 | 38.4 | <0.01 | <5.0E-09 |
| | 20 | 270 | 32 | 40.8 | 0.05 | 1.7E-08 |
| S6C20D | 20 | 290 | 27 | 26.6 | 0.12 | 5.0E-08 |
| | 20 | 290 | 15 | 26.9 | 0.09 | 7.1E-08 |
| | 20 | 290 | 15 | 42.2 | 0.24 | 1.8E-07 |
| | 20 | 300 | 71 | 30.1 | 0.83 | 1.4E-07 |
| | 20 | 320 | 47 | 25.8 | 0.39 | 9.5E-08 |
| S6C2E | 20 | 290 | 30 | 38.6 | 0.10 | 3.8E-08 |
| | 20 | 290 | 22 | 40.2 | 0.07 | 3.4E-08 |
| | 20 | 320 | 17 | 39.3 | 0.20 | 1.4E-07 |
| S6C2D | 20 | 320 | 61 | 29.6 | 0.55 | 1.1E-07 |
| S6C2F | 20 | 320 | 30 | 21.6 | 0.17 | 6.5E-08 |
| | 20 | 320 | 38 | 31.1 | 0.35 | 1.1E-07 |
| | 20 | 320 | 26 | 41.7 | 0.37 | 1.7E-07 |
| G316A8 | 20 | 320 | 55 | 32.4 | 0.57 | 1.2E-07 |
| | 20 | 310 | 33 | 34.4 | 0.11 | 4.0E-08 |
| | 20 | 290 | 66 | 34.9 | 0.21 | 3.7E-08 |
| | 20 | 270 | 32 | 35.1 | 0.05 | 1.8E-08 |
| | 20 | 300 | 91 | 35.2 | <0.01 | <5.0E-09 |
| S6C20-1 | 20 | 290 | 83 | 13.6 | 0.04 | 5.6E-09 |
| | 20 | 320 | 84 | 13.5 | <0.01 | <5.0E-09 |
| S6C20-2 | 20 | 290 | 56 | 14.4 | 0.09 | 1.9E-08 |
| | 20 | 290 | 63 | 19.3 | 0.21 | 3.8E-08 |
| | 20 | 290 | 21 | 20.6 | 0.03 | 1.5E-08 |
| | 20 | 290 | 48 | 24.0 | 0.21 | 5.1E-08 |
| | 20 | 290 | 50 | 25.7 | 0.29 | 6.8E-08 |
| | 20 | 290 | 35 | 29.7 | 0.28 | 9.1E-08 |
| GCS6C20-K | 20 | 360 | 30 | 32.5 | 0.52 | 2.0E-07 |
| GCS6C20-L | 20 | 340 | 34 | 32.9 | 0.79 | 2.7E-07 |
| GCS6C20-M | 20 | 340 | 30 | 32.9 | 0.88 | 3.4E-07 |
| GCS6C20-N | 20 | 350 | 30 | 32.9 | 0.86 | 3.3E-07 |
| GCS6C20-O | 20 | 360 | 30 | 32.1 | 0.36 | 1.4E-07 |
| G316-20-TS-1 | 20 | 250 | 409 | 31.7 | 0.28 | 7.9E-09 |

Table 7
SCC growth rates of 304SS (5–15%CW, T-S).

| Specimen no. | Cold work (%) | Temperature (°C) | Test time (days) | Apparent stress intensity factor (MPa√m) | Average crack length increment (mm) | Average crack growth rate (mm/s) |
|--------------|---------------|------------------|------------------|--|-------------------------------------|----------------------------------|
| G304B 1 | 5 | 290 | 72 | 20.8 | <0.01 | <5.0E-09 |
| | 5 | 290 | 58 | 25.8 | <0.01 | <5.0E-09 |
| | 5 | 290 | 58 | 31.2 | 0.16 | 3.3E-08 |
| G304B 2 | 5 | 320 | 182 | 30.9 | 0.07 | 4.6E-09 |
| G304C 1 | 10 | 310 | 68 | 30 | 0.10 | 1.7E-08 |
| | 10 | 320 | 38 | 31.1 | 0.08 | 2.9E-08 |
| | 10 | 290 | 34 | 31.4 | 0.08 | 2.9E-08 |
| | 10 | 270 | 29 | 31.6 | <0.01 | <5.0E-09 |
| | 10 | 280 | 51 | 31.6 | 0.04 | 1.0E-08 |
| | 10 | 300 | 64 | 31.6 | <0.01 | <5.0E-09 |
| G304-10-1 | 10 | 340 | 76 | 30 | <0.01 | <5.0E-09 |
| G304C 2 | 10 | 290 | 72 | 20.1 | <0.01 | <5.0E-09 |
| | 10 | 290 | 58 | 25.1 | 0.07 | 1.4E-08 |
| | 10 | 290 | 58 | 30.5 | 0.19 | 3.8E-08 |
| G304D 1 | 15 | 320 | 33 | 31.5 | 0.22 | 7.7E-08 |
| | 15 | 290 | 34 | 32.1 | 0.08 | 2.9E-08 |
| | 15 | 270 | 29 | 32.2 | <0.01 | <5.0E-09 |
| | 15 | 280 | 51 | 32.5 | 0.01 | <5.0E-09 |
| | 15 | 300 | 64 | 32.7 | 0.03 | 6.1E-09 |
| | 15 | 310 | 68 | 33 | 0.14 | 2.4E-08 |
| G304D 2 | 15 | 290 | 72 | 15.3 | <0.01 | <5.0E-09 |
| | 15 | 290 | 58 | 19 | 0.09 | 1.8E-08 |
| | 15 | 290 | 58 | 23.1 | 0.30 | 6.0E-08 |
| G304-15-2 | 15 | 340 | 76 | 34.2 | 0.60 | 9.2E-08 |
| G304-15-TS-3 | 15 | 330 | 61 | 31.8 | 0.13 | 2.40E-08 |
| G304-15-1 | 15 | 250 | 409 | 30.1 | 0.10 | 2.8E-09 |

Table 8
SCC growth rates of 304SS (20%CW, T-S).

| Specimen no. | Cold work (%) | Temperature (°C) | Test time (days) | Apparent stress intensity factor (MPa√m) | Average crack length increment (mm) | Average crack growth rate (mm/s) |
|--------------|---------------|------------------|------------------|--|-------------------------------------|----------------------------------|
| 304E 3 | 20 | 290 | 35 | 27.8 | 0.13 | 4.3E-08 |
| | 20 | 290 | 50 | 13.8 | 0.08 | 1.8E-08 |
| | 20 | 290 | 63 | 18.5 | 0.13 | 2.4E-08 |
| | 20 | 290 | 48 | 22.9 | 0.13 | 3.1E-08 |
| | 20 | 290 | 50 | 23.6 | 0.17 | 4.1E-08 |
| | 20 | 290 | 21 | 18.8 | 0.05 | 2.7E-08 |
| G304E 1 | 20 | 320 | 33 | 30.5 | 0.25 | 8.7E-08 |
| | 20 | 290 | 34 | 31 | 0.06 | 1.9E-08 |
| | 20 | 280 | 51 | 31.1 | 0.02 | 5.1E-09 |
| | 20 | 280 | 64 | 31.2 | 0.04 | 6.5E-09 |
| | 20 | 300 | 32 | 31.3 | 0.01 | <5.0E-09 |
| | 20 | 310 | 19 | 31.4 | 0.05 | 2.9E-08 |
| | 20 | 310 | 17 | 31.6 | 0.05 | 3.3E-08 |
| G304E 5 | 20 | 290 | 84 | 14 | 0.01 | <5.0E-09 |
| | 20 | 320 | 27 | 9.17 | <0.01 | <5.0E-09 |
| | 20 | 320 | 84 | 14 | 0.03 | 3.7E-09 |
| G304E 9 | 20 | 320 | 55 | 31.1 | 0.54 | 1.1E-07 |
| | 20 | 310 | 33 | 31.8 | 0.30 | 1.0E-07 |
| | 20 | 290 | 66 | 32.9 | 0.22 | 3.8E-08 |
| | 20 | 270 | 32 | 33.3 | 0.05 | 1.6E-08 |
| | 20 | 300 | 91 | 33.4 | 0.45 | 5.7E-08 |
| | 20 | 300 | 91 | 33.4 | 0.45 | 5.7E-08 |
| G304-20-4 | 20 | 340 | 76 | 32.8 | 0.98 | 1.5E-07 |
| G304-20-2 | 20 | 250 | 409 | 29.2 | 0.35 | 9.9E-09 |

the temperature was increased from 270 °C to 300 °C, the OGR of 304SS (20%CW) was increased, although retardation of the OGR ($<5 \times 10^{-9}$ mm/s) was observed in 316SS (20%CW). According to Ozawa et al. [36], similar retardations of crack propagation in Alloy 600 have been confirmed by OGR measurements using CT specimens.

The fracture surface of the 316SS (20%CW), as shown in Fig. 8a, indicated that unfractured metallic segments remained in the SCC area. The existence of the metallic segments meant that the SCC susceptibility was not homogeneous. If the unfractured segments resisted the crack mouth opening, the crack growth could be arrested. From this consideration, it should be noted that even if

the signal noise ratio is high enough and the test conditions are well controlled, reliability of CGRs in certain alloys is difficult to obtain. From this aspect, systematic investigations are required to elucidate the cracking phenomenon.

Figs. 8 and 9 show the fracture surfaces of 316SS (20%CW) and 304SS (20%CW) specimens; they exhibited similar surface morphologies. Typical IG facets were observed at the SCC area, and granular corrosion products, up to 21 μm in size, were scattered on the surfaces. Previously, it was reported that the corrosion products consisted of spinel type iron-rich oxide [15]. No obvious differences were observed between 316SS and 304SS.

In order to obtain systematic data, 83 crack growth tests were conducted using 38 specimens of 316SS with CW from 5% to 20% as shown in Tables 3–5. The influences of CW, test temperature and applied stress on CGR were examined. Since the CGR of 316SS under simulated PWR conditions is slower than that under the oxygenated condition, average CGR measurement times of 53 days were needed to improve the data accuracy. In many cases a longer test time (maximum: 409 days) was used, while 22 tests were evaluated as below the detection limit or had no crack initiation. When the PDM is applied to monitor crack growth, theoretically the detection limit depends on the signal to noise ratio. However, CGR data for less than 10 μm crack length were regarded as being for an invalid length to eliminate the unknown error. It should be noted that several tests did not apply the PDM due to unavailability of the facility; in those cases, periodical loading was not performed as a starter for crack initiation. The purpose of periodical loading is to induce the transition from the transgranular (TG) fatigue pre-crack to the IG crack. This could affect reproducibility of SCC growth rates especially in low susceptibility specimens by reducing the effect of crack initiation period. The required crack length for less scatter of CGR measurements and the detection limit under high temperature conditions are discussed later.

In the same way, 49 CGRs of 304SS with 5–20%CW were measured using 16 specimens, and 12 CGRs were evaluated as below the measurable limit or no cracking was observed as listed in Tables 6–8. Since relatively low temperature tests were performed on 304SS, average test time for each CGR measurement was about 69 days. The total number of suitable CGRs was 98, excluding the 35 data omitted because they were below the detection limit.

4. Discussion

4.1. Influence of cold work

Fig. 10 illustrates the influence of CW on the CGR in 316SS specimens exposed to simulated PWR primary water conditions. Since it is difficult to measure the CW ratio of an actual component, Vickers hardness was used instead to describe the effect of CW. The acceleration effect on CGRs by CW clearly appeared for both 320 °C and 300 °C conditions. According to Tsubota et al. [37], the critical hardness for initiation of SCC for 316L stainless steel under simulated BWR conditions was HV = 300. On the other hand, the cracks propagated even for HV = 184 with 316SS (5%CW). This discrepancy indicates that the critical hardness for initiation is higher than that for propagation as CGR under BWR conditions is generally faster than that under PWR conditions.

A comparable enhancement effect on yield strength for 316L, 304, 304L and 347L stainless steels is well documented [8,12,13,29,38]. Comparing the absolute value of CGRs is difficult by reason of different test conditions and materials, but the tendency for an increase in CGR by cold working was consistent with the reported data as shown in Fig. 11.

In addition, the enhancement effect by high yield strength has been reported not only for stainless steel, but also nickel-based

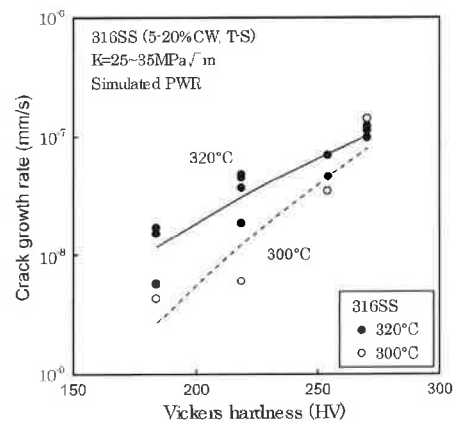


Fig. 10. Effect of hardness on crack growth rate of CW 316SS tested under simulated PWR primary water conditions. (Specimen Nos.: S6C5A, S6C10A, S6C10D, S6C10E, G8S6C10-4, S6C15A, S6C15D, S6C15E, S6C20D, S6C2E, G316A8.)

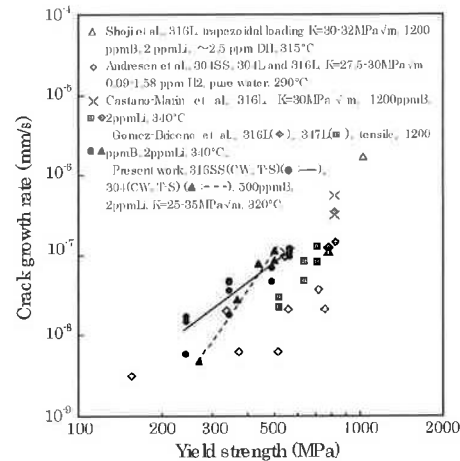


Fig. 11. Effect of yield strength on the crack growth rate of 316 and 316L under various simulated PWR primary water conditions [12,13,29,38]. (Specimen Nos.: S6C5A, S6C10A, S6C10E, G8S6C10-4, S6C15A, S6C15E, S6C20D, S6C2E, G316A8, G304B-2, G304C-1, G304D-1, G304E-1, G304E-9.)

alloys which have been used as nuclear reactor component materials. Speidel and Magdowski [39] measured the CGRs of Alloy 600 by a double cantilever beam (DCB) test and found the CGRs could be expressed using the yield strength to the third power. Fig. 12 compares 316SS, 304SS and Alloy 600 as a function of yield strength. While the test methods were different, the figure indicated that similar yield strength dependency was observed between stainless steels and nickel-based alloy.

The corrosion phenomenon of these alloys does not correspond to the CGRs [40], therefore the effect of yield strength might not correlate to corrosion factors. The proposed role of high yield strength has been described by Andresen et al. [41] and Shoji et al. [12]: the plastic zone size at a crack tip becomes smaller in high yield strength alloys to provide a higher strain gradient.

The theoretical yield strength dependence is not clear, but empirically it can be described as the following equation (Fig. 12).

$$\text{CGR} \propto \sigma_y^a \quad (a = 2 - 3) \quad (1)$$

4.2. Influence of stress intensity factor

The crack growth rate is generally induced by the applied stress which the results from this study exhibit clearly as shown in Figs. 13 and 14. The apparent K_{Ic} dependence on CGR often is empirically described by the following relation:

$$CGR \propto K_I^b \quad (b = 0.6 - 3.2) \quad (2)$$

where b is a constant that describes the K_{Ic} dependence. Fig. 13 shows the K_{Ic} dependence on 316SS indicated that 20%CW alloy provided a lower b value in comparison with 15%CW. However, it should be noted that this varying of trends was not obvious, if the data from $K_{Ic} = 13 \text{ MPa}\sqrt{\text{m}}$ were not there, there would be much slower CGRs with a fair amount of scatter due to difficulty of measurement. The CGRs of 316SS and 304SS obtained at 290 °C were slower and had more scatter as shown in Fig. 14. The statistical K_{Ic} dependence is discussed later, the obtained b for 316SS and 304SS ranged from 0.6 to 3.2.

The effect of K_{Ic} on CGRs has been evaluated for various alloys and water chemistry conditions as shown in Fig. 15. The acceleration effect by CW and temperature was recognized for several alloys, highest CGRs were observed for Alloy 600 with 31.9%CW in the S-T orientation. While CGRs were strongly influenced by the materials and test environment, comparable K dependences were observed in Alloy 600, 316SS and 304SS. This indicated that the influence of stress intensity on SCC was similar between nickel-based alloy and stainless steels under these conditions.

Regarding the threshold for the crack propagation, Scott [42] proposed that the threshold of Alloy 600 was 9 MPa $\sqrt{\text{m}}$ at 350 °C. The lowest K_{Ic} value of the present study was 13 MPa $\sqrt{\text{m}}$ for 316SS (15%CW). The existence of a threshold could not be elucidated because the data tended to be scattered for low OGR tests.

4.3. Influence of temperature on CGR

The temperature dependences of several cold-worked 316SS and 304SS specimens are shown in Figs. 16 and 17 respectively. The tests were performed under a constant load with an apparent stress intensity factor between 25 and 35 MPa $\sqrt{\text{m}}$. Arrhenius type temperature dependences were observed from 250 °C to 320 °C, but they disappeared above 330 °C in 15%CW and 10%CW 316SS specimens.

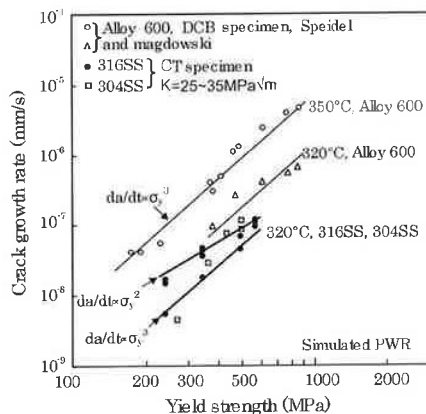


Fig. 12. Effect of yield strength on the crack growth rates of 316SS, 304SS and Alloy 600 [39]. (Specimen Nos.: S6C5A, S6C10A, S6C10E, G36C10-4, S6C15A, S6C15E, S6C20D, S6C2F, G316A8, G304E-2, G304C-1, G304D-1, G304E-1, G304E-9)

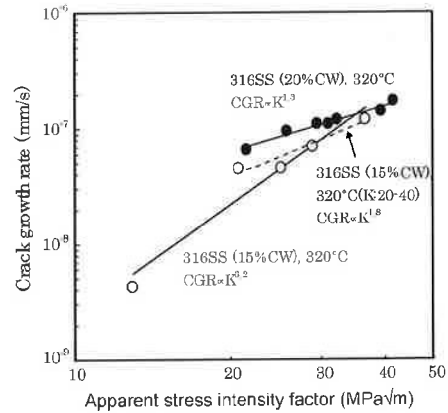


Fig. 13. Effect of stress intensity factor on the crack growth rates of 316SS with 20%CW and 15%CW at 320 °C. (Specimen Nos.: S6C20D, S6C2E, S6C2F, G316A8, S6C20-1, S6C15A, S6C15E, S6C15-4)

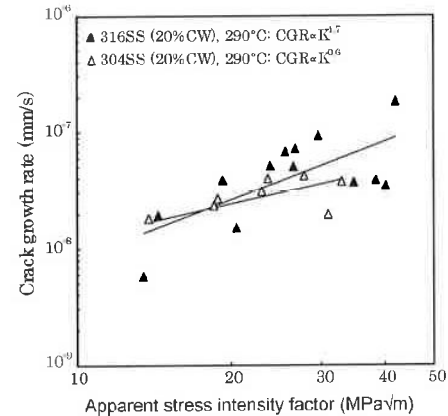


Fig. 14. Effect of stress intensity factor on the crack growth rates of 316SS (20%CW) and 304SS (20%CW) at 290 °C. (Specimen Nos.: S6C20D, S6C2E, G316A8, S6C20-1, S6C20-2, 304E-3, G304E-9)

Because the PDM could not be applied above 330 °C, true CGRs in high temperature were not elucidated, but the results implied that the CGRs were inhibited at higher temperature particular in lower percent CW alloys. One of the explanations for the suppression effect is decreasing the corrosion rates of stainless steels in simulated PWR primary water conditions [43]. The reason for the suppression effect above 330 °C was not clear, but a surface electro-chemical reaction seemed to be the rate limiting process for the corrosion of specimens and SCC.

The estimated apparent activation energies, which were obtained using the least squares method, were 75 kJ/mol, 81 kJ/mol and 145 kJ/mol in 316SS with 20%CW, 15%CW and 10%CW, respectively, as shown in Fig. 16. On the other hand, the respective apparent activation energies of 304SS (20%CW) and 304SS (15%CW) were calculated as 91 kJ/mol and 90 kJ/mol. Estimated apparent activation energies always include CGR measurement errors, but the trend of apparent activation energy decreases with increasing percent of CW has been reported by Rebak et al. [19], Moshier and Brown [20], and Cassagne and Gelpi [44] in Alloy 600. In addition, according to Shoji et al. [12], no consistent effect of temperature on crack growth rate was obtained for higher percent CW 304L

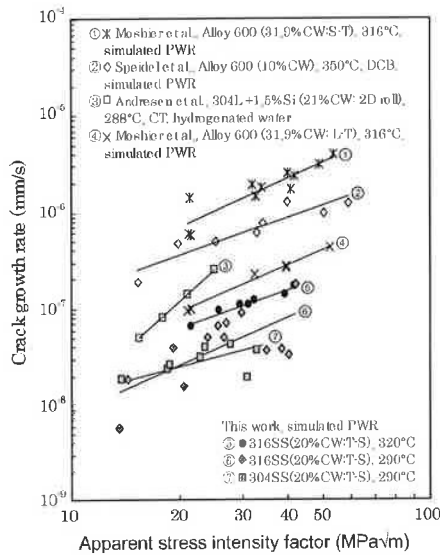


Fig. 15. Effect of stress intensity factor on CGR of various alloys in high temperature water [20,38,39]. (Specimen Nos.: S6C20D, S6C2E, S6C2F, G316AB, S6C20-1, S6C20-2, 304E3, G304E9.)

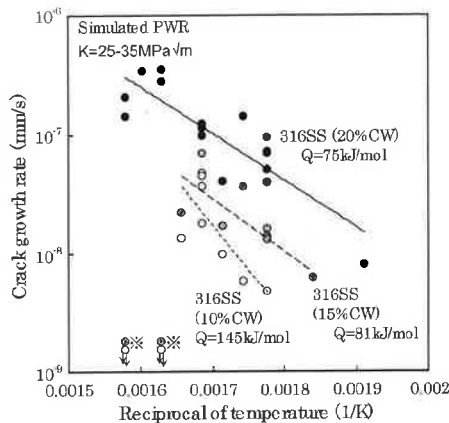


Fig. 16. Temperature dependence on crack growth rate of cold worked 316SS under simulated PWR primary water conditions. (Specimen Nos.: S6C20D, S6C2F, G316AB, S6C20-2, GCS6C20-K, GCS6C20-L, GCS6C20-M, GCS6C20-N, GCS6C20-O, G316-20-TS1, S6C15L, S6C15D, S6C15E, G316-15-TS-1, G316-15-TS-2, G316-15-TS-5, S6C10A, S6C10B, S6C10D, S6C10E, G36C10-4, G316-10-TS-2, G316-10-TS-3.) ※ Data from total crack length less than 0.01 mm.

and 316L, which had yield strength of 750–1000 MPa. On the contrary, Speidel and Magdowski [39] reported no significant influence of CW on the temperature dependence in experiments using double cantilever beam specimens. All these data implied that mechanical properties have some potential to change the activation energy but it is difficult to determine the accurate activation energy.

Fig. 18 shows the temperature dependence on CGRs of cold worked stainless steels and Alloy 600 as reported from several sources [17,29,30,38,45,46]. Reported apparent activation energies in CW stainless steels were around 60 kJ/mol, while slightly higher values ranging from 75 to 145 kJ/mol were obtained in this study.

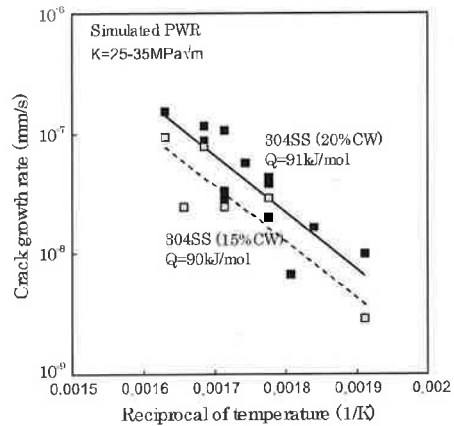


Fig. 17. Temperature dependence on crack growth rate of cold worked 304SS under simulated PWR primary water conditions (Specimen Nos.: G304D-1, G304-15-2, G304-15-TS-3, G304-15-1, 304E3, G304E-1, G304E-9, G304-20-4, G304-20-2.)

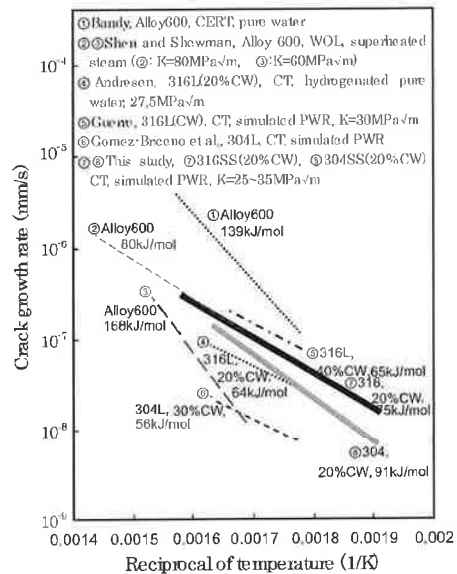


Fig. 18. Temperature dependence on crack growth rate of cold worked stainless steels and Alloy 600 under simulated PWR primary water and deaerated water conditions [17,29,30,38,45,46].

On the other hand, slightly higher apparent activation energies were reported for Alloy 600 ranging from 80 to 168 kJ/mol.

Arioka et al. [25] reported a similar temperature dependence for CGR in IG creep CGRs of 316SS. The CGRs of SCC were over 10 times higher, and a comparable thermal activation process might influence the crack growth.

4.4. Empirical formula for CGR calculation

This paper presents the influences of CW, stress intensity factor and temperature on the CGR of 316SS and 304SS. Each of the factors was precisely assumed as described above, but variability of data complicates the accurate prediction of CGRs. For instance

the coefficient for yield strength (a) varies from 2 to 3 (Eq. (1)), the coefficient for apparent $K(b)$ ranges from 0.6 to 3.2 (Eq. (2)) and activation energy varies from 75 to 145 kJ/mol. If the mechanism is fully understood and accuracy of CGR measurement is enough, it might be possible to use each obtained parameter. However, CGRs of CW stainless steels under PWR conditions tend to be scattered and the role of each parameter has not been clarified, then statistical data treatment presents a feasible way to evaluate the CGRs.

In the study, the empirical formula was established from the obtained correlations as described in Eq. (3). Factors for yield strength, apparent stress intensity factor and temperatures were calculated by multivariable analysis using all CGRs obtained in the study except for those evaluated for a crack length less than 0.01 mm:

$$\frac{da}{dt} = 9.5 \times 10^{-10} \times r_y^{2.9} \times K_a^{1.0} \times \exp\left(\frac{-84 \times 10^3}{RT}\right) \quad (3)$$

where da/dt is crack growth rate (mm/s), r_y is yield strength at test temperature, K_a is apparent stress intensity factor, R is gas constant (8.314 kJ/mol K) and T is absolute test temperature. SOC test results indicated the existence of a peak temperature, and the applicability range of the formula was between 250 °C and 320 °C. It should be noted that the base CGRs were for T-S orientation and cracking was branched, so technically, an absolute value for precise CGRs in operating power plants is not predictable.

Fig. 19 compares the calculated CGRs, which were derived from the empirical formula, and the measured CGRs; the data seemed to scatter in some extent. There are many reasons for variability of each measurement, for example crack arrest by an uncracked segment or specific material structures, and actual CGRs have some irregularities. In addition, PDM measurements of such low CGRs have some errors from electric noise, insulation of wires, etc. The empirical formula of Fig. 19 includes these irregularities and measurement errors from 98 CGRs. Theoretically, each factor might influence it mutually, then establishing the precise equation requires further fundamental studies.

Even though the precise CGR is not predictable, similar parameter dependences were observed between 316SS and 304SS. Both steel types were used with the same empirical formula and no obvious differences were observed. The results indicated that CGRs of 316SS and 304SS could be estimated using the same empirical formula.

Regarding the maintenance of operating power plants, the accuracy and margin of the safety ratio is important. Fig. 20 shows the

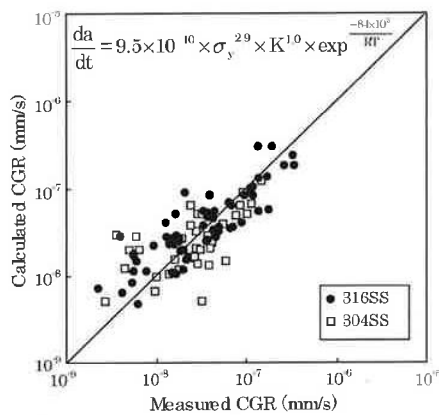


Fig. 19. Comparison of CGRs measured and calculated by the empirical formula.

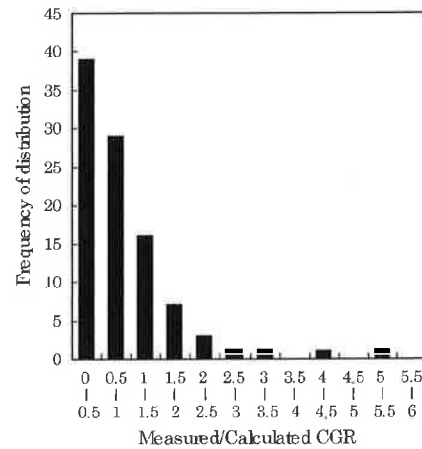


Fig. 20. Frequency of distribution as a function of measured/calculated CGR ratio.

frequency of distribution of measured/calculated CGR ratio: 92.8% of the measured CGRs did not exceed twice the calculated CGRs.

5. Conclusions

The crack growth rates of 316SS and 304SS under simulated PWR primary water conditions have been summarized to develop an empirical formula providing better engineering applications. Fifty-three cold worked compact tension specimens were employed to clarify the influences of yield strength, temperature dependence and stress intensity factors:

- (i) The influences of each parameter for 316SS and 304SS were similar, so the same empirical formula for crack growth rates could be applied. The estimated apparent activation energy was 84 kJ/mol and it was calculated from all the obtained crack growth rates. On the other hand, crack retardation was clearly observed above 330 °C in lower cold worked stainless steel specimens, therefore the applicability range of calculated activation energy was regarded as between 250 °C and 320 °C.
- (ii) The crack growth rates increased with increasing yield strength for 5% and 20% cold worked 316SS and 304SS specimens. These rates were proportional to the 2.9 power of yield strength at test temperature.
- (iii) The crack growth rates increased with increasing apparent stress intensity in the region between 13 MPa \sqrt{m} and 40 MPa \sqrt{m} , and these rates were proportional to the apparent yield strength.
- (iv) Cracking of T-S orientation specimens propagated through the grain boundary, and then branched off in two directions.

References

- [1] W. Bamford, J. Hall, A review of alloy 600 cracking on operating nuclear plants including alloy 82 and 182 weld behavior, in: Proc. of ICONE12, ASME, 2004.
- [2] D.W. Alley, A regulatory analysis and perspective regarding degradation of materials in light water reactors, in: Proc. of Corrosion 2011, Paper no. 11198, NACE, 2011.
- [3] G.S. Was, P.L. Andresen, Corrosion 63 (1) (2007) 19.
- [4] J.M. Boursier, S. Gallet, Y. Rouillon, et al., Stress corrosion cracking of austenitic stainless steels in PWR primary water: an update of metallurgical investigations performed on France withdrawn components, in: Proc. Int. Symp. Fontevraud 5, September 23–27, 2002.

- [5] T. Couvant, F. Moulart, L. Legras, et al., FWSOC of austenitic stainless steels of heaters of pressurizers, in: Proc. Int. Symp Fontevraud, 6, 2006.
- [6] Nuclear Industry Safety Agency (NISA), Cracks on the Inner Surface of the Welds at Primary Water Inlet and Outlet Nozzle to Steam Generators, NISA, February 5, 2008.
- [7] N. Totsuka, Z. Szklarska-Smialowska, Corrosion 44 (1988) 124.
- [8] P.L. Andresen, T.M. Angelii, W.R. Catlin, et al., Effect of deformation on SCC of unsensitized stainless steel, in: Proc. of Corrosion 2000, Paper no. 203, NACE, 2000.
- [9] P.L. Andresen, L.M. Young, W.R. Catlin, et al., Stress corrosion crack growth rate behavior of various grades of cold-worked stainless steel in high temperature water, in: Proc. of Corrosion 2002, Paper no. 2511, NACE, 2002.
- [10] K. Arioka, Effect of temperature, hydrogen and boric acid concentration on IGSCC susceptibility of annealed 316 stainless steel, in: Proc. Int. Symp. Fontevraud 5, September 23–27, 2002.
- [11] K. Arioka, T. Yamada, T. Takumi, Influence of boric acid, hydrogen concentration and grain boundary carbide on IGSCC behaviors of SUS 316 under PWR primary water, in: Proc. 11th Int. Conf. Environmental Degradation of Materials in Nuclear Power Systems-Water Reactors, Stevenson, August 10–14, 2003.
- [12] T. Shoji, G. Li, J. Kwon, S. Matsushima, et al., Quantification of yield strength effects on IGSCC of austenitic stainless steels in high temperature water, in: Proc. 11th Int. Conf. Environmental Degradation of Materials in Nuclear Power Systems-Water Reactors, Stevenson, August 10–14, 2003.
- [13] M.L. Castano Marin, M.S. Garcia Redondo, G.D. Velasco, et al., Crack growth rate of hardened austenitic stainless steels in BWR and PWR environments, in: Proc. 11th Int. Conf. Environmental Degradation of Materials in Nuclear Power Systems-Water Reactors, Stevenson, August 10–14, 2003.
- [14] F. Vaillant, T. Couvant, J.M. Boursier, et al., Stress corrosion cracking of cold-worked austenitic stainless steels in laboratory primary PWR environment, in: Proc. FVF2004, San Diego, CA, July 25–29, 2004.
- [15] T. Terachi, K. Fujii, K. Arioka, J. Nucl. Sci. Technol. 42 (2) (2005) 225.
- [16] T. Couvant, L. Legras, F. Vaillant, Effect of strain hardening on stress corrosion cracking of AISI 304L stainless steel in PWR primary environment at 360°C, in: Proc. 12th Int. Conf. Environmental Degradation of Materials in Nuclear Power Systems-Water Reactors, Salt Lake City, UT, August 14–18, 2005.
- [17] C. Guerre, O. Raquet, E. Herms, et al., SCC growth behavior of austenitic stainless steels in PWR primary water conditions, in: Proc. 12th Int. Conf. Environmental Degradation of Materials in Nuclear Power Systems-Water Reactors, Salt Lake City, UT, August 14–18, 2005.
- [18] K. Arioka, T. Yamada, T. Terachi, R.W. Staehle, Corrosion 62 (1) (2006) 74.
- [19] R.B. Rebak, Z. Xia, Z.S. Smialowska, Corrosion 51 (9) (1995) 689.
- [20] W.C. Moshier, C.M. Brown, Corrosion 56 (9) (2000) 307–320.
- [21] Y.C. Gao, K.C. Hwang, Elastic-plastic fields in steady crack growth in a strain-hardening material, in: Proc. 5th Int. Conf. on Fracture, Cannes, France, vol. 2, (1981) p. 669.
- [22] L.M. Young, P.L. Andresen, T.M. Angelii, Crack tip strain rate estimates based on continuum theory and experimental measurement, in: Proc. of Corrosion 2001, Paper no. 1131, NACE, 2001.
- [23] T. Shoji, T. Yamamoto, K. Watanabe, et al., “3 DFEEM simulation of EAC crack growth based on the deformation/oxidation mechanism, in: Proc. 11th Int. Conf. Environmental Degradation of Materials in Nuclear Power Systems-Water Reactors, Stevenson, August 10–14, 2003.
- [24] P.L. Andresen, M.M. Morra, W.R. Catlin, Effect of yield strength, corrosion potential, composition and stress intensity factor in SCC of stainless steels, in: Proc. of Corrosion 2004, Paper no. 4678, NACE, 2004.
- [25] K. Arioka, T. Yamada, T. Terachi, et al., Corrosion 63 (12) (2007) 1114.
- [26] S. Lozano-Perez, T. Yamada, T. Terachi, et al., Acta Mater. 57 (18) (2009) 5361.
- [27] K. Arioka, T. Yamada, T. Terachi, et al., Corrosion 62 (7) (2006) 568.
- [28] D.J. Gooch, Mater. Sci. Eng. 91 (1987) 45.
- [29] D. Gomez-Prisco, M. Sol Garcia, J. Lopez, SCC behavior of austenitic stainless steels in high temperature water effect of cold work, water chemistry and type of materials, in: Proc. 14th Int. Conf. Environmental Degradation of Materials in Nuclear Power Systems-Water Reactors, Virginia Beach, VA, August 23–27, 2009.
- [30] C. Guerre, O. Raquet, E. Herms, et al., SCC crack growth rate of cold-worked austenitic stainless steels in pwr primary water conditions, in: Proc. 13th Int. Conf. Environmental Degradation of Materials in Nuclear Power Systems-Water Reactors, Whistler, Canada, August 19–23, 2007.
- [31] Z. Lu, Y. Takeda, T. Shoji, J. Nucl. Mater. 383 (2008) 92.
- [32] Japan Stainless Steel Association, Stainless Steels Handbook, Nikkan Kogyo Shimbun, Ltd., Japan, 384, 1995 (in Japanese).
- [33] ASTM E 647-11, Standard Test Method for Measurement of Fatigue Crack Growth Rates, American Society for Testing and Materials, 2009.
- [34] E. Richey, D.S. Morton, Influence of specimen size on the SCC growth rate of Ni alloys exposed to high temperature water, in: Proc. of Corrosion 2006, Paper no. 6513, NACE, 2006.
- [35] ASTM E399-09, Standard Test Method for Plane-strain Fracture Toughness of Metallic Materials, American Society for Testing and Materials, 2011.
- [36] M. Ozawa, Y. Yamamoto, K. Nakata, et al., Establishment of experimental conditions for the SCC growth rate test of alloy 600 and Ni base weld metal in high temperature oxygenated water, in: Proc. 12th Int. Conf. Environmental Degradation of Materials in Nuclear Power Systems-Water Reactors, Salt Lake City, UT, August 14–18, 2005.
- [37] M. Tsubota, Y. Kanazawa, H. Inoue, The effect of cold work on the SCC susceptibility of austenitic stainless steels, in: Proc. 7th Int. Conf. Environmental Degradation of Materials in Nuclear Power Systems-Water Reactors, 1995, p. 519.
- [38] P.L. Andresen, M.M. Morra, J. Nucl. Mater. 383 (2008) 97.
- [39] M.O. Speidel, R. Magdowski, Stress corrosion cracking of stabilized austenitic stainless steels in various types of nuclear power plants, in: Proc. 9th Int. Conf. Environmental Degradation of Materials in Nuclear Power Systems-Water Reactors, Newport Beach, CA, August 1–5, 1999.
- [40] T. Terachi, T. Yamada, K. Arioka, S. Lozano-Perez, Role of corrosion in IFSCC of Fe- and Ni-based alloys, in: Proc. of the Int. Symp. on Research for Light Water Reactors, 2007, p. 215.
- [41] P.L. Andresen, L.M. Young, P.W. Emigh, R.M. Horn, Stress corrosion crack growth rate behavior of Ni alloys 182 and 600 in high temperature water, in: Proc. of Corrosion 2002, Paper no. 2510, NACE, 2002.
- [42] P. Scott, An analysis of primary water stress corrosion cracking in PWR steam generators, in: Proc. of the Specialists Meeting on Operating Experience with Steam Generators, Brussels, Belgium, 1991.
- [43] T. Terachi, T. Miyamoto, T. Yamada, K. Arioka, Mechanistic study of LFSCC of stainless steels, Temperature dependence of corrosion in hydrogenated water, in: Proc. of Nuclear Plant Chemistry Conf., Quebec City, Canada, October 3–7, 2010.
- [44] T. Cassagne, A. Gelpi, Crack growth rate measurements on alloy 600 steam generator turning in primary and hydrogenated AVT water, in: Proc. 6th Int. Conf. Environmental Degradation of Materials in Nuclear Power Systems-Water Reactors, San Diego, CA, August 1–5, 1993.
- [45] Y. Shen, P.G. Shewmon, Corrosion 47 (9) (1991) 712.
- [46] R. Bandy, D.C. Kooyen, Corrosion 40 (1984) 425.

4. 水平展開（類似個所の点検）

2章の「指示の原因検討」より、今回の加圧器スプレイライン配管溶接部の指示は、オーステナイト系ステンレス鋼の配管溶接部の内、表面機械加工時に形成された表面微細化層（硬化層）に起因する強加工SCCと考えられる。

強加工SCCについては、2章に記載のとおり材料、環境（温度）、応力に依存することから、強加工SCCの発生または進展の基準に基づき、追加点検対象を選定する。

なお、追加点検対象の選定においては、プラント運転に影響のある系統の配管・機器耐圧部の内、体積検査を要求される溶接部を対象とし、配管、機器の選定フローに基づき抽出を行う。

(1) 対象の選定フロー

プラント運転に影響のある系統の配管・機器耐圧部の内、体積検査を要求される溶接部を対象とし、図 4.1 に示す選定フローを用いて類似箇所の抽出及び追加点検対象の選定を行った。

プラント運転に影響のあるシステムの配管・機器耐圧部の内、体積検査を要求される溶接部

- ・プラント停止につながる系統：RCS, CVCS, MSS, FWS, CCWS
- ・安全上重要な系統：SIS, RHRS, CSS

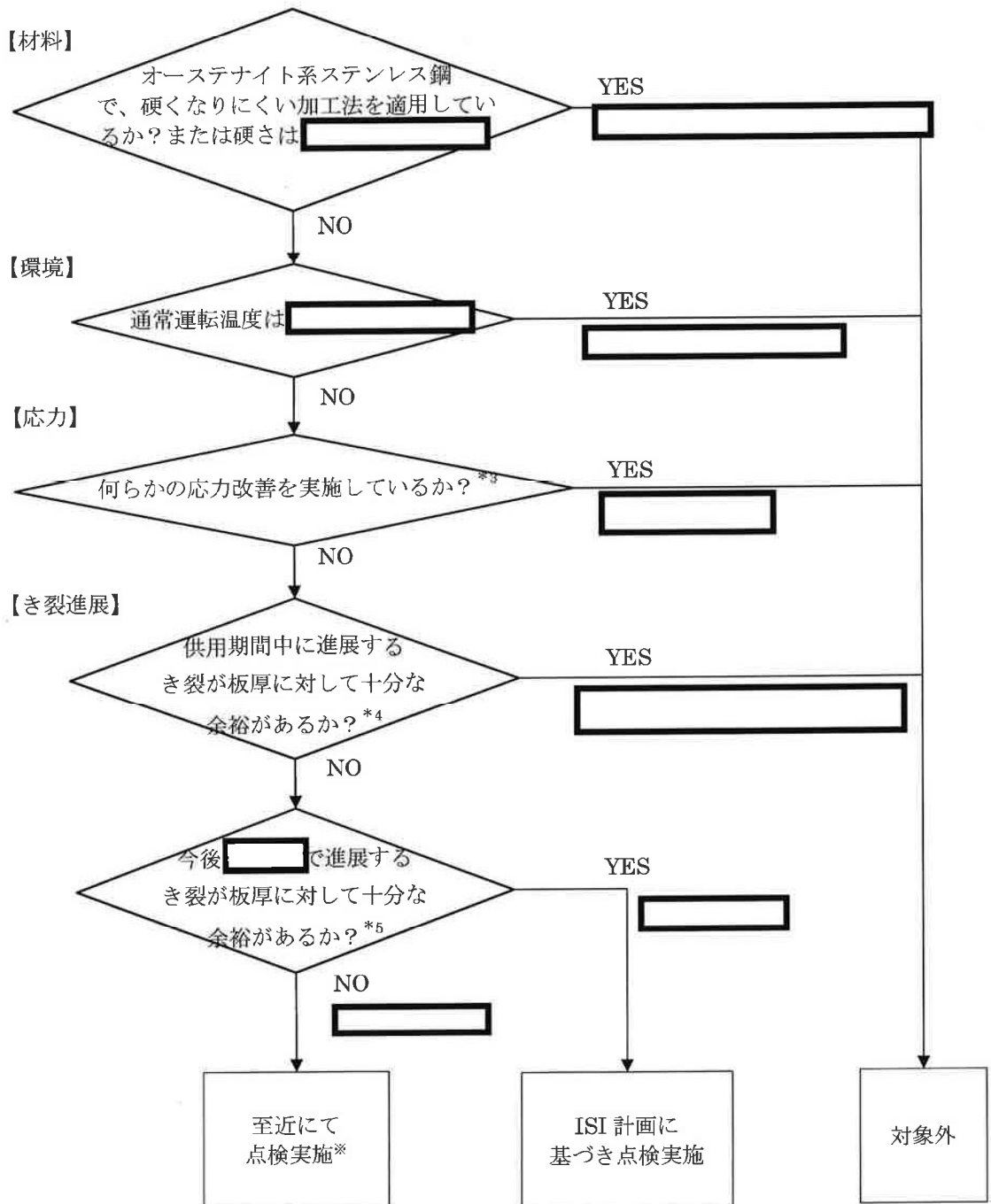
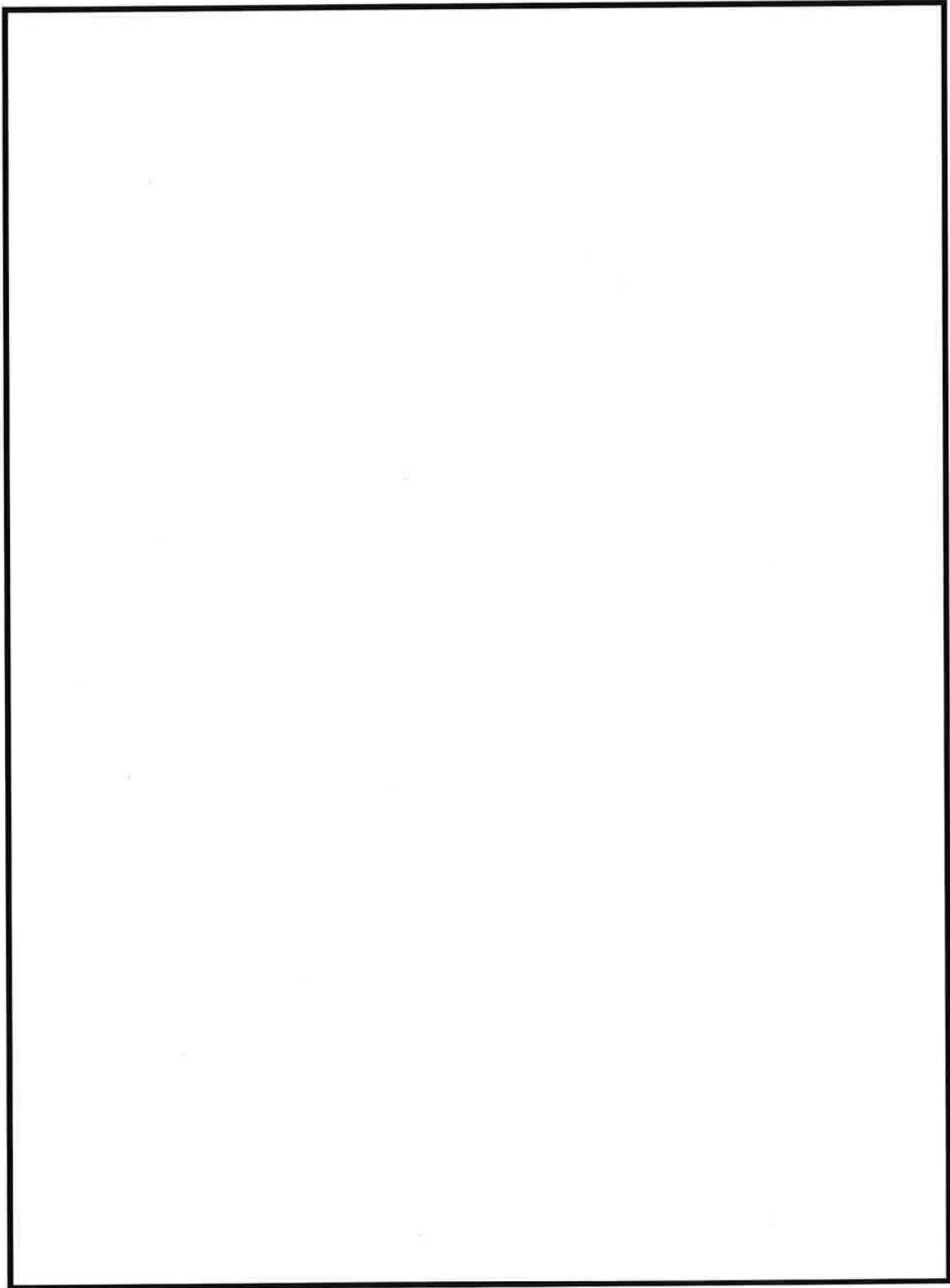


図 4.1 追加点検対象選定フロー

※被ばく量等を勘案し、計画的に点検を実施する。



(2) 対象箇所

(1) に示した選定フローに基づき抽出した対象箇所を下表に示す。

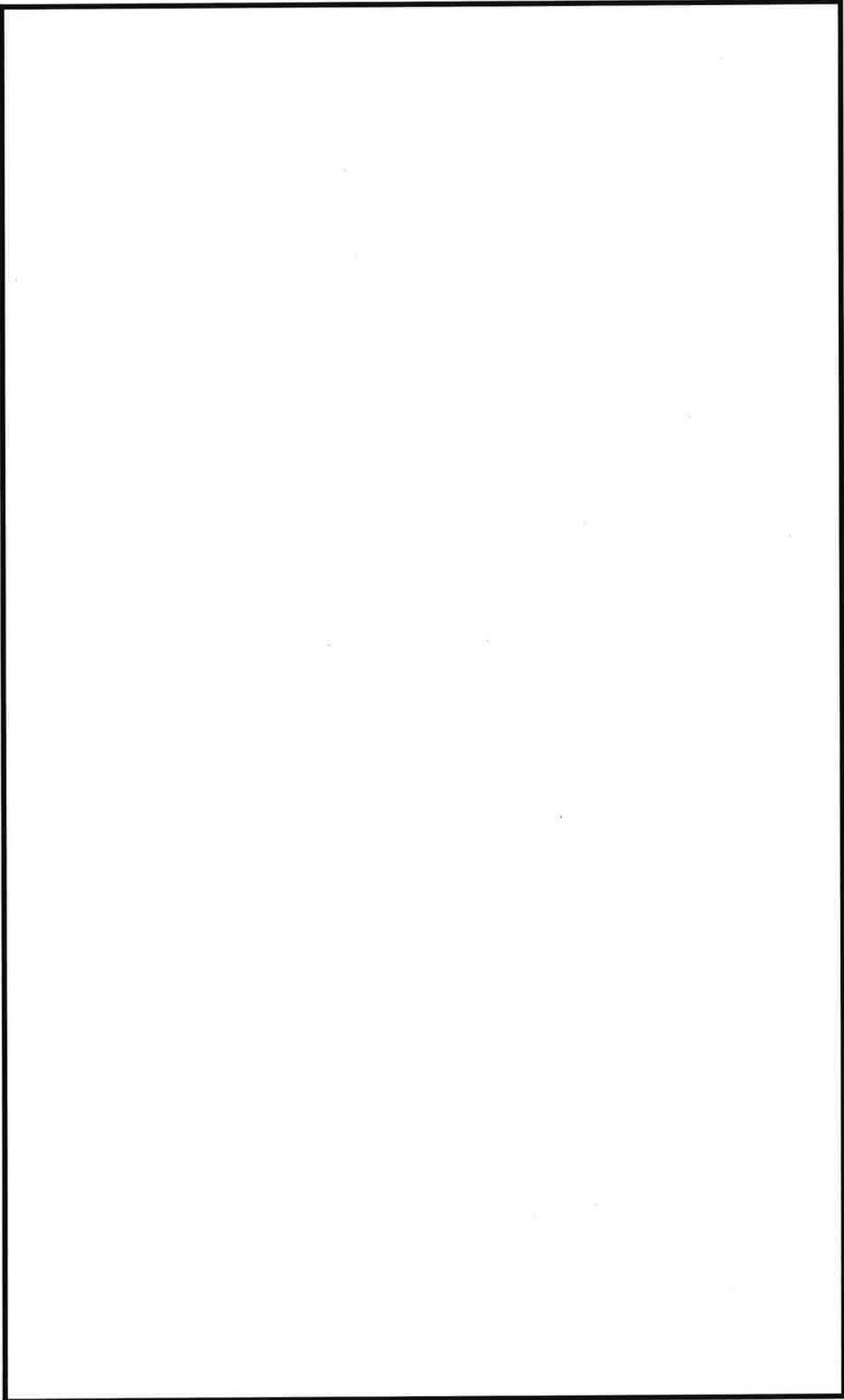
表 4.1 追加点検対象抽出結果

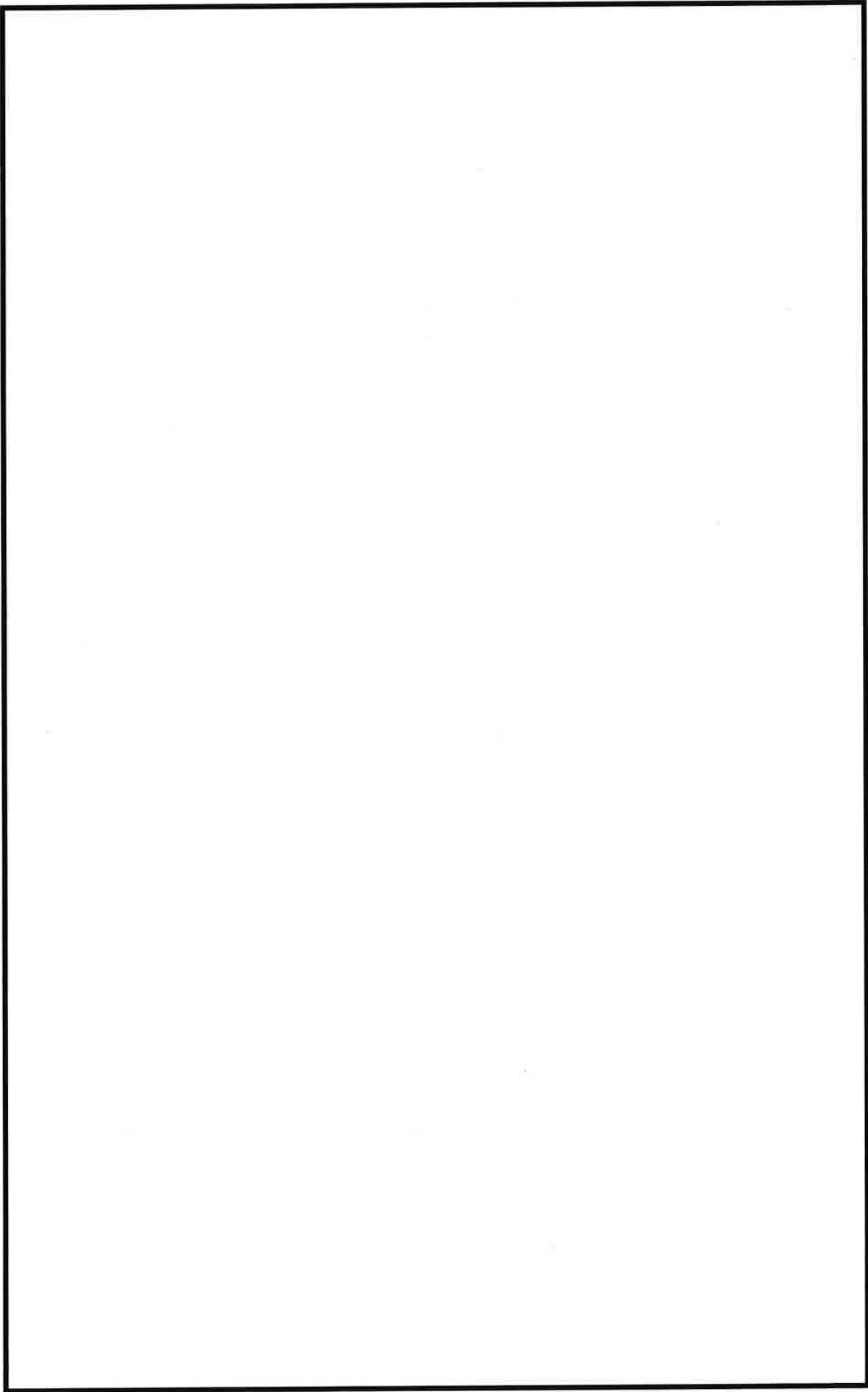
| | 箇所数 |
|--|-----|
| | 16 |
| | 3 |
| | 0 |
| | 0 |

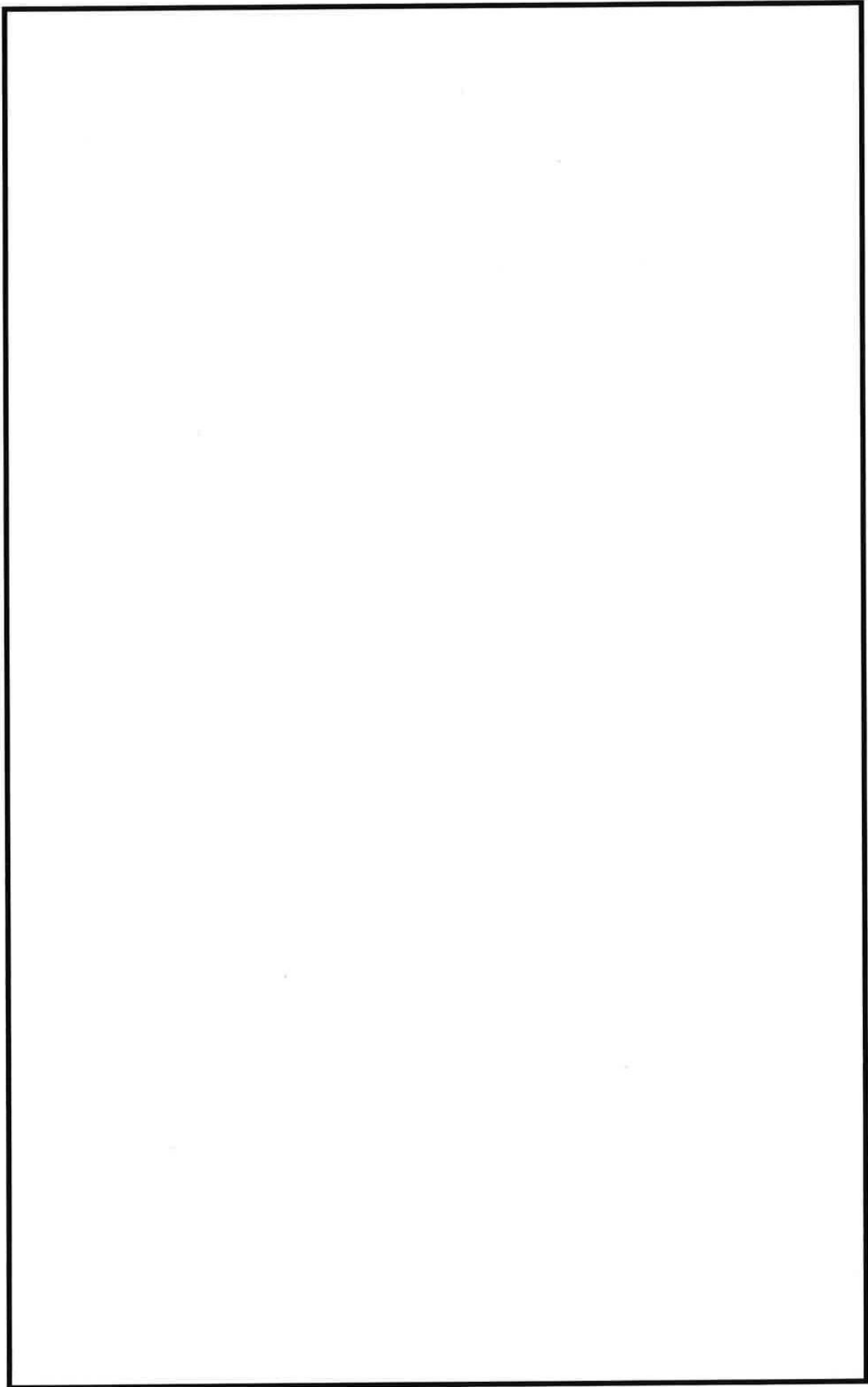
(3) 追加点検結果

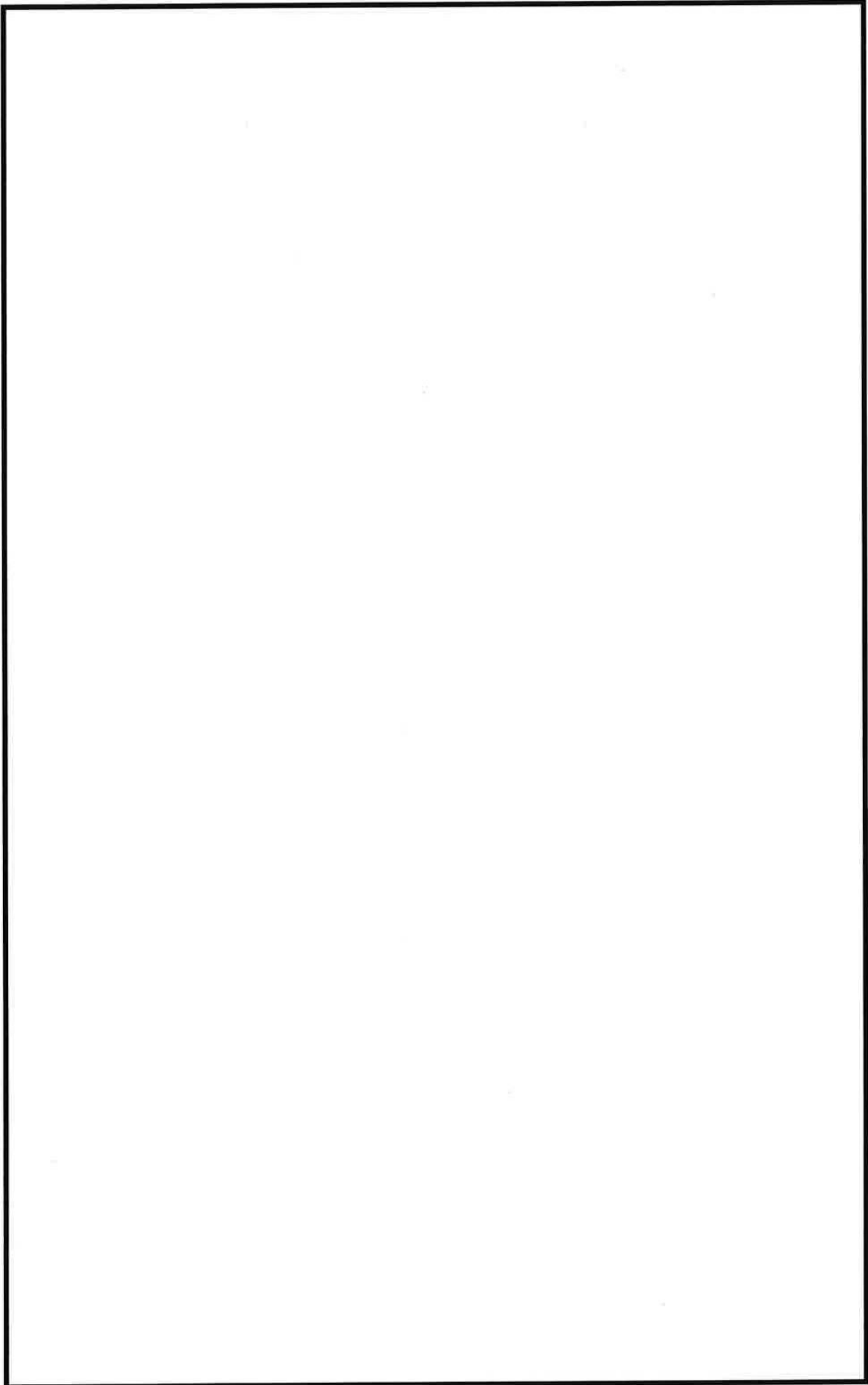
(2) に示した追加点検対象箇所について、追加点検を実施し、有意な指示が無いことを確認した。(添付-6 参照)

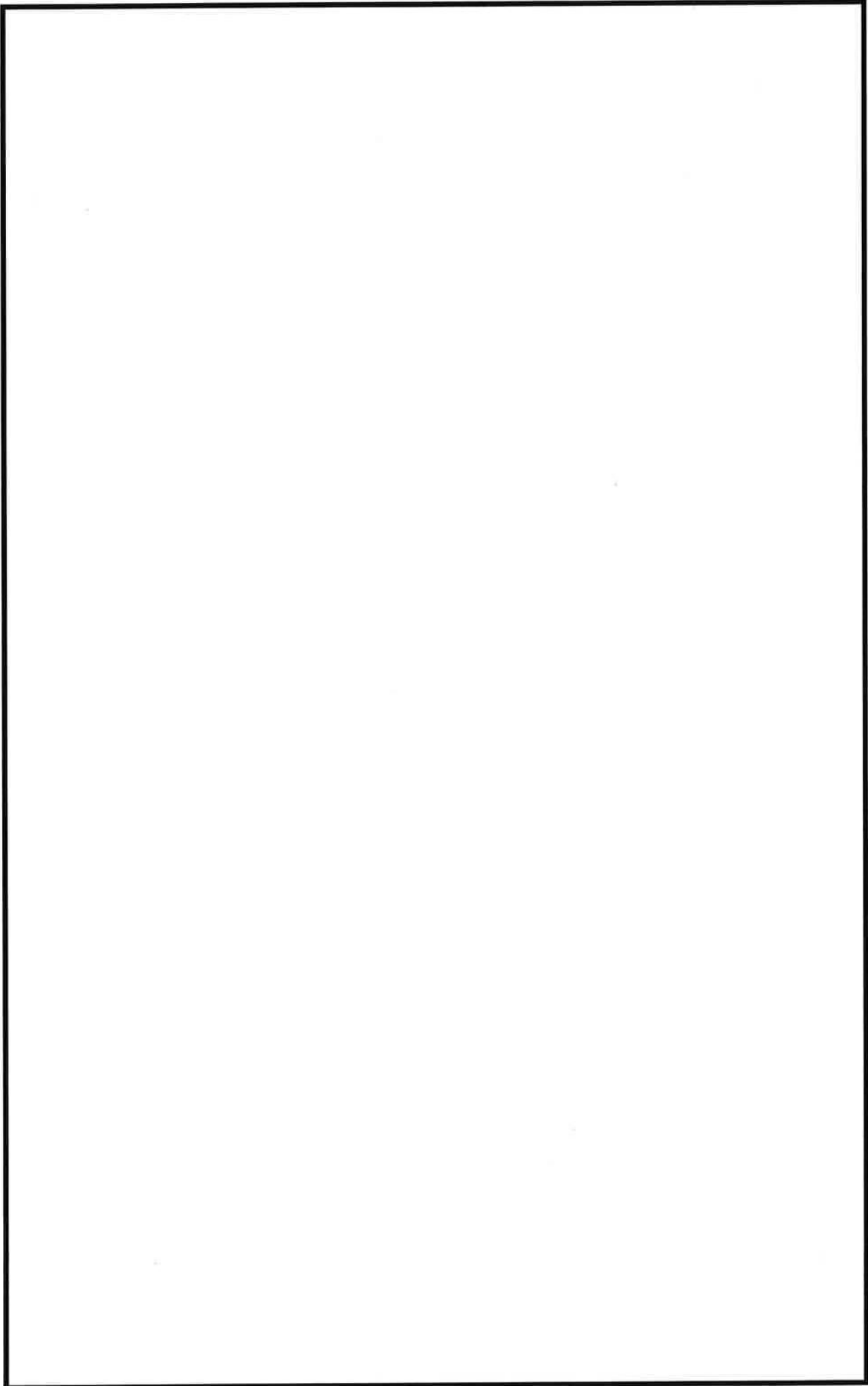
以上



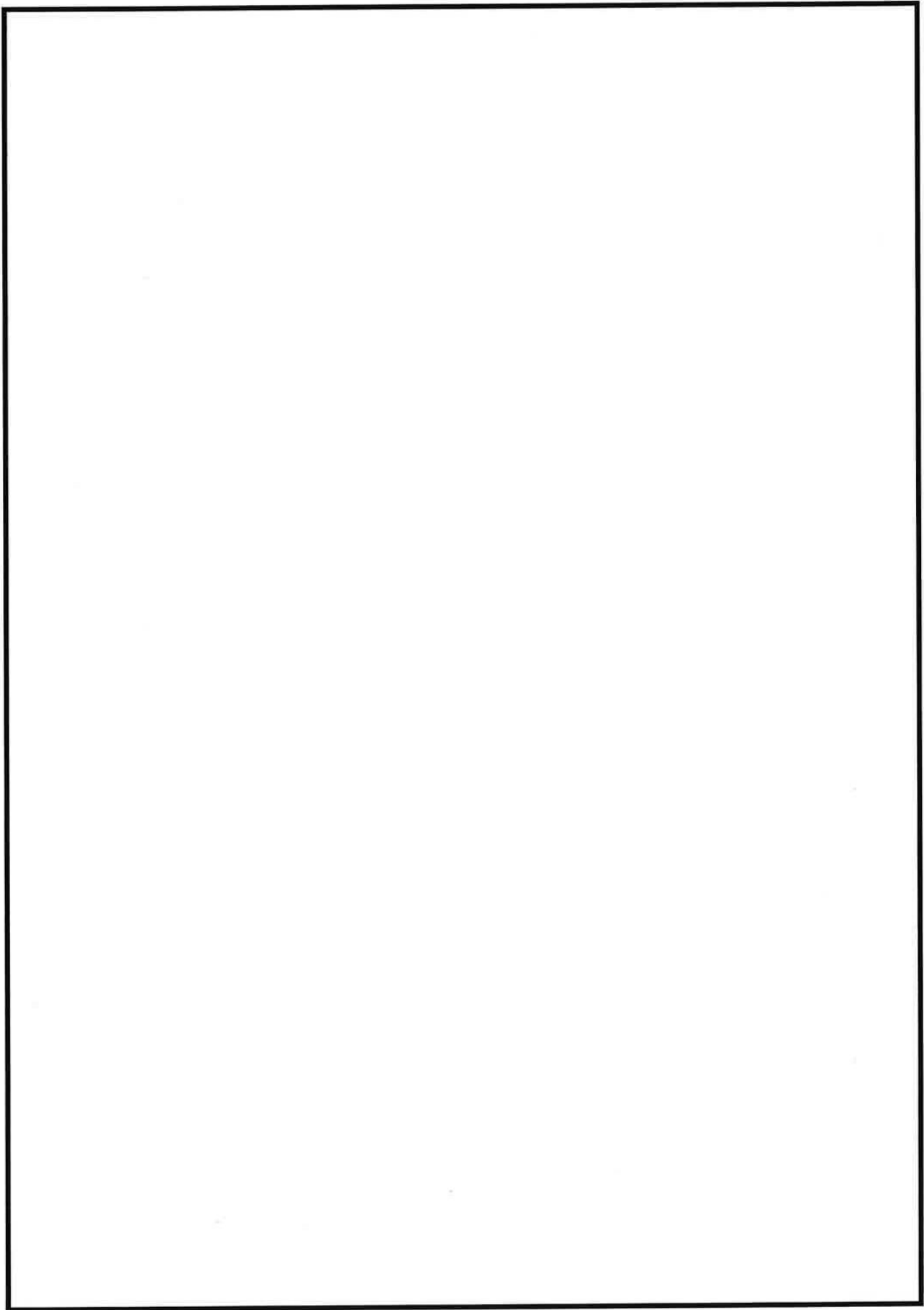


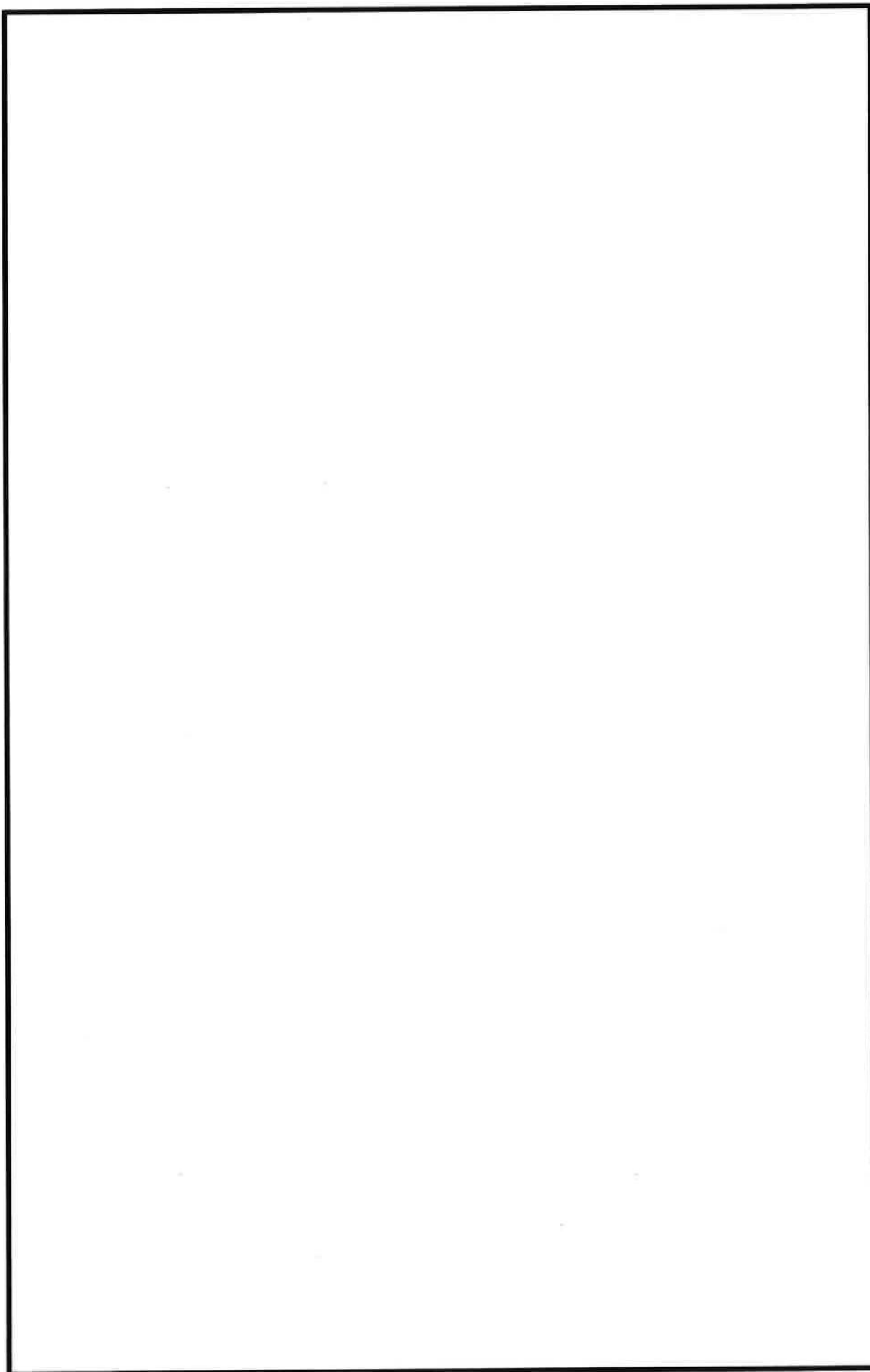


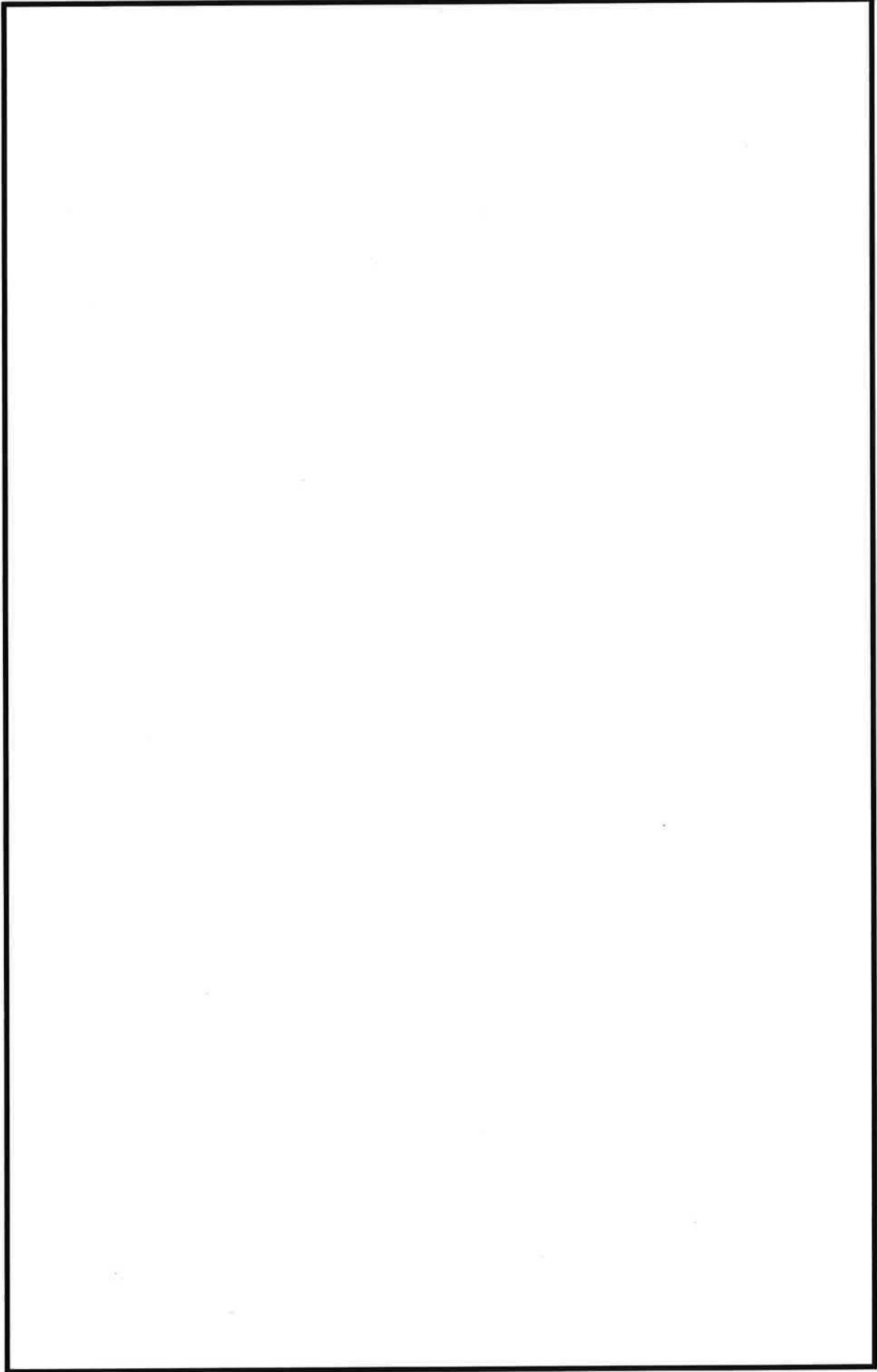


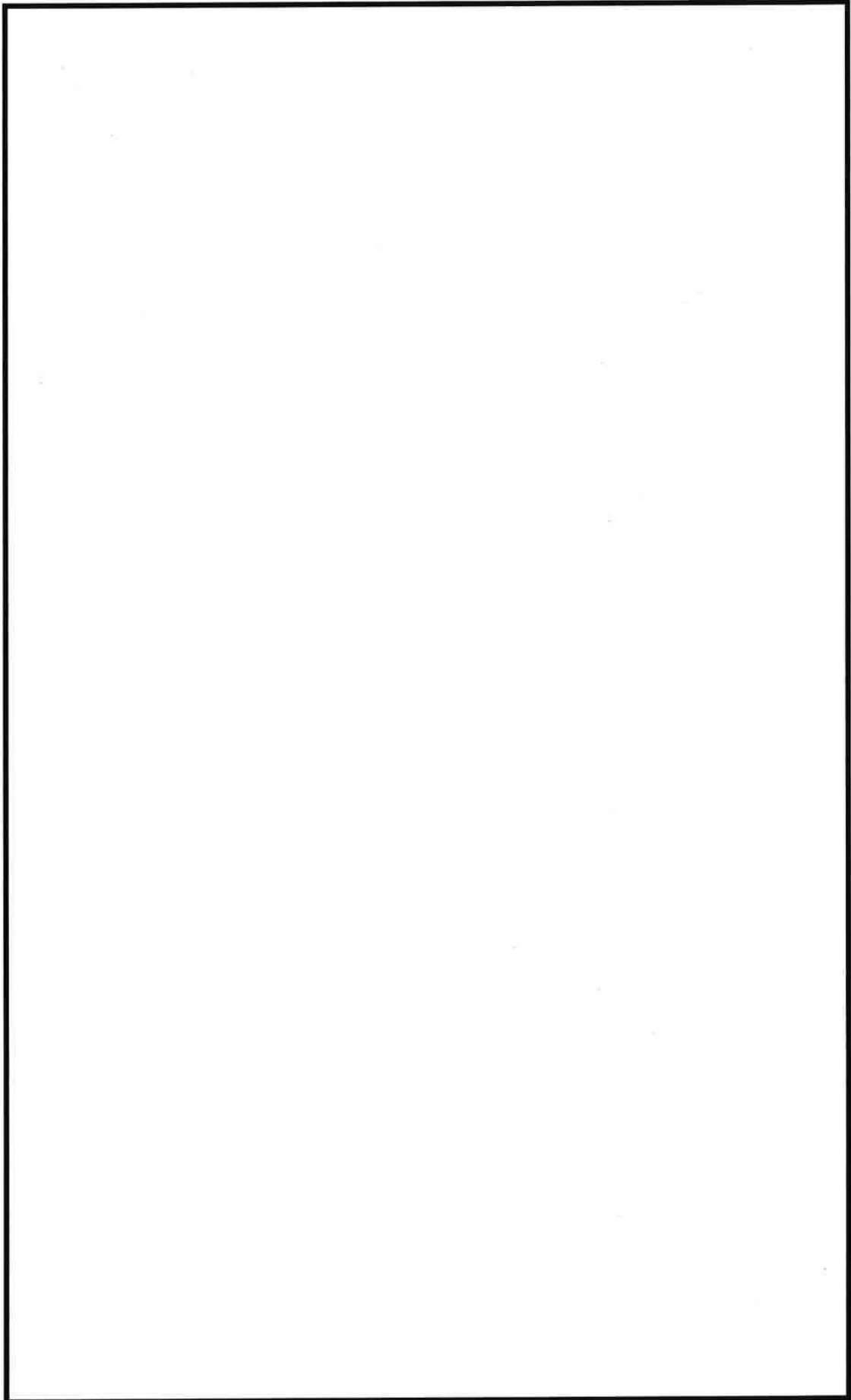


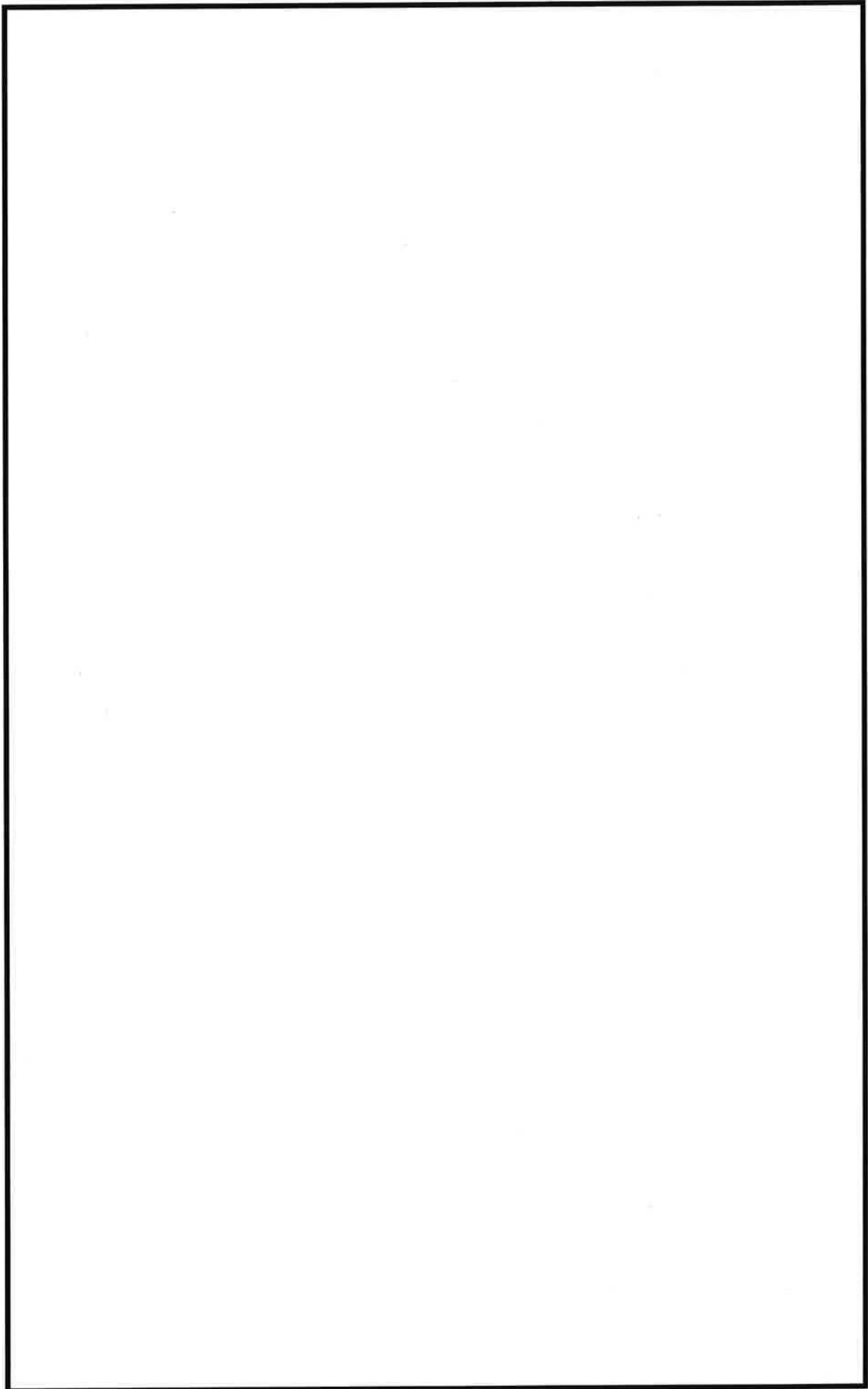


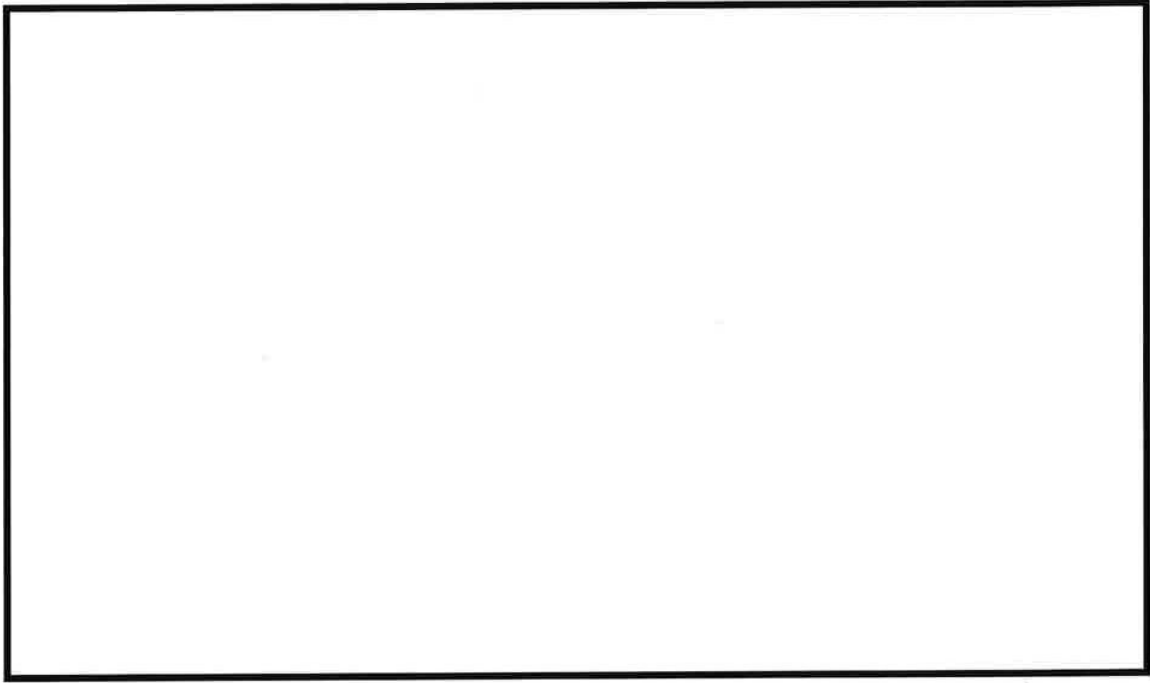












追加点検結果

本文図 4.1「追加点検対象選定フロー」に基づき至近にて点検実施対象に選定された溶接線 19 箇所について、供用期間中検査の 1 段階検査と同じ超音波探傷検査を実施した結果を示す。

(1)追加点検の対象

| 検査対象箇所 | 溶接番号 | |
|-------------------------|-------|--|
| 加圧器スプレイライン (A ループ) ① | FW-4 | |
| | SW-5 | |
| 加圧器スプレイライン (A ループ) ② | SW-20 | |
| | FW-21 | |
| | FW-22 | |
| | SW-23 | |
| | FW-24 | |
| 加圧器スプレイライン (D ループ) ① | SW-5 | |
| 加圧器スプレイライン (D ループ) ② | SW-2 | |
| | FW-3 | |
| | FW-4 | |
| | SW-5 | |
| | FW-6 | |

| 検査対象箇所 | 溶接線番号 |
|------------|-------|
| 加圧器スプレイライン | SW-10 |
| | FW-11 |
| | FW-28 |
| 加圧器逃がし弁ライン | FW-3 |
| | SW-4 |
| | SW-19 |

(2)追加点検の結果

追加点検では、いずれの溶接線でも有意な指示は認められなかった。点検結果記録を 3 例添付する。

| 検査対象箇所 | 溶接番号 | 有意な指示 | 結果添付 |
|----------------------|-------|-------|------|
| 加圧器スプレイライン (A ループ) ① | FW-4 | 無 | ○ |
| | SW-5 | 無 | ○ |
| 加圧器スプレイライン (A ループ) ② | SW-20 | 無 | |
| | FW-21 | 無 | |
| | FW-22 | 無 | |
| | SW-23 | 無 | |
| | FW-24 | 無 | |
| 加圧器スプレイライン (D ループ) ① | SW-5 | 無 | ○ |
| 加圧器スプレイライン (D ループ) ② | SW-2 | 無 | |
| | FW-3 | 無 | |
| | FW-4 | 無 | |
| | SW-5 | 無 | |
| | FW-6 | 無 | |
| 加圧器スプレイライン | SW-10 | 無 | |
| | FW-11 | 無 | |
| | FW-28 | 無 | |
| 加圧器逃がし弁ライン | FW-3 | 無 | |
| | SW-4 | 無 | |
| | SW-19 | 無 | |

以上

非破壊検査記録 (/)

(1) 検査の判定

| 項目番号 | カテゴリ | 機器名 | 検査の対象箇所 | 検査箇所 |
|-------|------|-----|---|----------------------|
| B9.11 | B-J | 配管 | 配管の同種金属溶接継手 (呼び径100A以上：周継手) 加圧器スプレイライン (Aループ) | FW-4 (H2-3911007) |

| 検査方法 | | 検査年月日 | 立会実績 | 結果 | 検査員 | 備考 |
|------|---------|--------------|------|----|-----|----|
| 体積検査 | 超音波探傷検査 | 年 月 日 | 有・無 | | | |
| 判定基準 | | 添付-1(4/4)に記載 | | | | |

非破壊検査記録 (/)

(2) 検査記録

検査年月日 _____ 年 月 日

助勢員 A _____

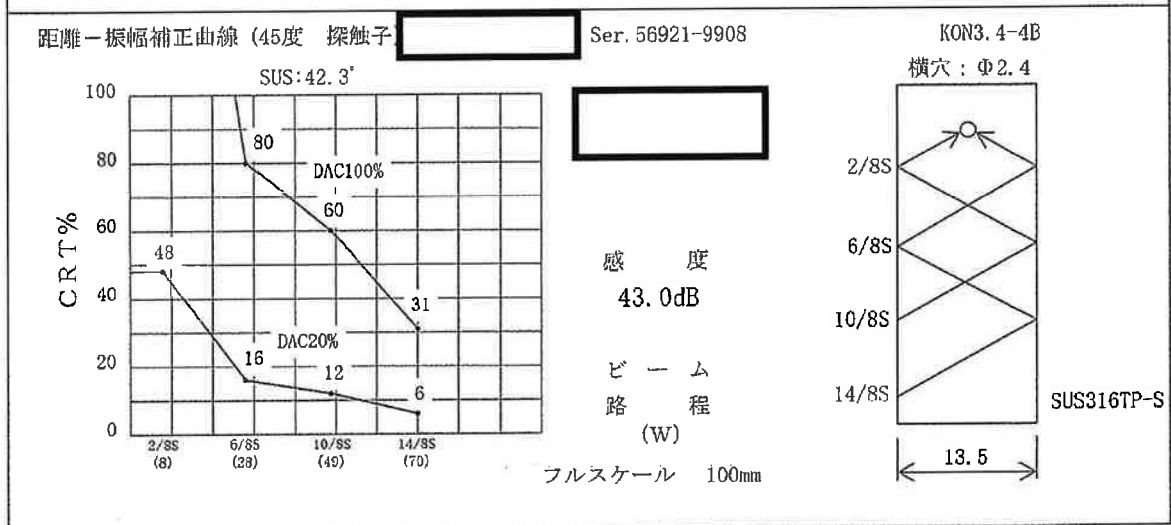
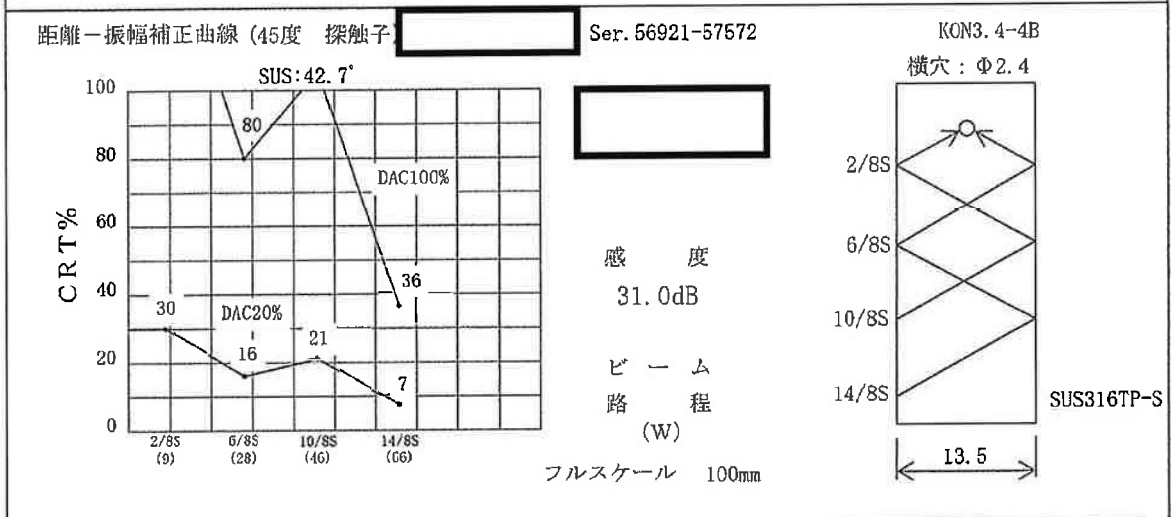
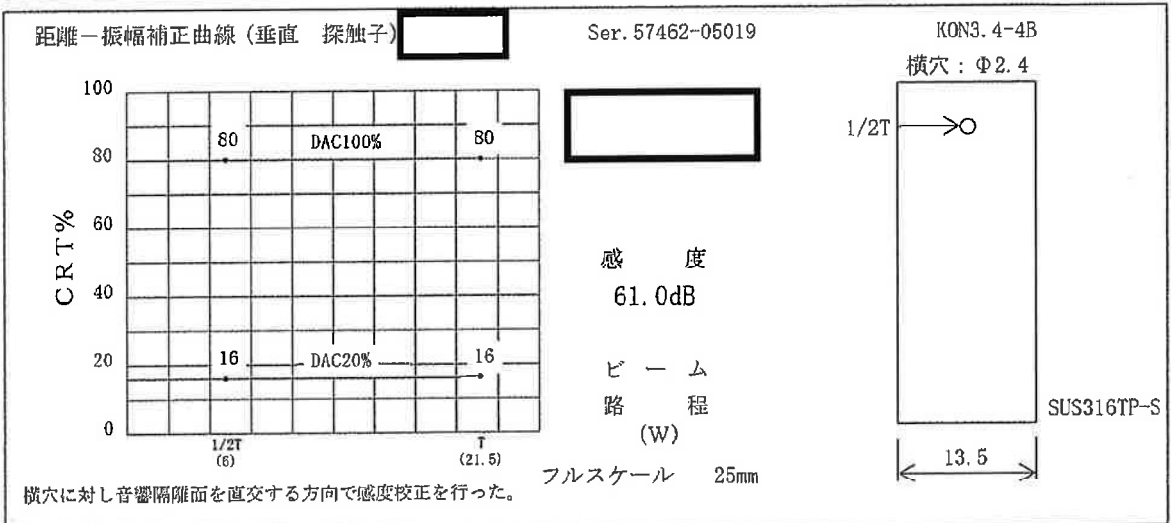
| 項目番号 | カテゴリ | 機器名 | 検査の対象箇所 | 検査箇所 | |
|--------|------|---------|---|----------------------|----|
| B9.11 | B-J | 配管 | 配管の同種金属溶接継手 (呼び径100A以上：周継手) 加圧器スプレイライン (Aループ) | FW-4 (H2-3911007) | |
| | | | | | |
| 検査実施結果 | 検査方法 | | 確認※ | 助勢員 A | 備考 |
| | 体積検査 | 超音波探傷検査 | | | |
| 確認項目 | | | 添付-1(4/4)に記載 | | |
| | | | | | |

※確認項目に対し異常がない場合は、「確認」欄に「レ」と記載する。

超音波探傷検査 (UT) 記録

検査箇所 加圧器スプレイライン (Aループ)

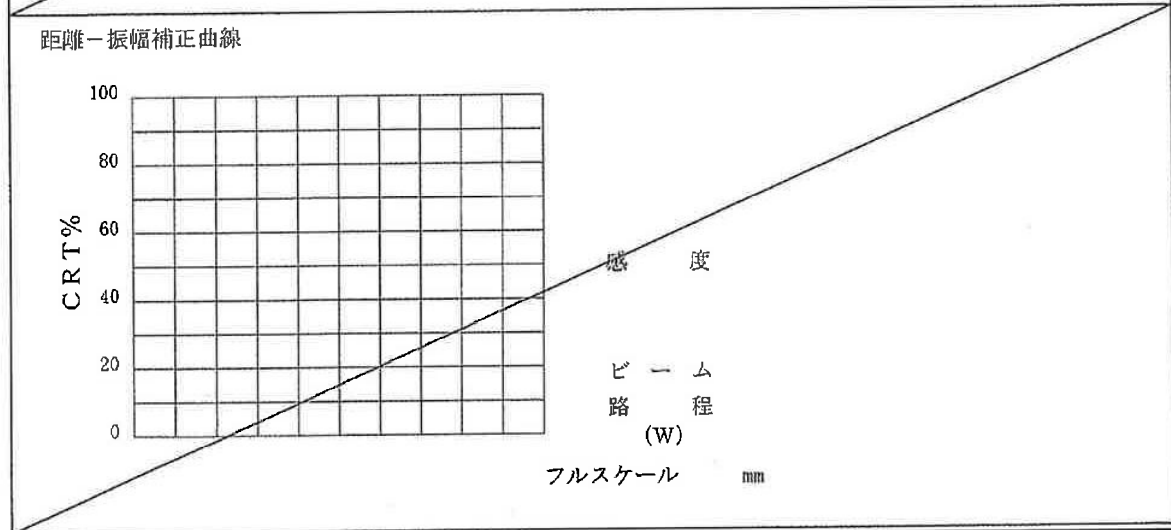
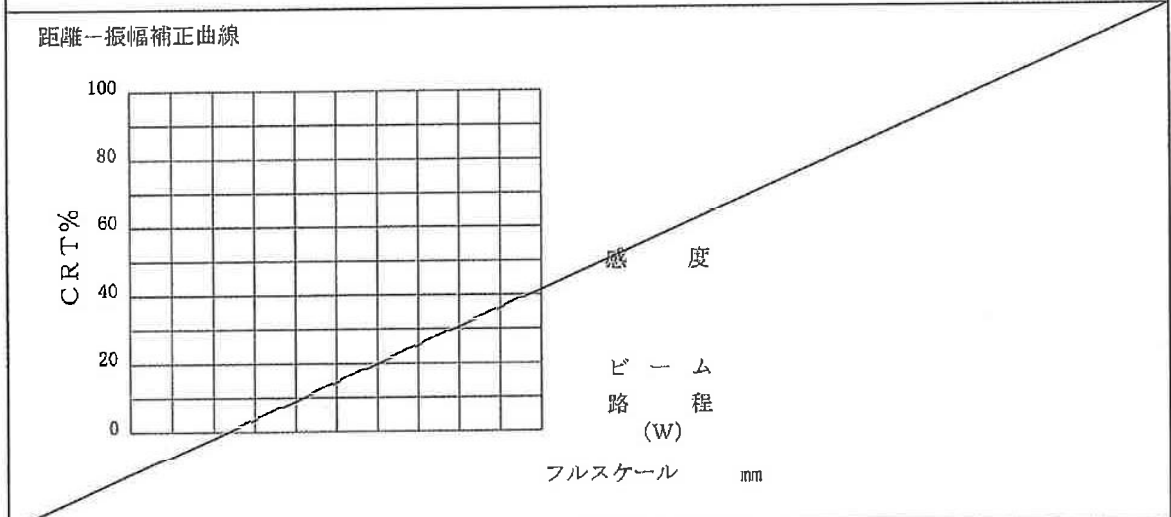
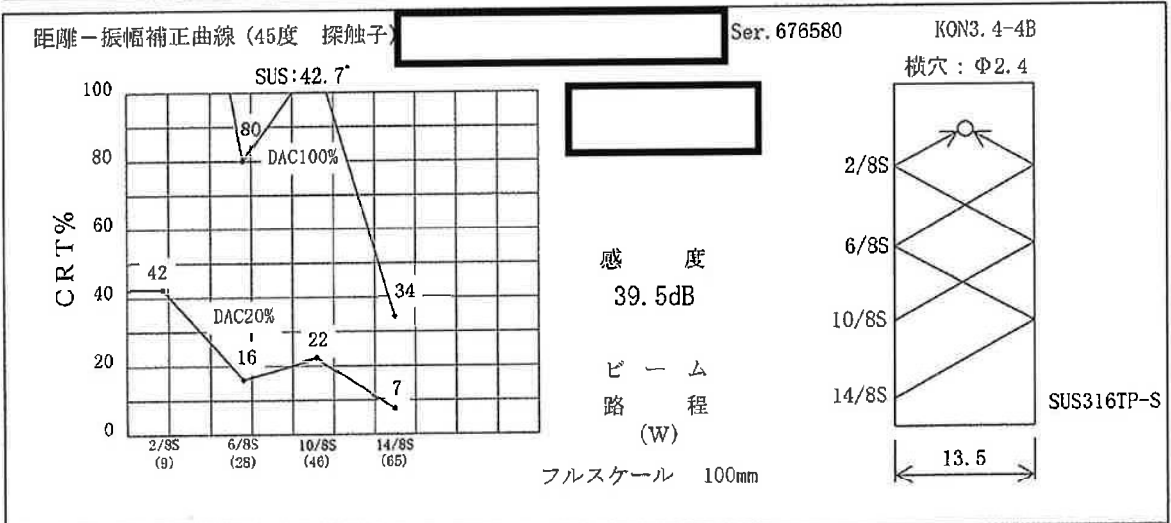
溶接線番号 FW-4 (H2-3911007)



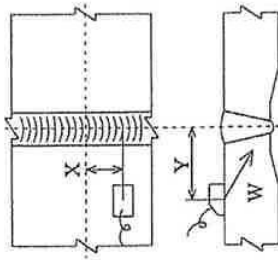
超音波探傷検査 (UT) 記録

検査箇所 加圧器スプレイライン (Aループ)

溶接線番号 FW-4(HI2-3911007)



超音波探傷データシート a (配管マインデンテーションの記録)



配管系統及びライン名 加圧器スプライン (Aループ) 溶接線番号 FW-4(H2-3911007)

上流側 管台 下流側 エルボ 探傷角度 45° (直角)

| No. | 探傷サイド | | ピーク指示部 | | | DAC20% | | DAC100% | | 備考 | |
|-----|-------|-----|----------|--------|--------|---------|---------|-------------------|-----------|-----|-----------|
| | 上流側 | 下流側 | X (mm) | Y (mm) | W (mm) | CRT (%) | DAC (%) | 指示範囲 (mm) | 指示長さ (mm) | | 指示長さ (mm) |
| 1 | ○ | | 0° +12 | 13 | 21.0 | 36 | 35 | 全周 | | | 裏波部* |
| 2 | ○ | | 30° +10 | 13 | 21.0 | 30 | 29 | 全周 | | | 裏波部* |
| 3 | ○ | | 120° +15 | 13 | 21.0 | 32 | 31 | 全周 | | | 裏波部* |
| 4 | ○ | | 180° +18 | 13 | 21.0 | 38 | 36 | 全周 | | | 裏波部* |
| 5 | ○ | | 240° +20 | 13 | 20.0 | 56 | 52 | 全周 | | | 裏波部* |
| 6 | ○ | | 330° +11 | 12 | 21.0 | 25 | 24 | 全周 | | | 裏波部* |
| 7 | ○ | | 240° +14 | 26 | 38.0 | 30 | 32 | 全周 | | | 外表面部 |
| 8 | | ○ | 0° +15 | 12 | 22.0 | 38 | 38 | 240° +0 ~ 120° +0 | 240 | 240 | 裏波部* |
| 9 | | ○ | 30° +20 | 12 | 19.0 | 36 | 32 | 240° +0 ~ 120° +0 | 240 | 240 | 裏波部* |
| 10 | | ○ | 60° +17 | 13 | 21.0 | 34 | 33 | 240° +0 ~ 120° +0 | 240 | 240 | 裏波部* |
| 11 | | ○ | 330° +8 | 13 | 21.0 | 60 | 57 | 240° +0 ~ 120° +0 | 240 | 240 | 裏波部* |

備考 * : 30° 毎の記録点間の最大エコー (ピーク) が前後の記録点のエコー高さを超える反射波を示す。

超音波探傷データシート b (配管インデクセーションの記録)

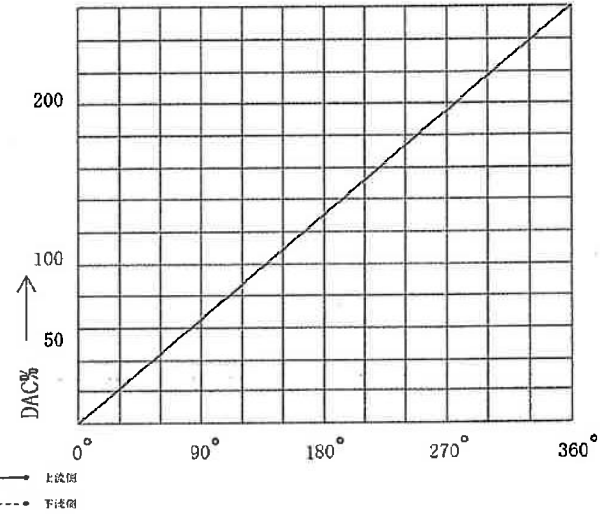
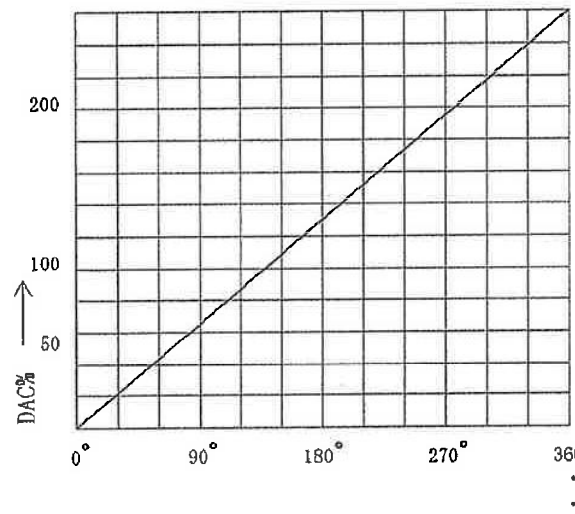
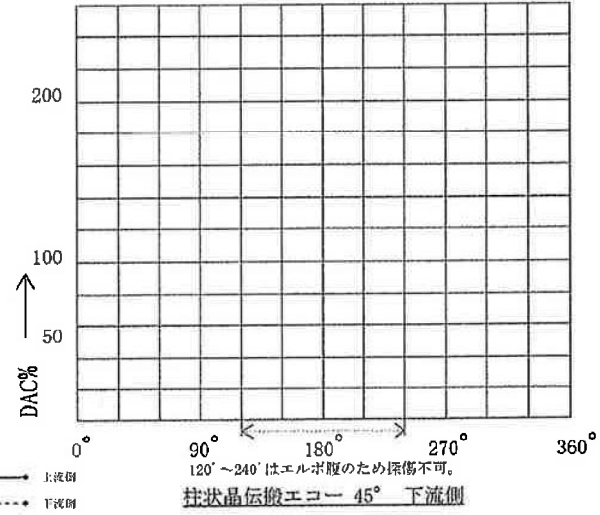
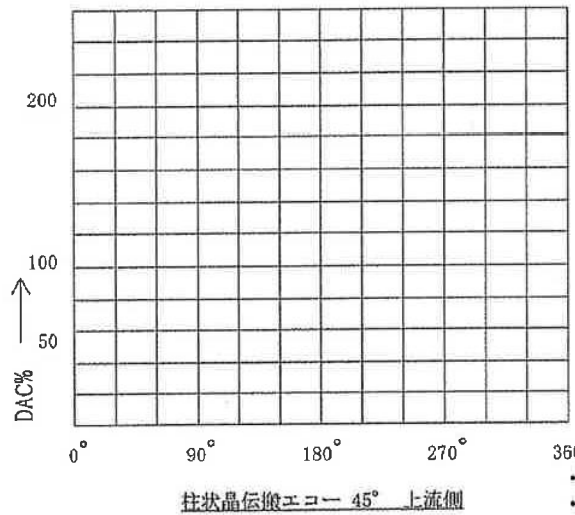
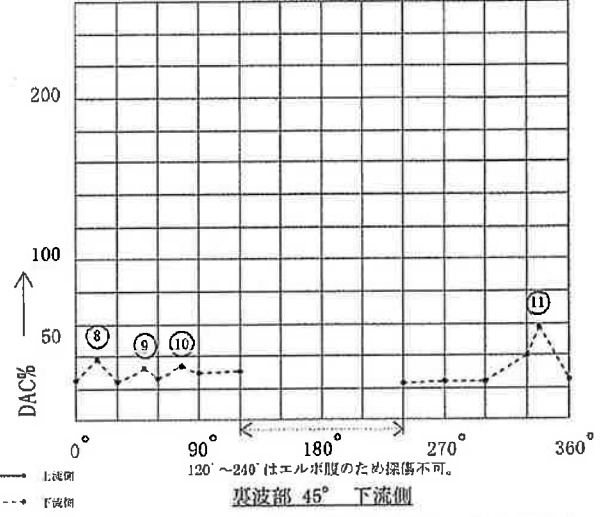
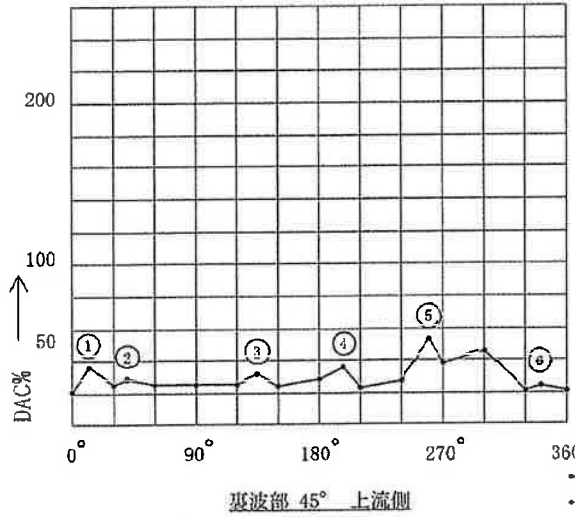
配管系統及びライン名 加圧器スプレイルライン (Aグループ) 溶接線番号 FW-4 (H2-3911007) 探傷角度 45° (直角)

| X位置 | 上 流 (管 台) | | | | | | 下 流 (エルボ) | | | | | | |
|--------|-------------|--------|---------|----------|--------|--------|-------------------------------|---------|--------|----------|---------|---------|-------------------------------|
| | 裏波部 | | | 柱状晶伝搬エコー | | | 裏波部 | | | 柱状晶伝搬エコー | | | |
| | Y (mm) | W (mm) | CRT (%) | DAC (%) | Y (mm) | W (mm) | CRT (%) | DAC (%) | Y (mm) | W (mm) | CRT (%) | DAC (%) | |
| 0° | 12 | 20.0 | 22 | 21 | | | | | 11 | 21.0 | 26 | 25 | |
| 3 0° | 13 | 21.0 | 26 | 25 | | | | | 13 | 22.0 | 24 | 24 | |
| 6 0° | 13 | 21.0 | 26 | 25 | | | | | 13 | 20.0 | 28 | 26 | |
| 9 0° | 14 | 21.0 | 26 | 25 | | | | | 13 | 22.0 | 30 | 30 | |
| 1 2 0° | 13 | 21.0 | 26 | 25 | | | | | 11 | 18.0 | 36 | 31 | |
| 1 5 0° | 13 | 21.0 | 25 | 24 | | | | | — | — | — | — | |
| 1 8 0° | 13 | 21.0 | 30 | 29 | | | | | — | — | — | — | |
| 2 1 0° | 13 | 20.0 | 25 | 23 | | | | | — | — | — | — | |
| 2 4 0° | 12 | 19.0 | 30 | 27 | | | | | 13 | 20.0 | 25 | 23 | |
| 2 7 0° | 13 | 21.0 | 40 | 38 | | | | | 13 | 22.0 | 24 | 24 | |
| 3 0 0° | 12 | 20.0 | 50 | 46 | | | | | 11 | 18.0 | 28 | 24 | |
| 3 3 0° | 13 | 21.0 | 22 | 21 | | | | | 12 | 22.0 | 40 | 40 | |
| | | | | | | | 120° ~ 240° はエルボ腹のため探傷不可。 | | | | | | 120° ~ 240° はエルボ腹のため探傷不可。 |
| | | | | | | | 空白欄は隣接する30°芯2点以上にまたがる反射波を認めず。 | | | | | | 空白欄は隣接する30°芯2点以上にまたがる反射波を認めず。 |

超音波探傷データシートc (配管-インディケーションのマップ)

配管系統及びライン名 加圧器スプレイライン (Aループ)

溶接線番号 FW-4(H2-3911007)



インデイクေးションの位置

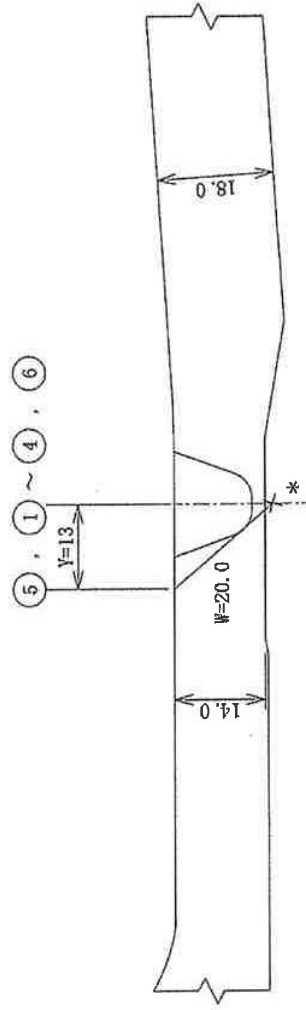
縮尺：1/1

単位：mm

配管系統及びライン名 加圧器スプレイライン(Aループ)



溶接線番号 FW-4(H2-3911007)



上流側 (管 台)

下流側 (エルボ)

*：ビーム路程、Y距離を計測し作図した結果、裏波部に位置する。

インデイクエーションの位置

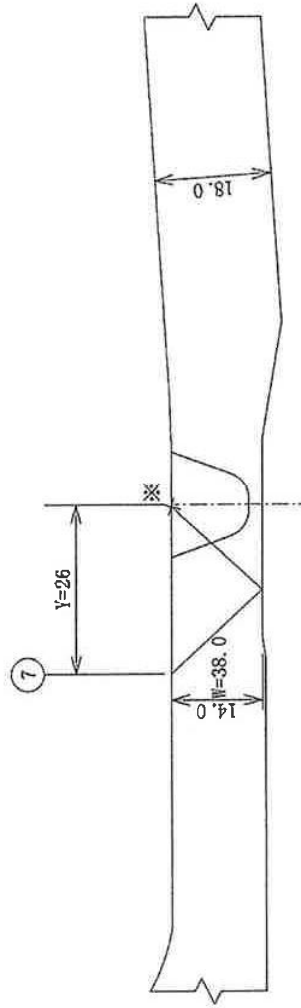
縮尺：1/1

単位：mm

配管系統及びライン名 加圧器スプレイライン (Aループ)



溶接線番号 FW-4 (H2-3911007)



上流側 (管 台)

下流側 (エルボ)

※：ビームの到達点の波形の変化を指で確認。

インデイクေးションの位置

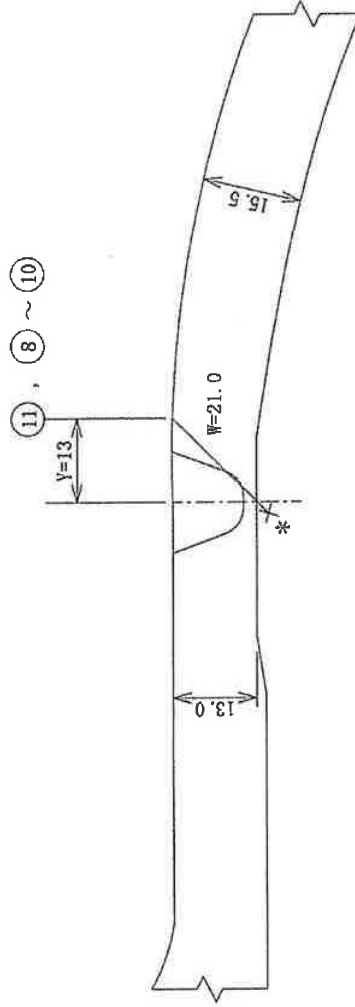
縮尺：1/1

単位：mm

配管系統及びライン名 加圧器スプレライン(エルブ)



溶接継番号 FW-4(H2-3911007)



上流側 (管 台)

下流側 (エルボ)

* : ビーム路程、Y距離を計測し作図した結果、裏波部に位置する。

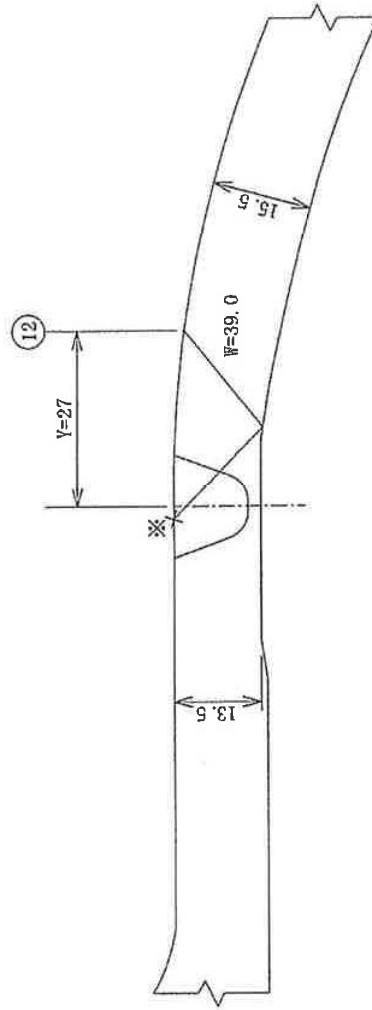
インデイクエーションの位置

縮尺：1/1

単位：mm

配管系統及びライン名 加圧器スプレイン (Aループ)

溶接線番号 FW-4 (H2-3911007)



上流側 (管台)

下流側 (エルボ)

※：ビームの到達点の波形の変化を指で確認。

超音波探傷データシート b (配管インデケーションの記録)

探傷角度 45° (小型探触子) (直角)

溶接線番号 FW-4 (H2-3911007)

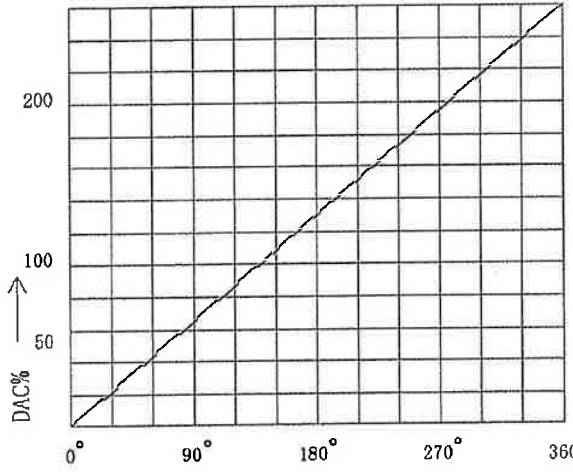
配管系統及びライン名 加圧器スプレイレイン (Aグループ)

| X位置 | 流 (管台) | | | | | | | | | | | | 流 (エルボ) | | | | | |
|------|--------|--------|---------|---------|--------|--------|---------|---------|--------|--------|---------|---------|---------|--------|---------|---------|--|--|
| | 裏波部 | | | | | | 裏波部 | | | | | | 裏波部 | | | | | |
| | Y (mm) | W (mm) | CRT (%) | DAC (%) | Y (mm) | W (mm) | CRT (%) | DAC (%) | Y (mm) | W (mm) | CRT (%) | DAC (%) | Y (mm) | W (mm) | CRT (%) | DAC (%) | | |
| 0° | | | | | | | | | | | | | | | | | | |
| 30° | | | | | | | | | | | | | | | | | | |
| 60° | | | | | | | | | | | | | | | | | | |
| 90° | | | | | | | | | | | | | | | | | | |
| 120° | | | | | | | 11 | 19.0 | 40 | 29 | 0 | 15.0 | 70 | 42 | | | | |
| 150° | | | | | | | 12 | 19.0 | 38 | 27 | 0 | 15.0 | 55 | 33 | | | | |
| 180° | | | | | | | 13 | 19.0 | 45 | 32 | 0 | 16.0 | 96 | 60 | | | | |
| 210° | | | | | | | 13 | 18.0 | 64 | 44 | 0 | 16.0 | 58 | 36 | | | | |
| 240° | | | | | | | 12 | 18.0 | 62 | 42 | 0 | 15.0 | 62 | 37 | | | | |
| 270° | | | | | | | | | | | | | | | | | | |
| 300° | | | | | | | | | | | | | | | | | | |
| 330° | | | | | | | | | | | | | | | | | | |

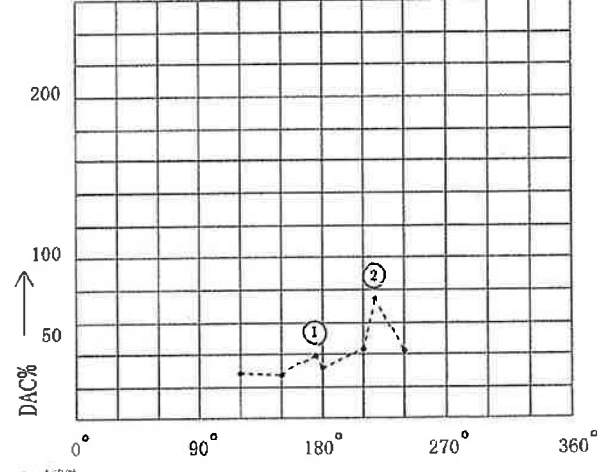
超音波探傷データシートc (配管-インディケーションのマップ)

配管系統及びライン名 加圧器スプレライン (Aループ)

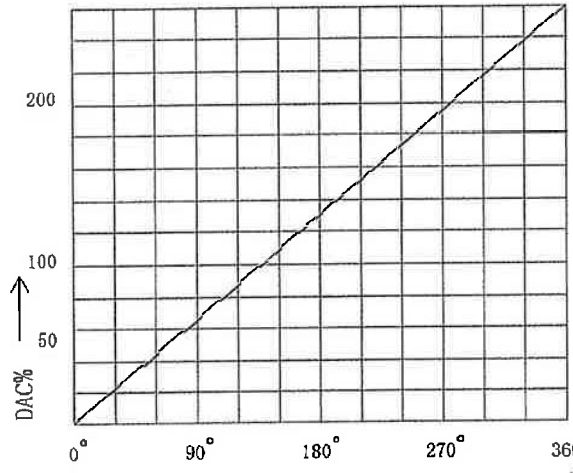
溶接線番号 FW-4(H2-3911007) (小型探触子)



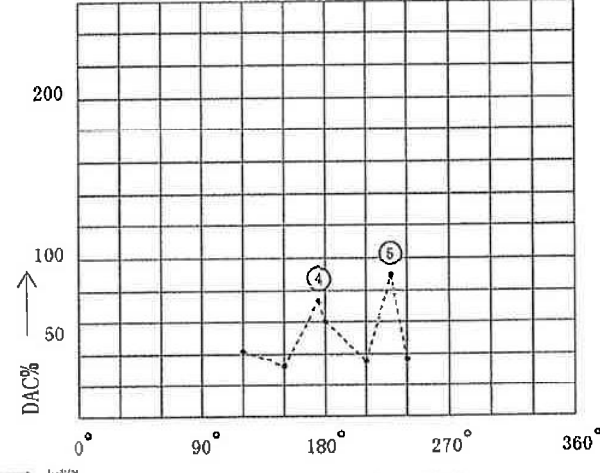
裏波部 45° 上流側



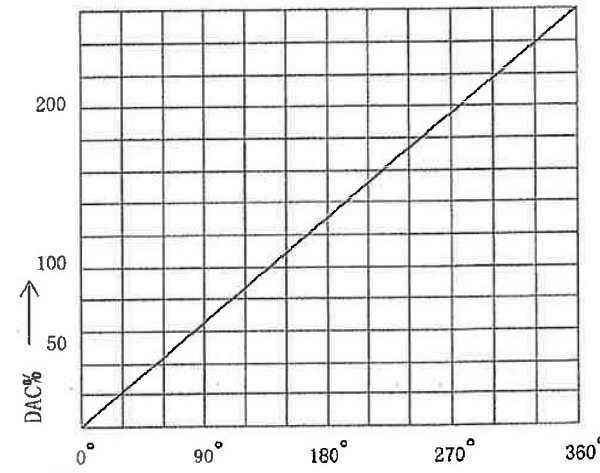
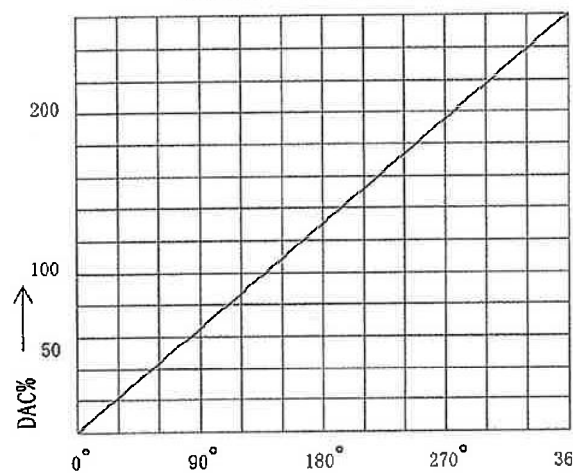
裏波部 45° 下流側



柱状晶伝搬エコー 45° 上流側



柱状晶伝搬エコー 45° 下流側



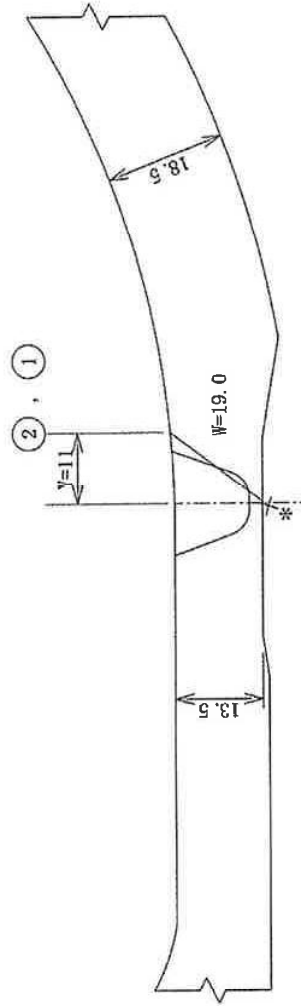
インデケーションの位置

縮尺：1/1

単位：mm

配管系統及びライン名 加圧器スプレイライン (Aループ)

溶接線番号 FW-4(H2-3911007)



上流側 (管 台)

下流側 (エルボ)

* : ビーム路程、Y距離を計測し作図した結果、裏波部に位置する。

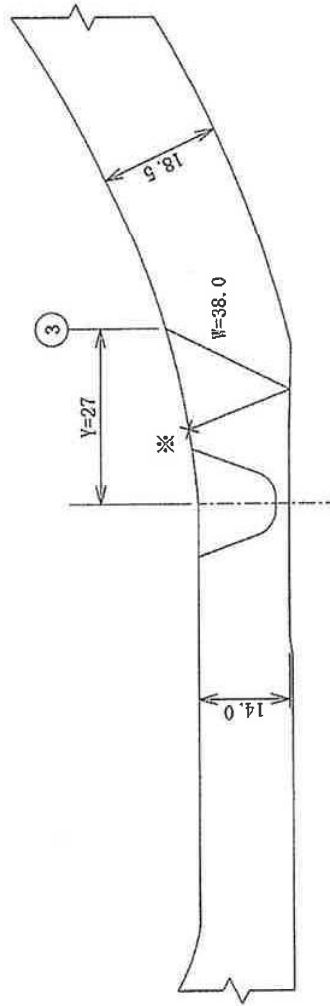
インデケーションの位置

縮尺：1/1
単位：mm

配管系統及びライン名 加圧器スプレイライン(Aループ)



溶接線番号 FW-4(H2-3911007)



上流側 (管 台)

下流側 (エルボ)

※：ピームの到達点の波形の変化を指で確認。

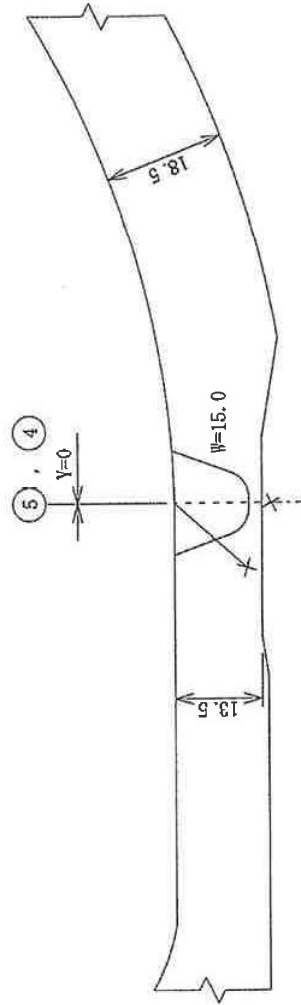
インデイクエーションの位置

縮尺：1/1
単位：mm

配管系統及びライン名 加圧器スプレイルライン (Aループ)



溶接線番号 FW-4 (H2-3911007)



上流側 (管 台)

下流側 (エルボ)

---: 破線の線に進んだと思われる。

非破壊検査記録 (/)

(1) 検査の判定

| 項目番号 | カテゴリ | 機器名 | 検査の対象箇所 | 検査箇所 |
|-------|------|-----|---|----------------------|
| B9.11 | B-J | 配管 | 配管の同種金属溶接継手 (呼び径100A以上：周継手) 加圧器スプレイライン (Aループ) | SW-5 (H2-3911007) |

| 検査方法 | | 検査年月日 | 立会実績 | 結果 | 検査員 | 備考 |
|------|---------|--------------|------|----|-----|----|
| 体積検査 | 超音波探傷検査 | 年 月 日 | 有・無 | | | |
| 判定基準 | | 添付-1(4/4)に記載 | | | | |

非 破 壊 検 査 記 録 (/)

(2) 検査記録

検査年月日 _____ 年 月 日

助 勢 員 A _____

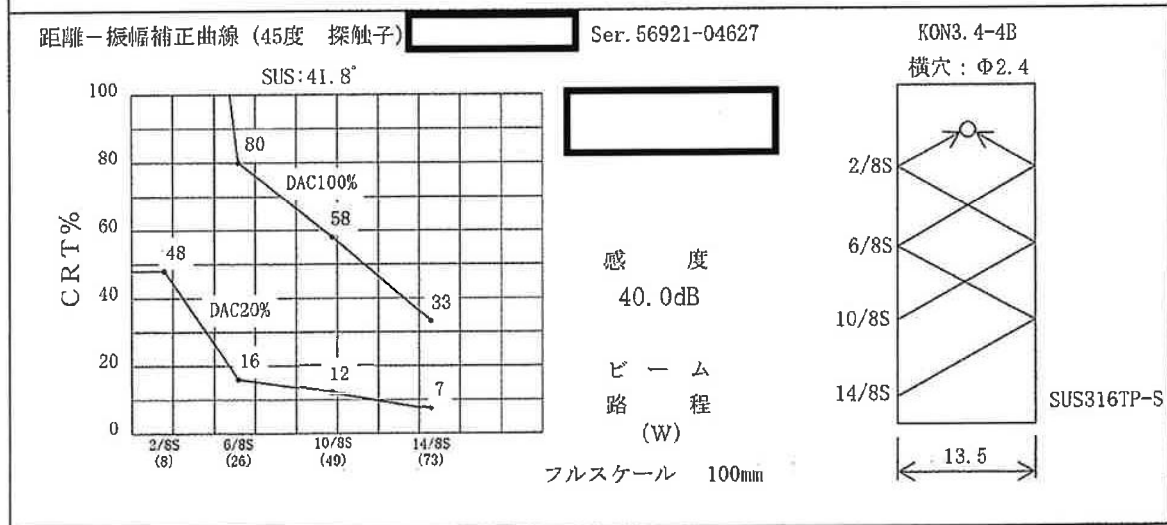
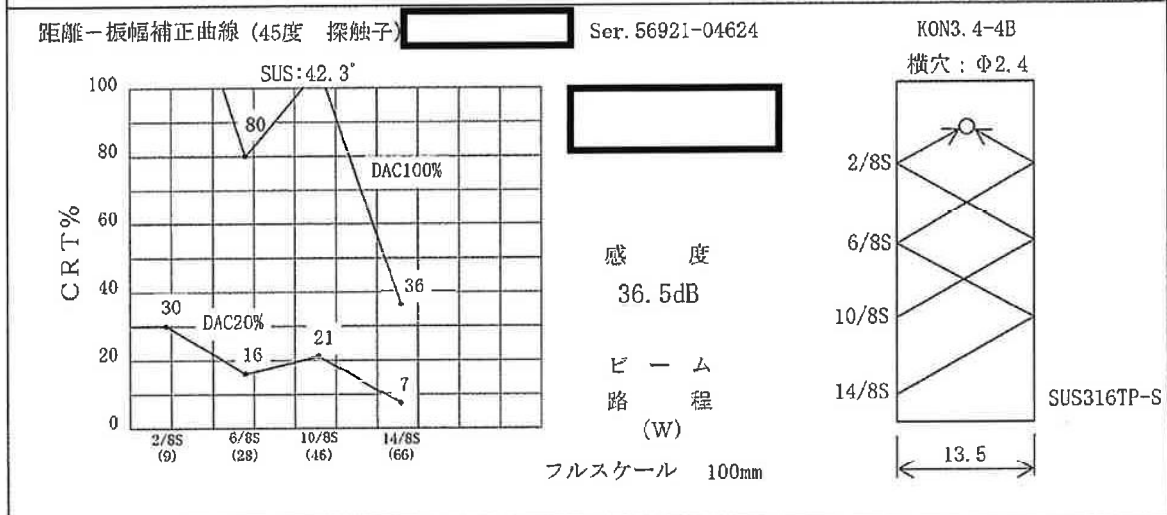
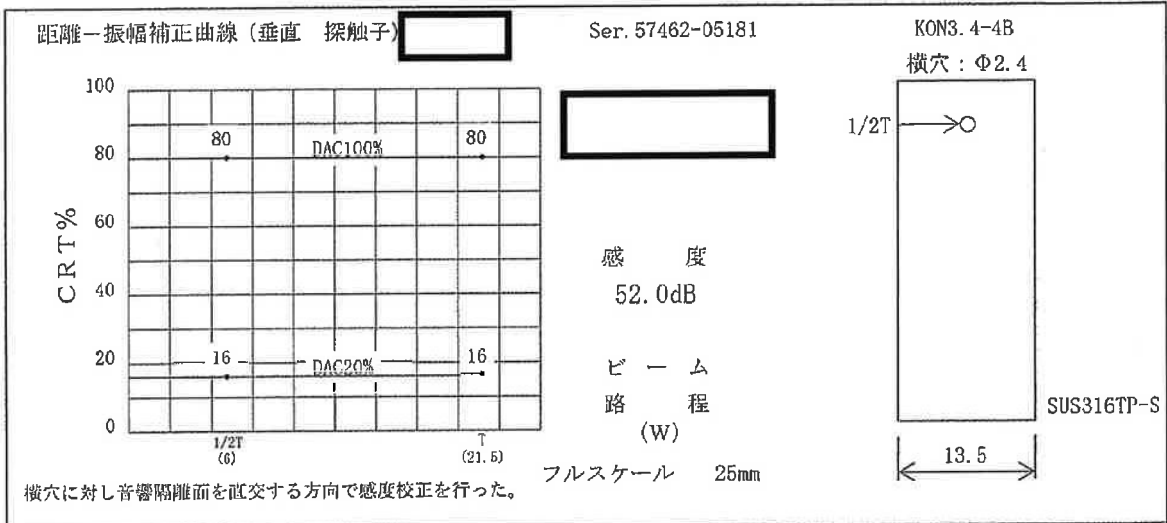
| 項目番号 | カテゴリ | 機 器 名 | 検 査 の 対 象 箇 所 | 検 査 箇 所 | |
|---------|---------|---------|---|----------------------|-----|
| B9.11 | B-J | 配管 | 配管の同種金属溶接継手 (呼び径100A以上;周継手) 加圧器スプレイライン (Aループ) | SW-5 (H2-3911007) | |
| | | | | | |
| 検査実施結果 | 検 査 方 法 | | 確認※ | 助 勢 員 A | 備 考 |
| | 体積検査 | 超音波探傷検査 | | | |
| 確 認 項 目 | | | 添付-1(4/4)に記載 | | |
| | | | | | |

※確認項目に対し異常がない場合は、「確認」欄に「レ」と記載する。

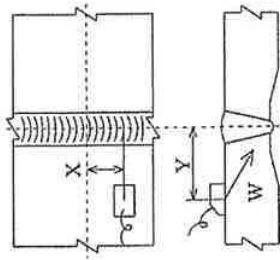
超音波探傷検査 (UT) 記録

検査箇所 加圧器スプレイライン (Aループ)

溶接線番号 SW-5 (H2-3911007)



超音波探傷データシート a (配管インデクセーションの記録)

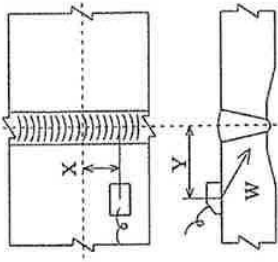


配管系統及びライン名 加圧器スプレイレイン (Aループ) 溶接線番号 SW-6(H2-3911007)
 上流側 エルボ 下流側 パイプ 探傷角度 45° (直角)

| 探傷サイド | ピーク指示部 | | | DAC20% | | | DAC100% | | 備考 | |
|-------|--------|-----|-------|---------|---------|----------|-------------------|----------|-------------------|----------|
| | 上流側 | 下流側 | W(mm) | CRT (%) | DAC (%) | 指示長さ(mm) | 指示範囲(mm) | 指示長さ(mm) | | 指示範囲(mm) |
| ○ | 30° | -3 | 13 | 20.0 | 75 | 69 | 240° +0 ~ 120° +0 | 240 | | 裏波部* |
| ○ | 60° | +8 | 12 | 19.0 | 40 | 36 | 240° +0 ~ 120° +0 | 240 | | 裏波部* |
| ○ | 90° | +1 | 11 | 19.0 | 40 | 36 | 240° +0 ~ 120° +0 | 240 | | 裏波部* |
| ○ | 240° | +17 | 12 | 20.0 | 61 | 56 | 240° +0 ~ 120° +0 | 240 | | 裏波部* |
| ○ | 300° | -7 | 13 | 20.0 | 32 | 30 | 240° +0 ~ 120° +0 | 240 | | 裏波部* |
| ○ | 300° | +11 | 13 | 22.0 | 30 | 30 | 240° +0 ~ 120° +0 | 240 | | 裏波部* |
| ○ | 330° | +20 | 13 | 21.0 | 40 | 38 | 240° +0 ~ 120° +0 | 240 | | 裏波部* |
| ○ | 300° | +20 | 25 | 34.0 | 30 | 34 | 240° +0 ~ 120° +0 | 240 | | 外表面部 |
| ○ | 30° | -5 | 12 | 21.0 | 120 | 114 | 全周 | 360 | 30° ~ 30° -6 ~ -4 | 裏波部* |
| ○ | 60° | +9 | 13 | 20.0 | 50 | 46 | 全周 | 360 | | 裏波部* |
| ○ | 150° | -15 | 13 | 20.0 | 55 | 51 | 全周 | 360 | | 裏波部* |

備考 * : 30° 毎の記録点間の最大エコー (ピーク) が前後の記録点のエコー高さを超える反射波を示す。

超音波探傷データシート a (配管インデントーションの記録)



配管系統及びライン名 加圧器スプレライン (Aループ) 溶接線番号 SW-5 (H2-3911007)
 上流側 エルボ 下流側 パイプ 探傷角度 45° (直角)

| 探傷サイド | ピーク指示部 | | | DAC20% | | DAC100% | | 備考 |
|-------|--------|-----|-----|-----------|-----------|-----------|-----------|------|
| | 上流側 | 下流側 | パイプ | 指示範囲 (mm) | 指示長さ (mm) | 指示範囲 (mm) | 指示長さ (mm) | |
| 12 | ○ | ○ | ○ | 30 | 29 | 全周 | 360 | 裏波部* |
| 13 | ○ | ○ | ○ | 35 | 34 | 全周 | 360 | 裏波部* |
| 14 | ○ | ○ | ○ | 50 | 48 | 全周 | 360 | 裏波部* |
| 15 | ○ | ○ | ○ | 38 | 34 | 全周 | 360 | 裏波部* |
| 16 | ○ | ○ | ○ | 32 | 31 | 全周 | 360 | 裏波部* |
| 17 | ○ | ○ | ○ | 52 | 48 | 全周 | 360 | 裏波部* |
| 18 | ○ | ○ | ○ | 48 | 44 | 全周 | 360 | 裏波部* |
| 19 | ○ | ○ | ○ | 30 | 34 | 全周 | 360 | 外表面部 |
| | | | | 以下 | 余白 | | | |
| | | | | | | | | |
| | | | | | | | | |
| | | | | | | | | |

備考 * : 30° 毎の記録点間の最大エコー (ピーク) が前後の記録点のエコー高さを超える反射波を示す。

超音波探傷データシートb (配管インデケーションの記録)

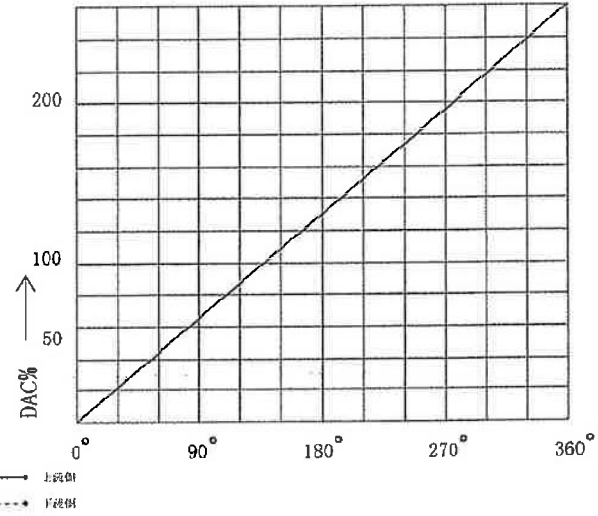
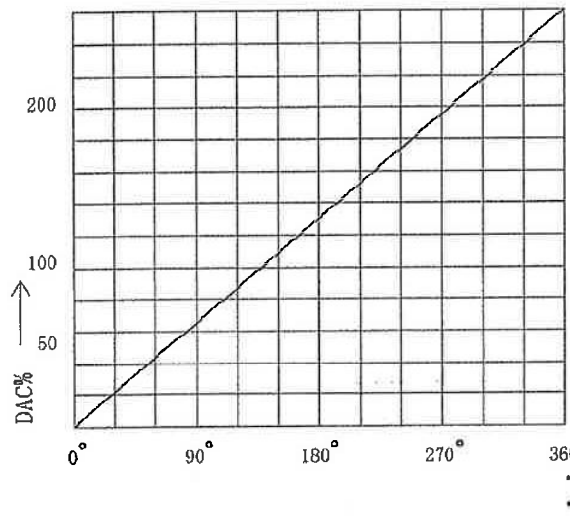
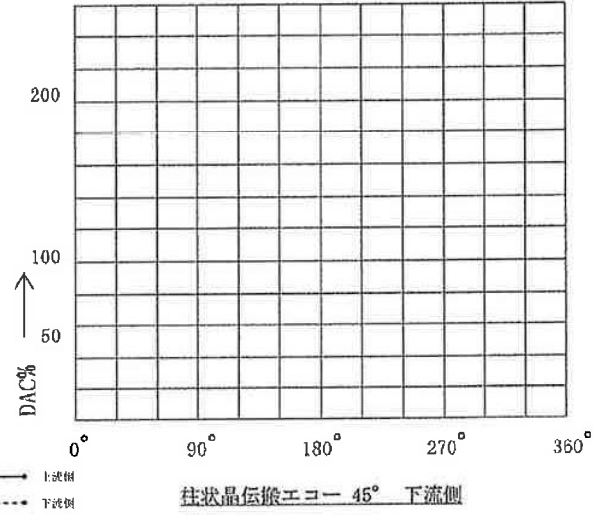
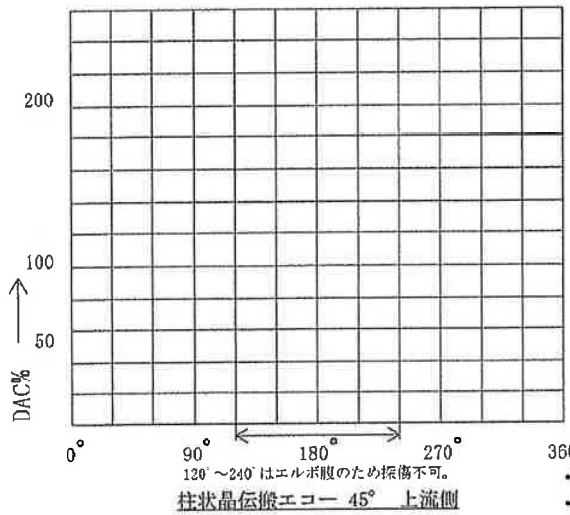
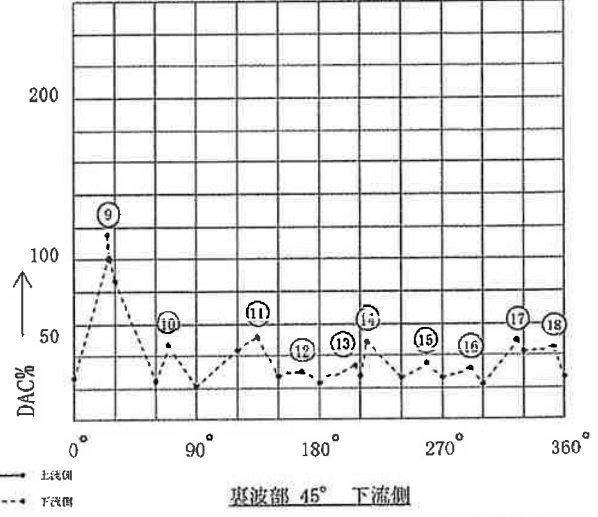
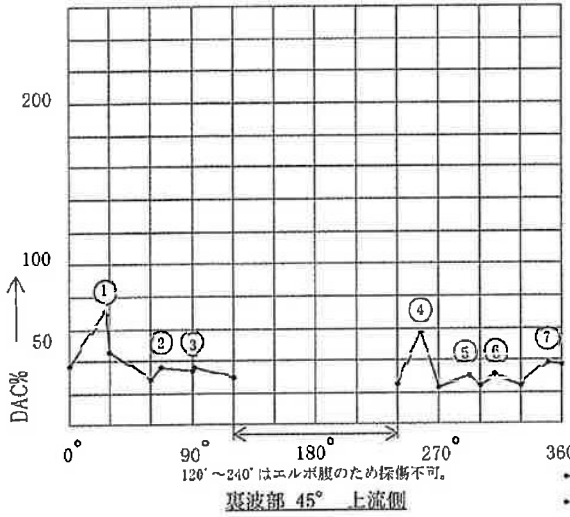
配管系統及びライン名 加圧器スプレイライン (Aグループ) 溶接線番号 SP-5 (H2-3911007) 探傷角度 45° (直角)

| X位置 | 上 流 (エルボ) | | | | | | 下 流 (パイプ) | | | | | | |
|------|-------------------------|--------|---------|----------|--------|--------|-------------------------|---------|--------|----------|---------|---------|-------------------------------|
| | 裏波部 | | | 柱状晶伝播エコー | | | 裏波部 | | | 柱状晶伝播エコー | | | |
| | Y (mm) | W (mm) | CRT (%) | DAC (%) | Y (mm) | W (mm) | CRT (%) | DAC (%) | Y (mm) | W (mm) | CRT (%) | DAC (%) | |
| 0° | 13 | 22.0 | 37 | 37 | | | | | 12 | 20.0 | 28 | 26 | |
| 30° | 11 | 20.0 | 50 | 46 | | | | | 12 | 21.0 | 90 | 86 | |
| 60° | 12 | 21.0 | 30 | 29 | | | | | 12 | 20.0 | 26 | 24 | |
| 90° | 12 | 19.0 | 38 | 34 | | | | | 12 | 20.0 | 22 | 21 | |
| 120° | 12 | 20.0 | 32 | 30 | | | | | 12 | 20.0 | 48 | 44 | |
| 150° | — | — | — | — | — | — | — | — | 13 | 21.0 | 28 | 27 | |
| 180° | — | — | — | — | — | — | — | — | 13 | 21.0 | 24 | 23 | |
| 210° | — | — | — | — | — | — | — | — | 13 | 20.0 | 30 | 28 | |
| 240° | 12 | 21.0 | 26 | 25 | | | | | 13 | 20.0 | 28 | 26 | |
| 270° | 11 | 20.0 | 25 | 23 | | | | | 13 | 19.0 | 29 | 26 | |
| 300° | 14 | 21.0 | 25 | 24 | | | | | 13 | 20.0 | 23 | 22 | |
| 330° | 13 | 21.0 | 25 | 24 | | | | | 12 | 21.0 | 45 | 43 | |
| | 120°~240° はエルボ腹のため探傷不可。 | | | | | | 120°~240° はエルボ腹のため探傷不可。 | | | | | | 空白欄は隣接する30°お2点以上にまたがる反射波を認めず。 |
| | 120°~240° はエルボ腹のため探傷不可。 | | | | | | 120°~240° はエルボ腹のため探傷不可。 | | | | | | |

超音波探傷データシートc (配管-インディケーションのマップ)

配管系統及びライン名 加圧器スプレイライン (Aループ)

溶接線番号 SW-5(H2-3911007)



インデイクေးションの位置

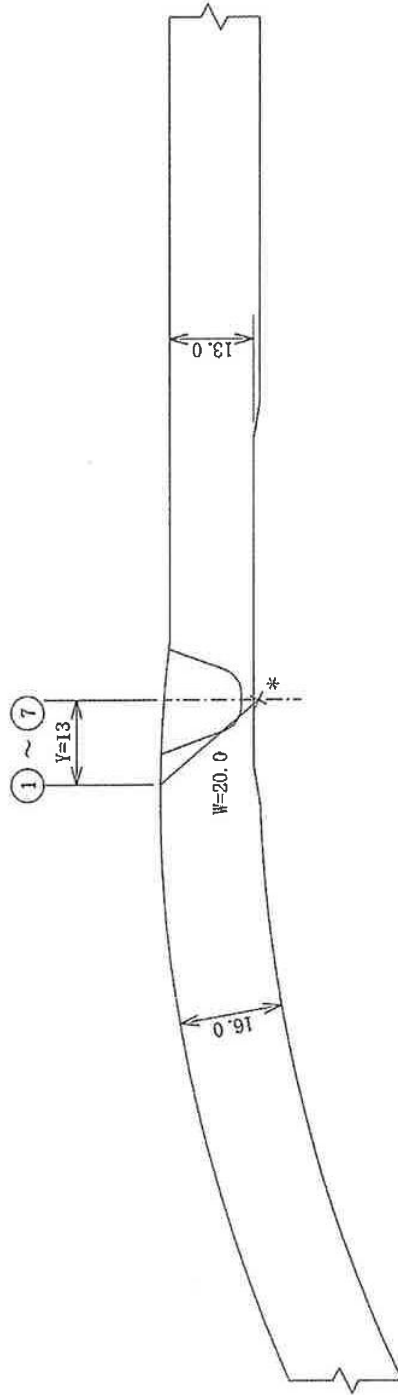
縮尺：1/1

単位：mm

配管系統及びライン名 加圧器スプレイライン (Aグループ)



溶接線番号 SW-5(H2-3911007)



上流側 (エルボ)

下流側 (パイプ)

* : ビーム路程、Y距離を計測し作図した結果、裏被部に位置する。

インデイクエーションの位置

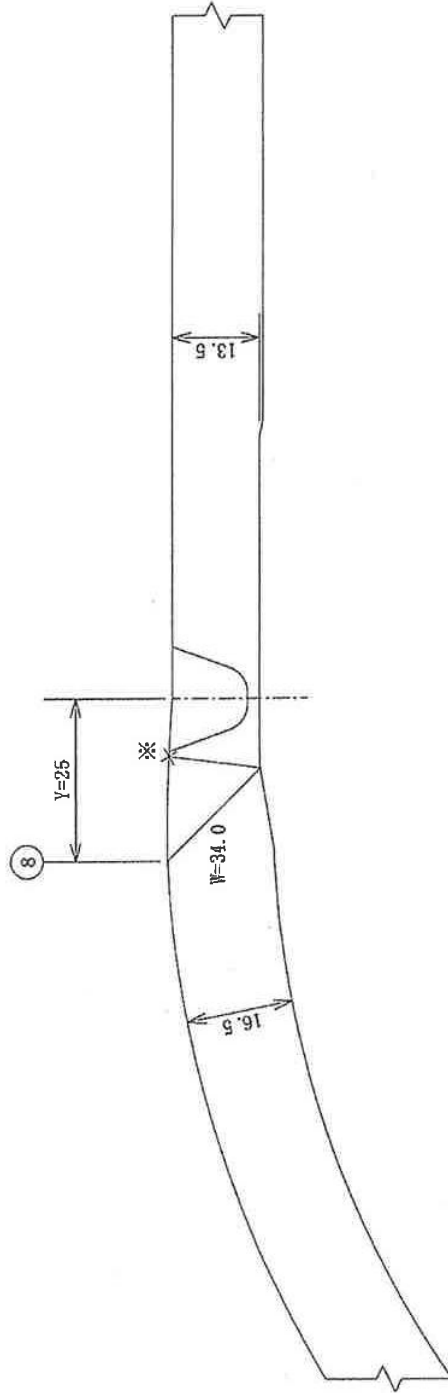
縮尺: 1/1

単位: mm

配管系統及びライン名 加圧器スプレイライン (Aループ)



溶接線番号 SW-5 (H2-3911007)



上流側 (エルボ)

下流側 (パイプ)

※: ビームの到達点の波形の変化を指で確認。

インデイクエーションの位置

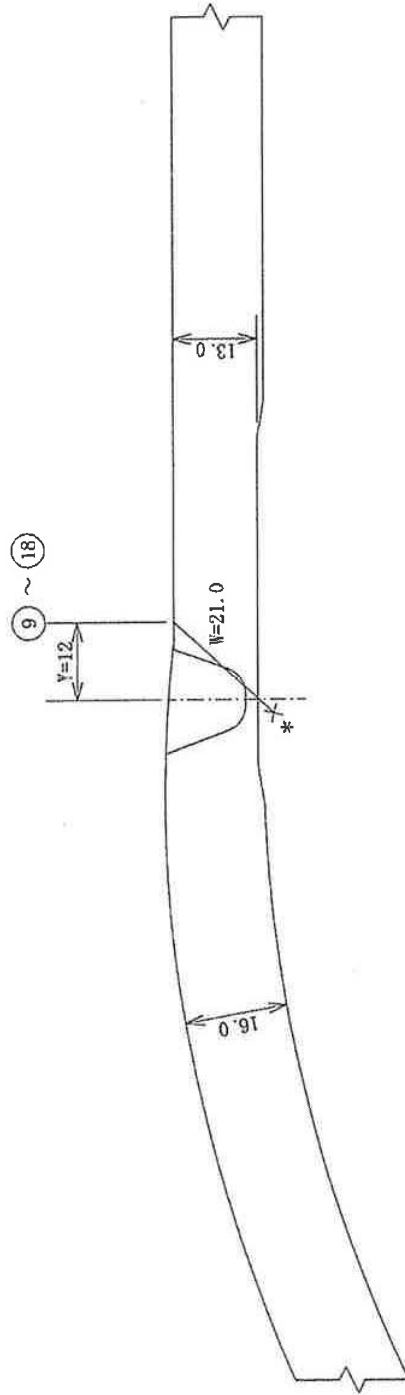
縮尺: 1/1

単位: mm

配管系統及びライン名 加圧器スプレイン (Aループ)



溶接線番号 SW-5 (H2-3911007)



上流側 (エルボ)

下流側 (パイプ)

* : ビーム路程、Y距離を計測し作図した結果、裏波部に位置する。

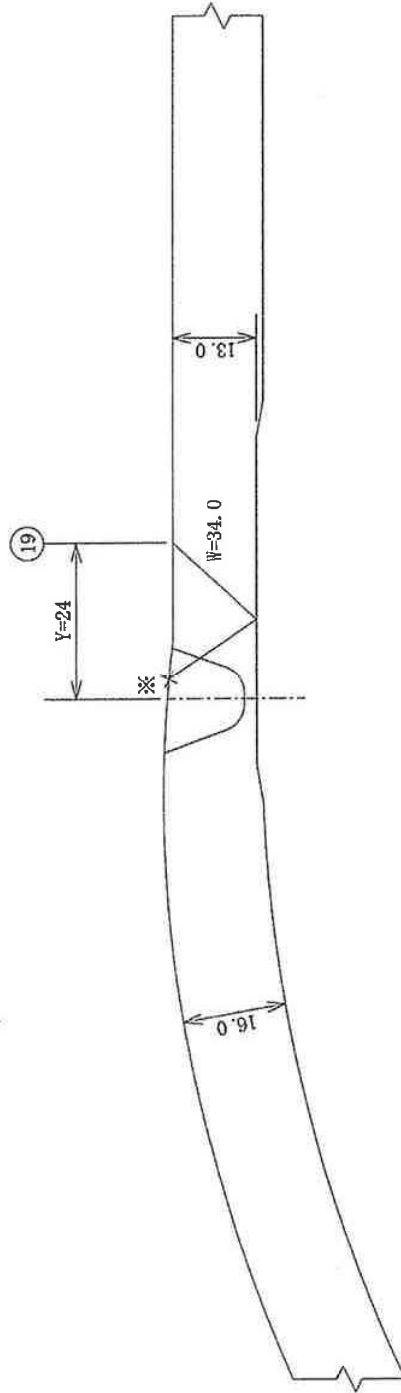
インデイクエーションの位置

縮尺：1/1
単位：mm

配管系統及びライン名 加圧器スプレライン (Aループ)



溶接線番号 SW-5 (H2-3911007)

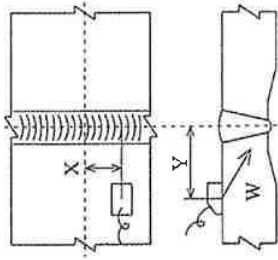


上流側 (エルボ)

下流側 (パイプ)

※：ビームの到達点の波形の変化を指で確認。

超音波探傷データシート a (配管-インデイングেশョンの記録)



配管系統及びライン名 加圧器スプレイレイン (A.ループ) 溶接線番号 SW-5 (H2-3911007)
 上流側 エルボ 下流側 パイプ 探傷角度 45° (小型探触子) (直角)

| 探傷サイト | ピーク指示部 | | | DAC 20% | | DAC 100% | | 備考 | | |
|-------|--------|-----|----------|---------|---------|----------|-----------|-------------------|-----------|------|
| | 上流側 | 下流側 | Y (mm) | W (mm) | CRT (%) | DAC (%) | 指示長さ (mm) | | 指示長さ (mm) | |
| 1 | ○ | | 120° +16 | 12 | 22.0 | 46 | 38 | 120° +0 ~ 240° +0 | 120 | 裏波部* |
| 2 | ○ | | 150° +6 | 12 | 21.0 | 35 | 28 | 120° +0 ~ 240° +0 | 120 | 裏波部* |
| 3 | ○ | | 210° -5 | 11 | 20.0 | 85 | 64 | 120° +0 ~ 240° +0 | 120 | 裏波部* |
| 4 | ○ | | 240° -11 | 11 | 20.0 | 78 | 58 | 120° +0 ~ 240° +0 | 120 | 裏波部* |
| 5 | ○ | | 180° +3 | 18 | 36.0 | 52 | 55 | 120° +0 ~ 240° +0 | 120 | 外表面部 |
| | | | | | | 以下 | 余白 | | | |
| | | | | | | | | | | |
| | | | | | | | | | | |
| | | | | | | | | | | |
| | | | | | | | | | | |
| | | | | | | | | | | |
| | | | | | | | | | | |
| | | | | | | | | | | |

備考 * : 30° 毎の記録点間の最大エコー (ピーク) が前後の記録点のエコー高さを超える反射波を示す。

超音波探傷データシートb (配管インデケーションの記録)

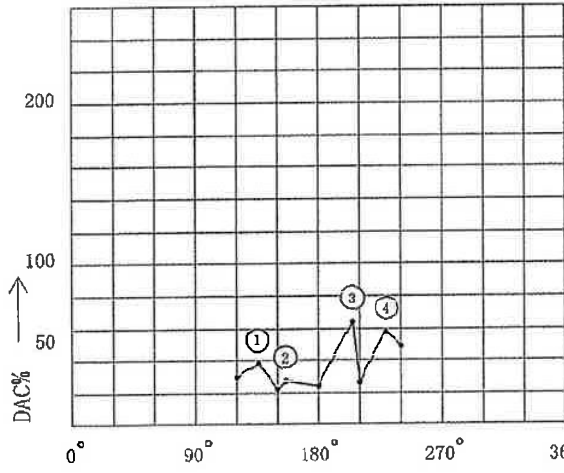
配管系統及びライン名 加圧器スプレイレイン (Aグループ) 溶接線番号 SW-5 (H2-3911007) 探傷角度 45° (小型探触子) (直角)

| X位置 | 流 (エルボ) | | | | | | | | | | | | 流 (パイプ) | | | | | | | | | | | |
|------|-------------------------------|--------|---------|---------|--------|--------|----------|---------|--------|--------|---------|---------|-----------|--------|---------|---------|--------|--------|----------|---------|--|--|--|--|
| | 裏波部 | | | | | | 柱状晶伝搬エコー | | | | | | 裏波部 | | | | | | 柱状晶伝搬エコー | | | | | |
| | Y (mm) | W (mm) | CRT (%) | DAC (%) | Y (mm) | W (mm) | CRT (%) | DAC (%) | Y (mm) | W (mm) | CRT (%) | DAC (%) | Y (mm) | W (mm) | CRT (%) | DAC (%) | Y (mm) | W (mm) | CRT (%) | DAC (%) | | | | |
| 0° | | | | | | | | | | | | | | | | | | | | | | | | |
| 30° | | | | | | | | | | | | | | | | | | | | | | | | |
| 60° | | | | | | | | | | | | | | | | | | | | | | | | |
| 90° | | | | | | | | | | | | | | | | | | | | | | | | |
| 120° | 11 | 20.0 | 40 | 30 | | | | | | | | | | | | | | | | | | | | |
| 150° | 12 | 22.0 | 26 | 22 | | | | | | | | | | | | | | | | | | | | |
| 180° | 11 | 21.0 | 30 | 24 | | | | | | | | | | | | | | | | | | | | |
| 210° | 11 | 20.0 | 35 | 26 | | | | | | | | | | | | | | | | | | | | |
| 240° | 12 | 20.0 | 65 | 49 | | | | | | | | | | | | | | | | | | | | |
| 270° | | | | | | | | | | | | | | | | | | | | | | | | |
| 300° | | | | | | | | | | | | | | | | | | | | | | | | |
| 330° | | | | | | | | | | | | | | | | | | | | | | | | |
| | 空白欄は隣接する30°芯2点以上にまたがる反射底を認めず。 | | | | | | | | | | | | | | | | | | | | | | | |

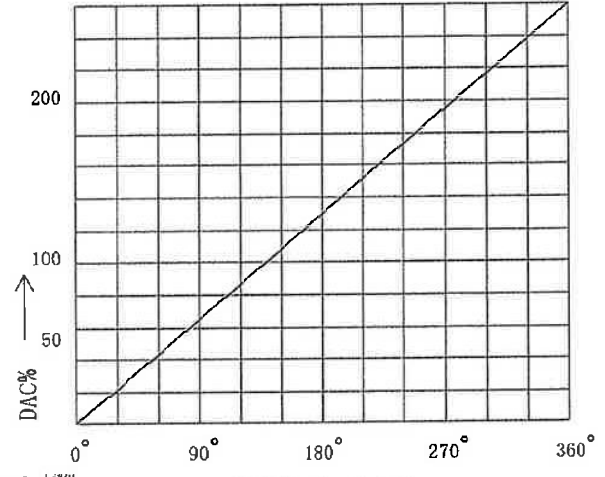
超音波探傷データシートc (配管-インディケーションのマップ)

配管系統及びライン名 加圧器スプレイライン (Aループ)

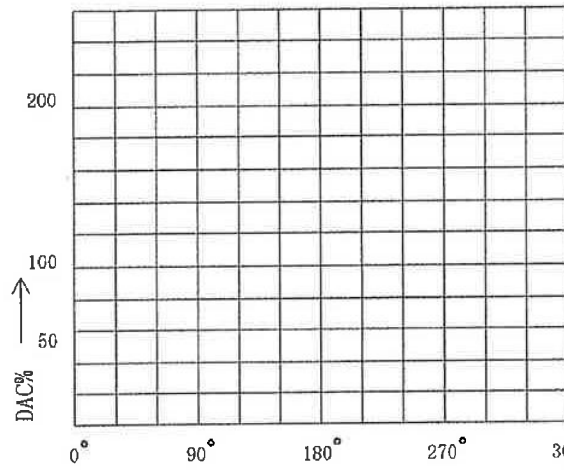
溶接線番号 SW-5(H2-3911007) (小型探触子)



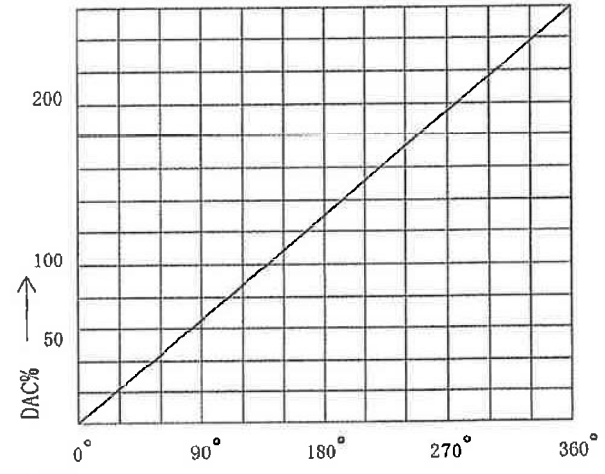
裏波部 45° 上流側



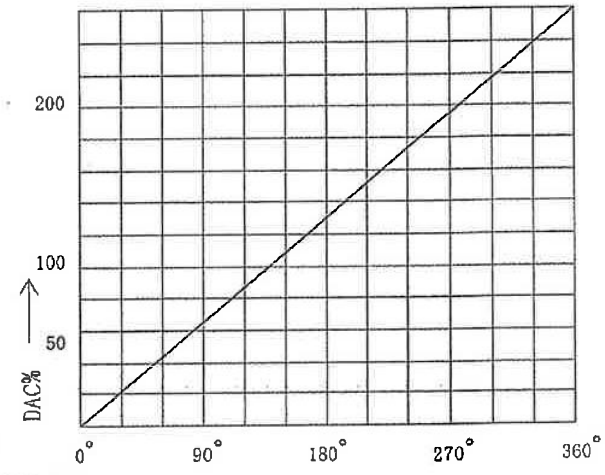
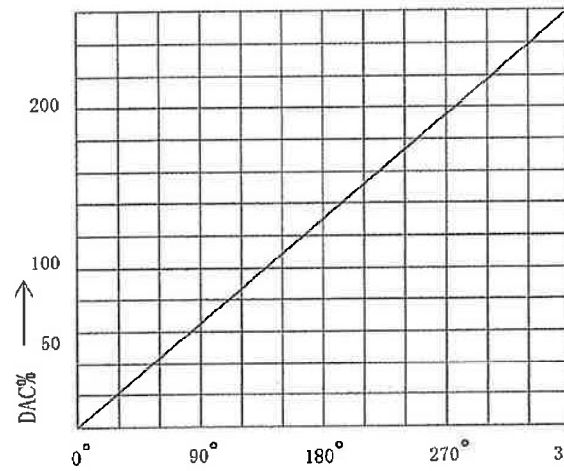
裏波部 45° 下流側



柱状晶伝搬エコー 45° 上流側



柱状晶伝搬エコー 45° 下流側



インデケーションの位置

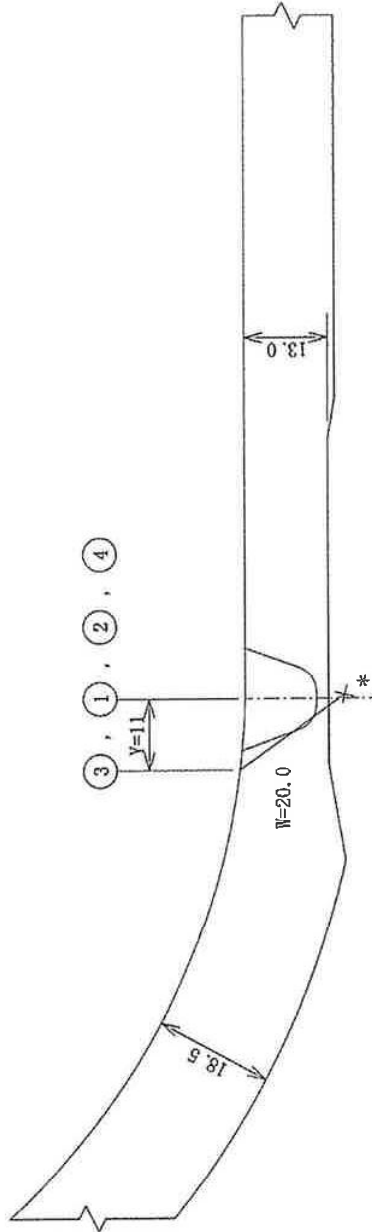
縮尺：1/1

単位：mm

配管系統及びライン名 加圧器スプレインライン (Aループ)



溶接線番号 SW-5 (H2-3911007)



上流側 (エルボ)

下流側 (パイプ)

* : ビーム路程、Y距離を計測し作図した結果、裏波部に位置する。

インデイクエーションの位置

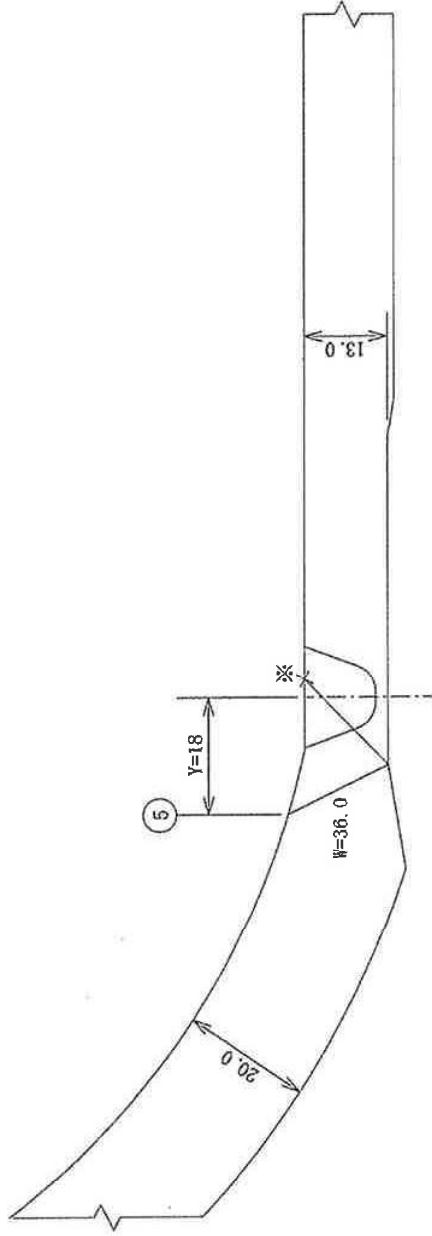
縮尺：1/1

単位：mm

配管系統及びライン名 加圧器スプレライン (A/ループ)



溶接線番号 SW-5(H2-3911007)

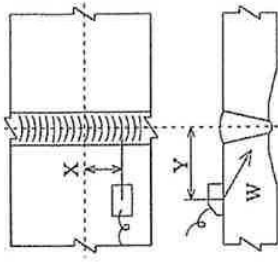


上流側 (エルボ)

下流側 (パイプ)

※：ビームの到達点の波形的変化を指で確認。

超音波探傷データシート a (配管インデケーションの記録)



配管系統及びライン名 加圧器スプレイルライン (Aループ) 溶接線番号 SW-5 (H2-3911007)
 上流側 エルボ 下流側 パイプ 探傷角度 60° (直角)

| 探傷サイド | ピーク指示部 | | | DAC20% | | DAC100% | | 備考 | | | | | | | | | | | | | | |
|-------|--------|-----|-----|-----------|-----------|-----------|-----------|---------|-----|---------|-----|-----------|-------------|-----------|----|-----------|-------------------|-----------|---|----|------|--|
| | 上流側 | 下流側 | 指示部 | 指示範囲 (mm) | 指示長さ (mm) | 指示範囲 (mm) | 指示長さ (mm) | | | | | | | | | | | | | | | |
| 1 | ○ | 30° | -7 | Y (mm) | 19 | W (mm) | 24.0 | CRT (%) | 160 | DAC (%) | 102 | 指示範囲 (mm) | 0° ~ 30° +0 | 指示長さ (mm) | 30 | 指示範囲 (mm) | 30° ~ 30° -8 ~ -6 | 指示長さ (mm) | 2 | 備考 | 裏波部* | |
| | | | | | | | | 以下 | 余白 | | | | | | | | | | | | | |
| | | | | | | | | | | | | | | | | | | | | | | |
| | | | | | | | | | | | | | | | | | | | | | | |
| | | | | | | | | | | | | | | | | | | | | | | |
| | | | | | | | | | | | | | | | | | | | | | | |
| | | | | | | | | | | | | | | | | | | | | | | |
| | | | | | | | | | | | | | | | | | | | | | | |
| | | | | | | | | | | | | | | | | | | | | | | |
| | | | | | | | | | | | | | | | | | | | | | | |

備考 * : 30° 毎の記録点間の最大エコー (ピーク) が前後の記録点のエコー高さを超える反射波を示す。

超音波探傷データシートb (配管インデケーションの記録)

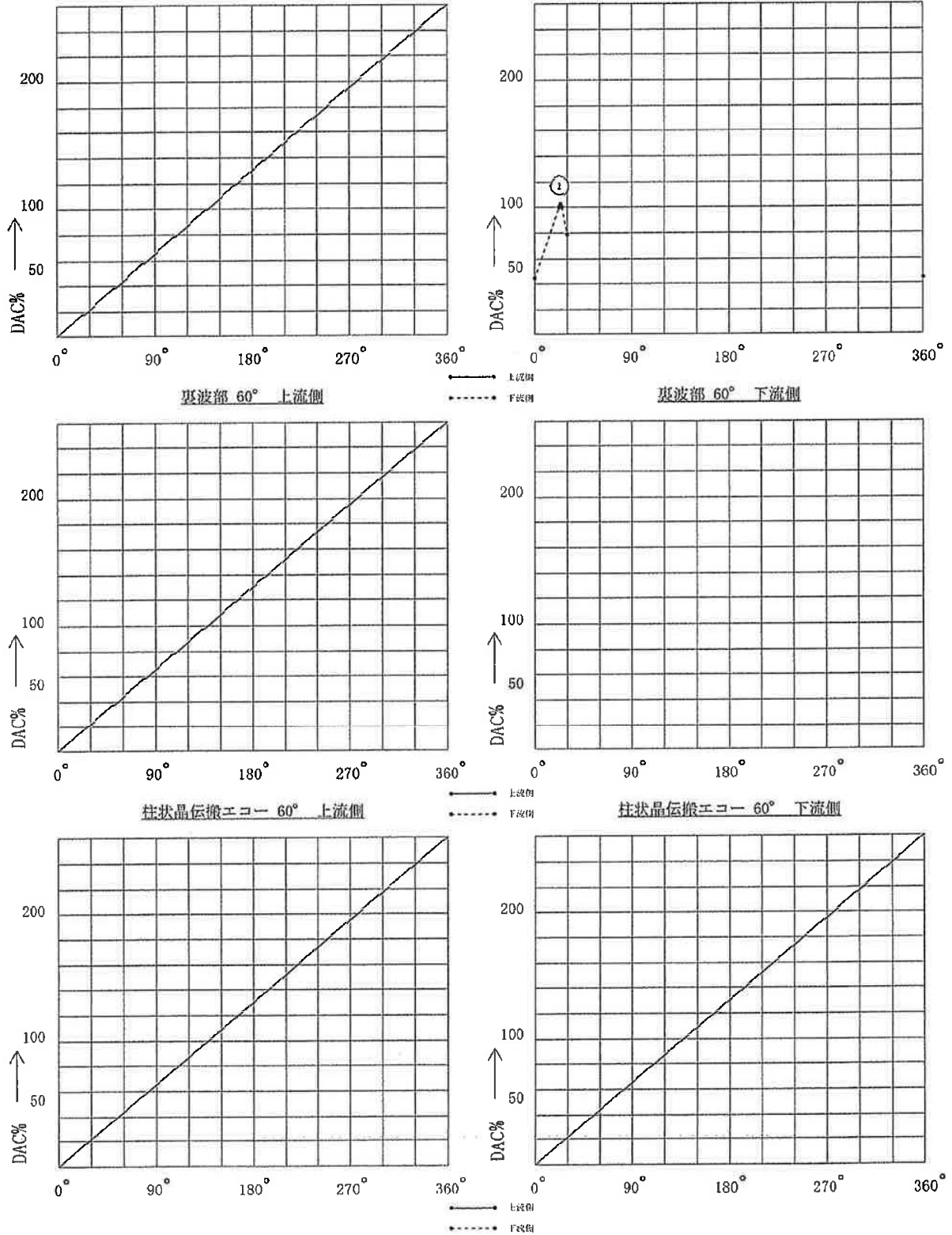
配管系統及びライン名 加圧器スプレイレイン (Aグループ) 溶接線番号 SW-5 (H2-3911007) 探傷角度 60° (直角)

| X位置 | 流 (エルボ) | | | | | | | | | | 流 (パイプ) | | | | | | | | | |
|------|-------------------------------|--------|---------|---------|--------|----------|---------|---------|--------|--------|-----------|---------|--------|----------|---------|---------|--|--|--|--|
| | 裏波部 | | | | | 柱状晶伝線エコー | | | | | 裏波部 | | | 柱状晶伝線エコー | | | | | | |
| | Y (mm) | W (mm) | CRT (%) | DAC (%) | Y (mm) | W (mm) | CRT (%) | DAC (%) | Y (mm) | W (mm) | CRT (%) | DAC (%) | Y (mm) | W (mm) | CRT (%) | DAC (%) | | | | |
| 0° | | | | | | | | | | | | | 18 | 24.0 | 70 | 45 | | | | |
| 30° | | | | | | | | | | | | | 18 | 23.0 | 130 | 79 | | | | |
| 60° | | | | | | | | | | | | | | | | | | | | |
| 90° | | | | | | | | | | | | | | | | | | | | |
| 120° | | | | | | | | | | | | | | | | | | | | |
| 150° | | | | | | | | | | | | | | | | | | | | |
| 180° | | | | | | | | | | | | | | | | | | | | |
| 210° | | | | | | | | | | | | | | | | | | | | |
| 240° | | | | | | | | | | | | | | | | | | | | |
| 270° | | | | | | | | | | | | | | | | | | | | |
| 300° | | | | | | | | | | | | | | | | | | | | |
| 330° | | | | | | | | | | | | | | | | | | | | |
| | 空白欄は隣接する30°芯2点以上にまたがる反射波を認めず。 | | | | | | | | | | | | | | | | | | | |

超音波探傷データシートc (配管-インディケーションのマップ)

配管系統及びライン名 加圧器スプレイライン (Aループ)

溶接線番号 SW-5(H2-3911007)



インデイクエーションの位置

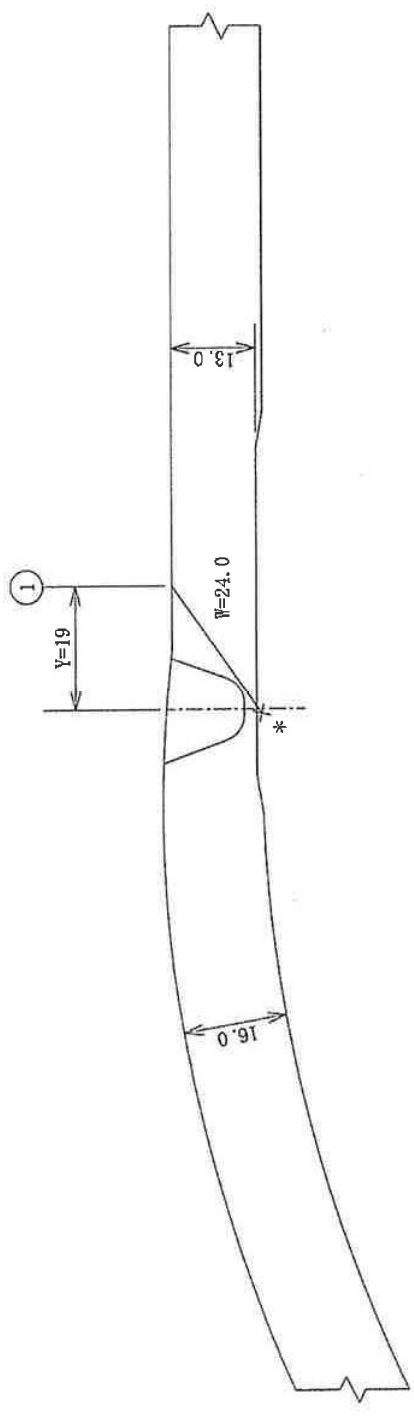
縮尺：1/1

単位：mm

配管系統及びライン名 加圧器スプレイライン (Aループ)



溶接線番号 SW-5 (H2-3911007)



下流側 (パイプ)

上流側 (エルボ)

* : ビーム路程、Y距離を計測し作図した結果、裏波部に位置する。

非破壊検査記録 (/)

(1) 検査の判定

| 項目番号 | カテゴリ | 機器名 | 検査の対象箇所 | 検査箇所 |
|-------|------|-----|---|----------------------|
| B9.11 | B-J | 配管 | 配管の同種金属溶接継手 (呼び径100A以上：周継手) 加圧器スプレイライン (Dループ) | SW-5 (H2-3911015) |

| 検査方法 | | 検査年月日 | 立会 実績 | 結果 | 検査員 | 備考 |
|----------|-------------|--------------|----------|----|-----|----|
| 体積 検査 | 超音波 探傷検査 | 年 月 日 | 有・無 | | | |
| 判定基準 | | 添付-1(4/4)に記載 | | | | |

非破壊検査記録 (/)

(2) 検査記録

検査年月日 _____ 年 月 日

助勢員 A _____

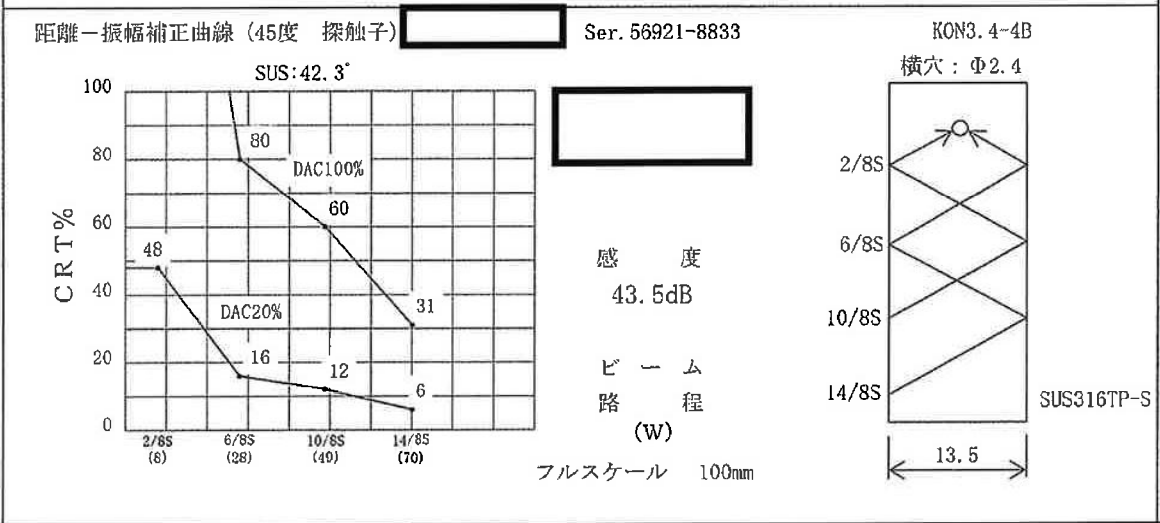
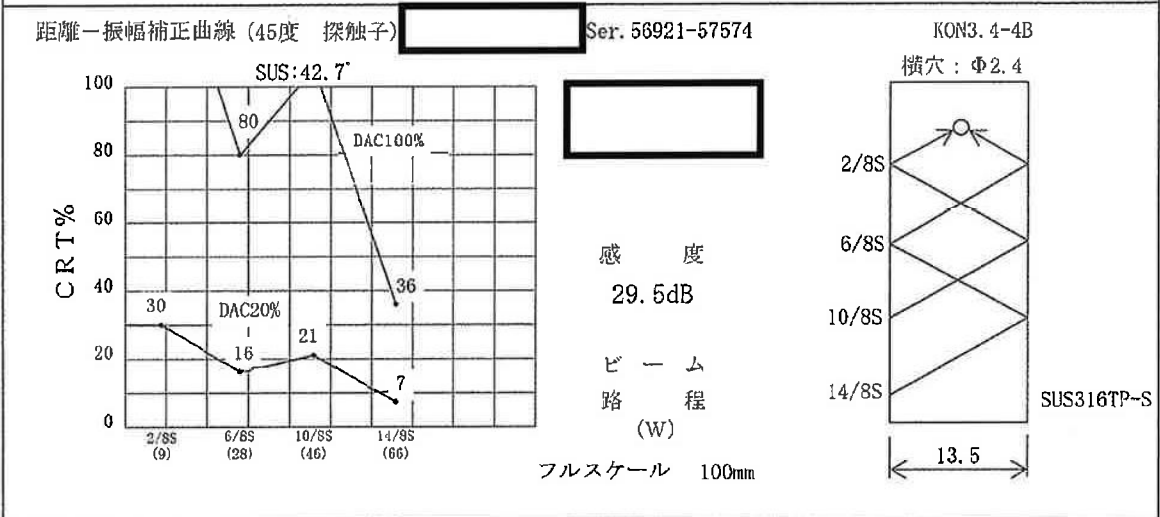
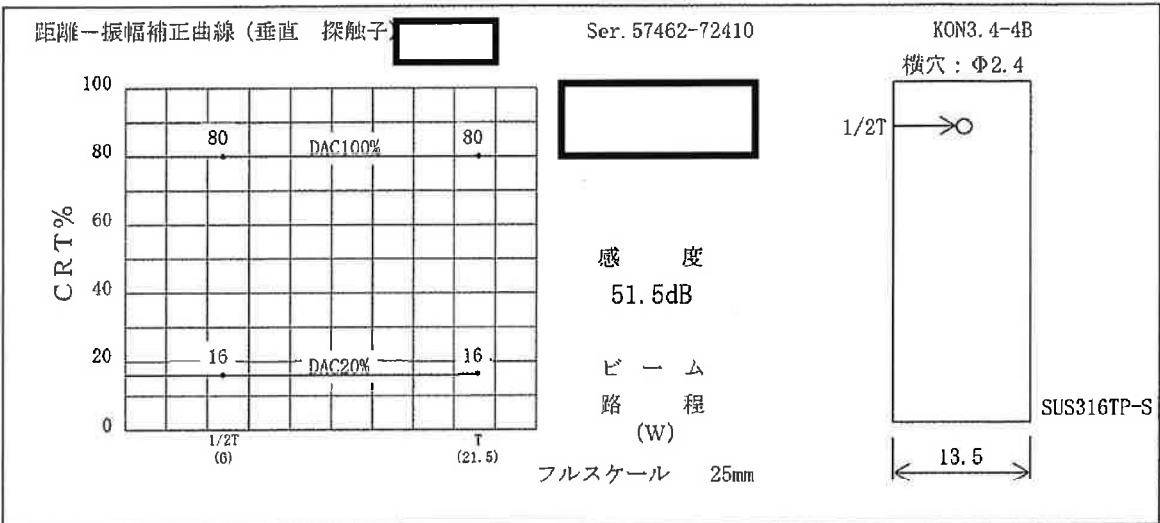
| 項目番号 | カテゴリ | 機器名 | 検査の対象箇所 | 検査箇所 | |
|--------|------|---------|---|----------------------|----|
| B9.11 | B-J | 配管 | 配管の同種金属溶接継手 (呼び径100A以上：周継手) 加圧器スプレイライン (Dループ) | SW-5 (H2-3911015) | |
| | | | | | |
| 検査実施結果 | 検査方法 | | 確認※ | 助勢員 A | 備考 |
| | 体積検査 | 超音波探傷検査 | | | |
| 確認項目 | | | 添付-1(4/4)に記載 | | |
| | | | | | |

※確認項目に対し異常がない場合は、「確認」欄に「レ」と記載する。

超音波探傷検査 (UT) 記録

検査箇所 加圧器スプレイライン (Dループ)

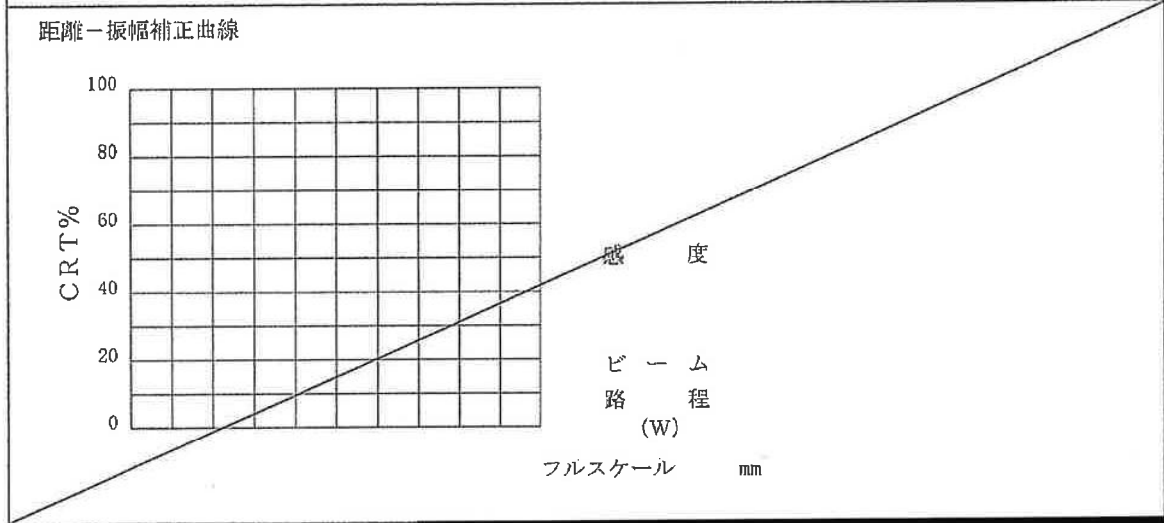
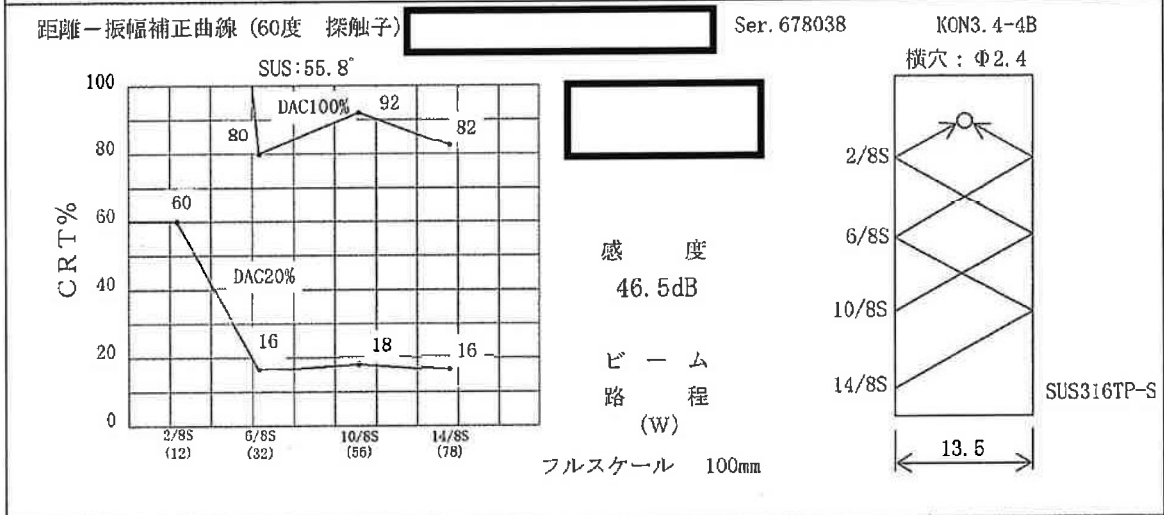
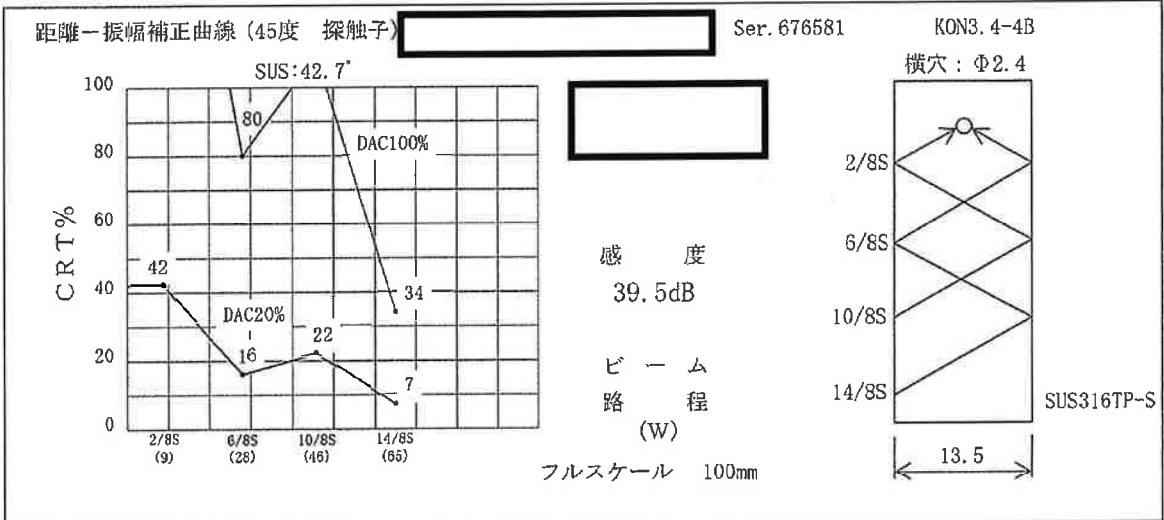
溶接線番号 SW-5 (H2-3911015)



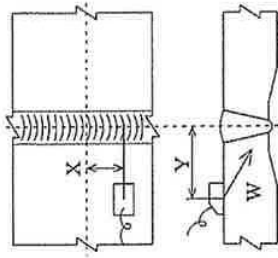
超音波探傷検査 (UT) 記録

検査箇所 加圧器スプレイライン (Dループ)

溶接線番号 SW-5(H2-3911015)



超音波探傷データシート a (配管インデクセーションの記録)

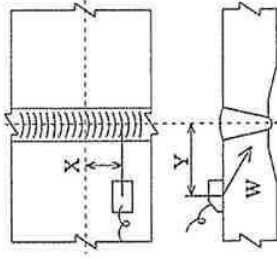


配管系統及びライン名 加圧器スプレライン (Dループ) 溶接線番号 SW-5 (H2-3911015)
 上流側 エルボ 下流側 パイプ 探傷角度 45° (直角)

| 探傷サイド | ピーク指示部 | | | DAC20% | | | DAC100% | | 備考 |
|-------|---------|-----|------|-----------|-----------|--------------------|-----------|-----------|-----------|
| | 上流側 | 下流側 | パイプ | 指示範囲 (mm) | 指示長さ (mm) | 指示長さ (mm) | 指示範囲 (mm) | 指示長さ (mm) | |
| 1 ○ | 90° +11 | 14 | 19.0 | 37 | 33 | 240° +16 ~ 120° +0 | 224 | 224 | 裏波部* |
| 2 ○ | 270° -7 | 13 | 18.0 | 62 | 54 | 240° +16 ~ 120° +0 | 224 | 224 | 裏波部 |
| 3 ○ | 270° +6 | 14 | 20.0 | 38 | 35 | 240° +16 ~ 120° +0 | 224 | 224 | 裏波部* |
| 4 ○ | 300° +6 | 14 | 21.0 | 39 | 37 | 240° +16 ~ 120° +0 | 224 | 224 | 裏波部* |
| 5 ○ | 330° +4 | 14 | 21.0 | 47 | 45 | 240° +16 ~ 120° +0 | 224 | 224 | 裏波部* |
| 6 ○ | 30° +9 | 25 | 37.0 | 53 | 58 | 240° +0 ~ 120° +0 | 240 | 240 | 外表面部 |
| 7 ○ | 0° +2 | 1 | 16.0 | 67 | 54 | 240° +0 ~ 120° +0 | 240 | 240 | 柱状晶伝搬エコー* |
| 8 ○ | 30° +5 | 0 | 15.0 | 58 | 46 | 240° +0 ~ 120° +0 | 240 | 240 | 柱状晶伝搬エコー* |
| 9 ○ | 90° -17 | 0 | 15.0 | 56 | 44 | 240° +0 ~ 120° +0 | 240 | 240 | 柱状晶伝搬エコー* |
| 10 ○ | 90° +9 | 1 | 15.0 | 62 | 49 | 240° +0 ~ 120° +0 | 240 | 240 | 柱状晶伝搬エコー* |
| 11 ○ | 240° +8 | 0 | 15.0 | 35 | 28 | 240° +0 ~ 120° +0 | 240 | 240 | 柱状晶伝搬エコー* |

備考 * : 30° 毎の記録点間の最大エコー (ピーク) が前後の記録点のエコー高さを超える反射波を示す。

超音波探傷データシート a (配管インデインケーションの記録)



配管系統及びライン名 加圧器スプレインライン (Dループ)

溶接線番号 SW-5(H2-3911015)

上流側 エルボ

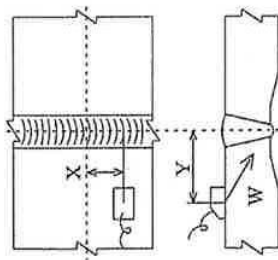
下流側 パイプ

探傷角度 45° (直角)

| 探傷サイド | ピーク指示部 | | | DAC 20% | | DAC 100% | | 備考 |
|-------|----------|-----|--------|---------|---------|---------------------------|-----------|-----------|
| | 上流側 | 下流側 | W (mm) | CRT (%) | DAC (%) | 指示長さ (mm) | 指示長さ (mm) | |
| ○ | 300° +5 | 0 | 15.0 | 39 | 31 | 240° ~ +0 +0 ~ 120° +0 | 240 | 柱状晶伝搬エコー* |
| ○ | 30° -8 | 14 | 21.0 | 45 | 43 | 0° ~ +11 30° ~ -2 | 17 | 裏波部 |
| ○ | 60° -6 | 14 | 20.0 | 29 | 27 | 60° ~ -13 60° ~ -3 | 10 | 裏波部 |
| ○ | 60° +7 | 14 | 20.0 | 26 | 24 | 60° ~ +2 60° ~ +10 | 8 | 裏波部 |
| ○ | 90° +5 | 14 | 20.0 | 27 | 25 | 90° ~ +4 90° ~ +6 | 2 | 裏波部 |
| ○ | 90° +10 | 13 | 20.0 | 25 | 23 | 90° ~ +9 90° ~ +11 | 2 | 裏波部 |
| ○ | 180° -13 | 14 | 20.0 | 40 | 37 | 150° ~ +11 180° ~ -7 | 12 | 裏波部 |
| ○ | 180° +17 | 13 | 20.0 | 68 | 63 | 180° ~ +7 210° ~ -1 | 22 | 裏波部 |
| ○ | 240° -10 | 13 | 20.0 | 49 | 45 | 210° ~ +13 240° ~ -2 | 15 | 裏波部 |
| ○ | 270° +12 | 14 | 21.0 | 29 | 28 | 270° ~ +8 300° ~ -7 | 15 | 裏波部 |
| ○ | 300° +7 | 13 | 20.0 | 42 | 39 | 300° ~ +3 300° ~ +16 | 13 | 裏波部 |

備考 * : 30° 毎の記録点間の最大エコー (ピーク) が前後の記録点のエコー高さを超える反射波を示す。

超音波探傷データシート a (配管インデケーションの記録)



配管系統及びライン名 加圧器スプレイレイン (Dループ) 溶接線番号 SW-5(H2-3911015)
 上流側 エルボ 下流側 パイプ 探傷角度 45° (直角)

| 探傷サイド | ピーク指示部 | | | DAC 20% | | DAC 100% | | 備考 | |
|-------|----------|-----|------|-----------|-----------|------------|------------|-----|----------|
| | 上流側 | 下流側 | 指示部 | 指示範囲 (mm) | 指示長さ (mm) | 指示範囲 (mm) | 指示長さ (mm) | | |
| ○ | 330° +8 | 14 | 21.0 | 44 | 42 | 330° ~ -12 | 0° ~ -8 | 34 | 裏波部 |
| ○ | 270° +13 | 24 | 35.0 | 55 | 62 | 全周 | | 360 | 外表面部 |
| ○ | 30° +5 | 0 | 15.0 | 57 | 45 | 30° ~ -10 | 30° ~ +9 | 19 | 柱状晶伝搬エコー |
| ○ | 60° -4 | 0 | 15.0 | 36 | 29 | 60° ~ -7 | 60° ~ +1 | 8 | 柱状晶伝搬エコー |
| ○ | 60° +10 | 0 | 15.0 | 36 | 29 | 60° ~ +6 | 60° ~ +12 | 6 | 柱状晶伝搬エコー |
| ○ | 90° -7 | 1 | 16.0 | 32 | 26 | 90° ~ -11 | 90° ~ -4 | 7 | 柱状晶伝搬エコー |
| ○ | 120° -5 | 1 | 16.0 | 43 | 35 | 120° ~ -11 | 120° ~ -2 | 9 | 柱状晶伝搬エコー |
| ○ | 150° +13 | 0 | 15.0 | 62 | 49 | 150° ~ +7 | 150° ~ +19 | 12 | 柱状晶伝搬エコー |
| ○ | 330° -16 | 0 | 15.0 | 36 | 29 | 300° ~ +8 | 330° ~ -8 | 14 | 柱状晶伝搬エコー |
| ○ | 330° +11 | 0 | 15.0 | 32 | 26 | 330° ~ +9 | 0° ~ -12 | 9 | 柱状晶伝搬エコー |
| | | | | | 余白 | | | | |

備考

超音波探傷データシート b (配管インデケーションの記録)

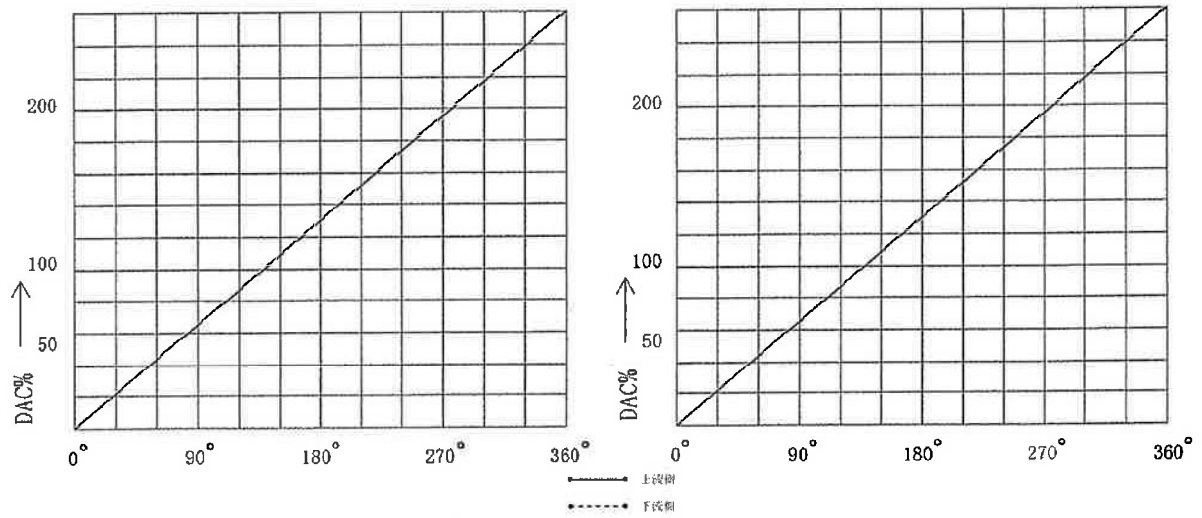
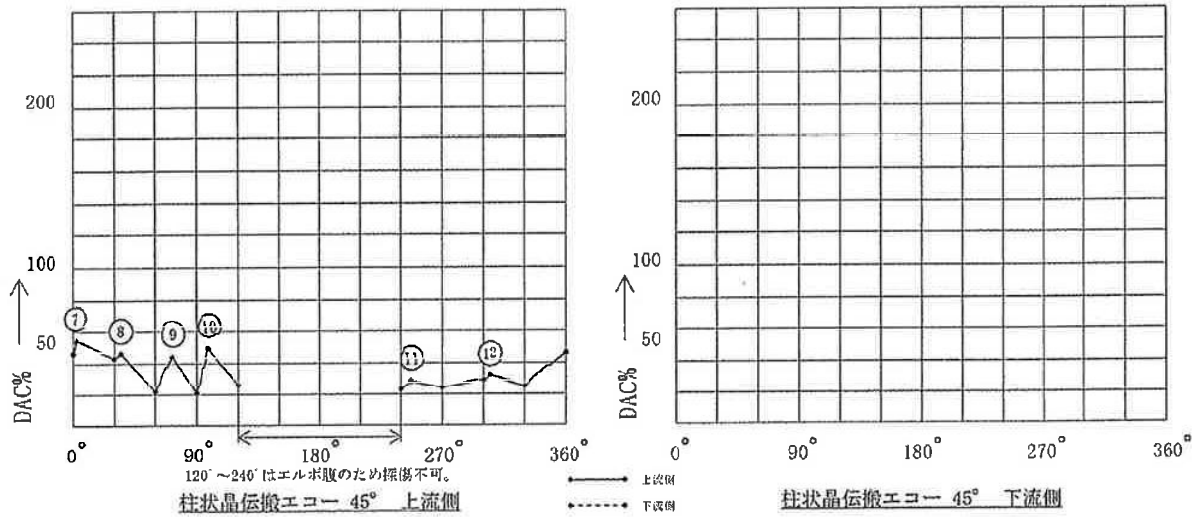
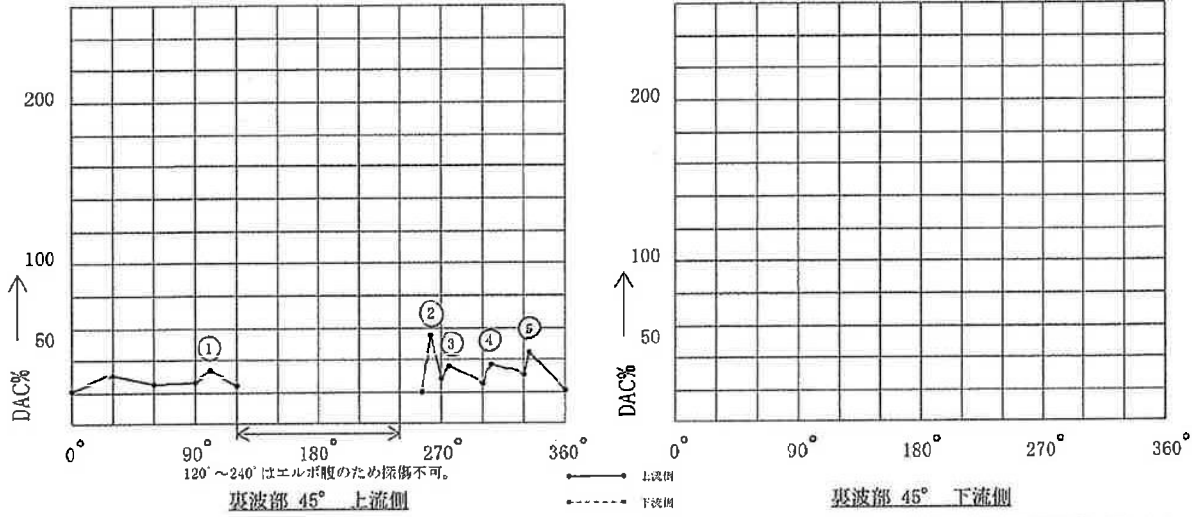
配管系統及びライン名 加圧器スプライン (Dループ) 溶接線番号 SW-5 (H2-391101E) 探傷角度 45° (直角)

| X位置 | 上 流 (エルボ) | | | | | | 下 流 (パイプ) | | | | | |
|------|-------------------------------|--------|---------|----------|--------|--------|-------------------------------|---------|--------|----------|---------|---------|
| | 裏波部 | | | 柱状晶伝線エコー | | | 裏波部 | | | 柱状晶伝線エコー | | |
| | Y (mm) | W (mm) | CRT (%) | DAC (%) | Y (mm) | W (mm) | CRT (%) | DAC (%) | Y (mm) | W (mm) | CRT (%) | DAC (%) |
| 0° | 13 | 21.0 | 22 | 21 | 1 | 16.0 | 56 | 46 | | | | |
| 30° | 14 | 21.0 | 32 | 31 | 1 | 16.0 | 53 | 43 | | | | |
| 60° | 14 | 20.0 | 27 | 25 | 1 | 15.0 | 28 | 22 | | | | |
| 90° | 14 | 20.0 | 28 | 26 | 1 | 16.0 | 26 | 21 | | | | |
| 120° | 14 | 22.0 | 24 | 24 | 0 | 15.0 | 33 | 26 | | | | |
| 150° | — | — | — | — | — | — | — | — | | | | |
| 180° | — | — | — | — | — | — | — | — | | | | |
| 210° | — | — | — | — | — | — | — | — | | | | |
| 240° | | | | | 0 | 15.0 | 29 | 23 | | | | |
| 270° | 13 | 19.0 | 32 | 29 | 1 | 16.0 | 29 | 24 | | | | |
| 300° | 13 | 19.0 | 28 | 25 | 1 | 16.0 | 36 | 29 | | | | |
| 330° | 13 | 21.0 | 32 | 31 | 1 | 16.0 | 31 | 25 | | | | |
| | 120°~240° はエルボ順のため探傷不可。 | | | | | | 120°~240° はエルボ順のため探傷不可。 | | | | | |
| | 空白欄は隣接する30°芯2点以上にまたがる反射波を認めず。 | | | | | | 空白欄は隣接する30°芯2点以上にまたがる反射波を認めず。 | | | | | |

超音波探傷データシート c (配管-インディケーションのマップ)

配管系統及びライン名 加圧器スプレイライン (Dループ)

溶接線番号 SW-5(H2-3911015)



インデイクエーションの位置

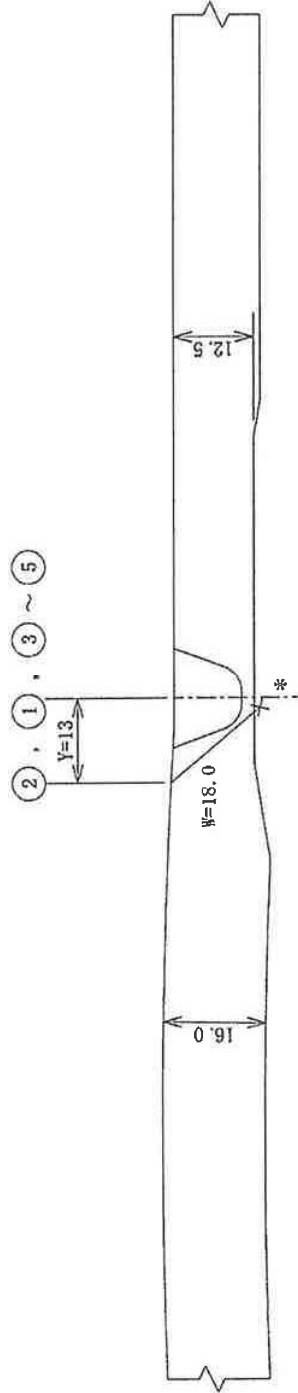
縮尺：1/1

単位：mm

配管系統及びライン名 加圧器スプレイン (Dループ)



溶接線番号 SW-5 (H2-3911015)



上流側 (エルボ)

下流側 (パイプ)

* : ビーム路程、Y距離を計測し作図した結果、裏波部に位置する。

インデイクエーションの位置

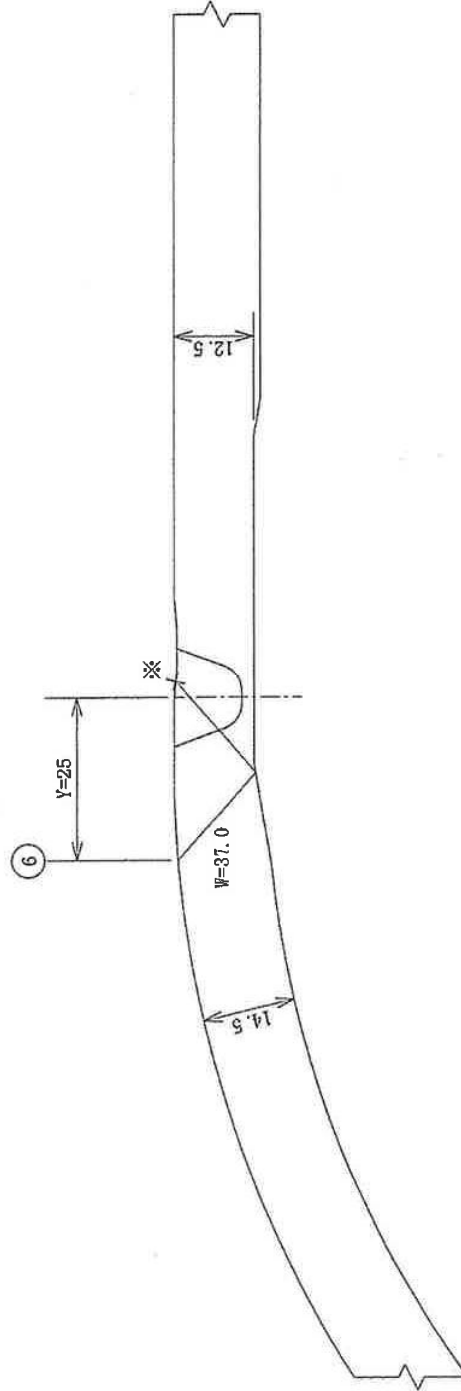
縮尺：1/1

単位：mm

配管系統及びライン名 加圧器スプレイライン (Dループ)



溶接線番号 SW-5 (H2-3911016)



上流側 (エルボ)

下流側 (パイプ)

※：ビームの到達点の波形の変化を指で確認。

インデイクエーションの位置

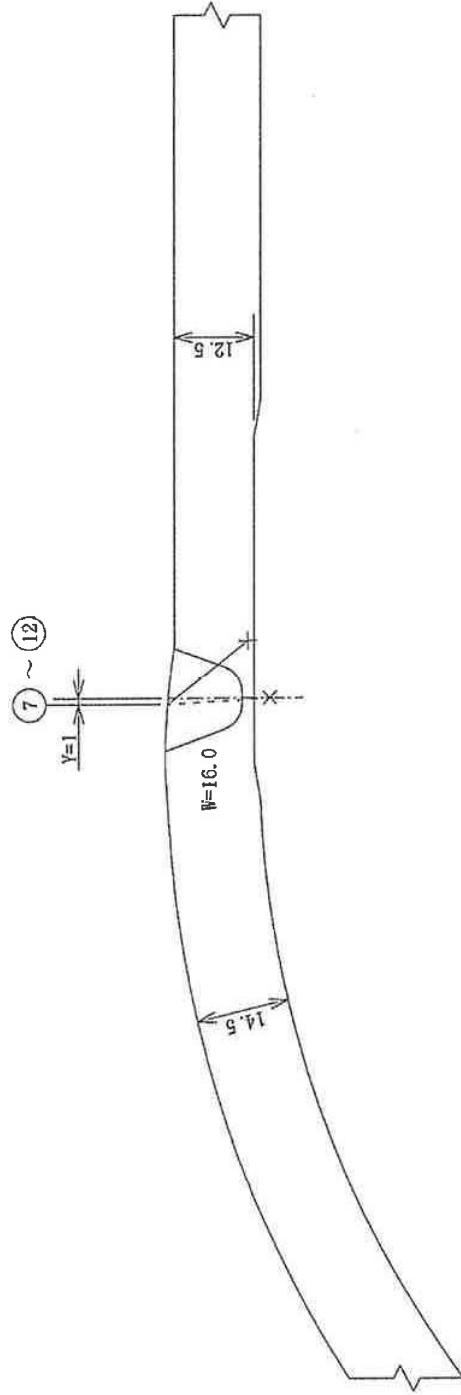
縮尺：1/1

単位：mm

配管系統及びライン名 加圧器スプレイン (Dループ)



溶接線番号 SN-5 (H2-3911015)



上流側 (エルボ)

下流側 (パイプ)

---: 破線の様に進んだと思われる。

インデイクエーションの位置

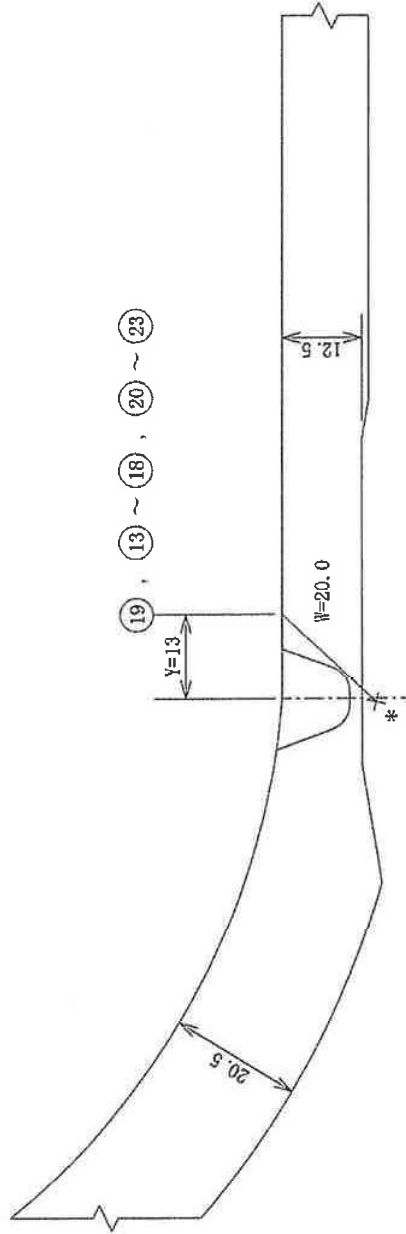
縮尺：1/1

単位：mm

配管系統及びライン名 加圧器スプレイン (Dループ)



溶接線番号 SN-5(H2-3911015)



上流側 (エルボ)

下流側 (パイプ)

* : ビーム路程、Y距離を計測し作図した結果、裏波部に位置する。

インデケーションの位置

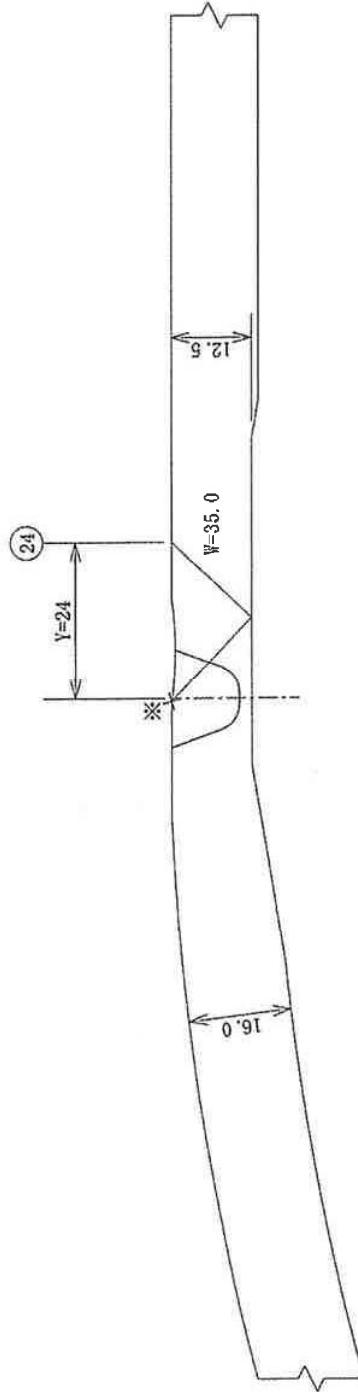
縮尺：1/1

単位：mm

配管系統及びライン名 加圧器スプレイン (Dループ)



溶接線番号 SW-5 (H2-3911015)



上流側 (エルボ)

下流側 (パイプ)

※：ビームの到達点の波形的変化を指で確認。

インデケーションの位置

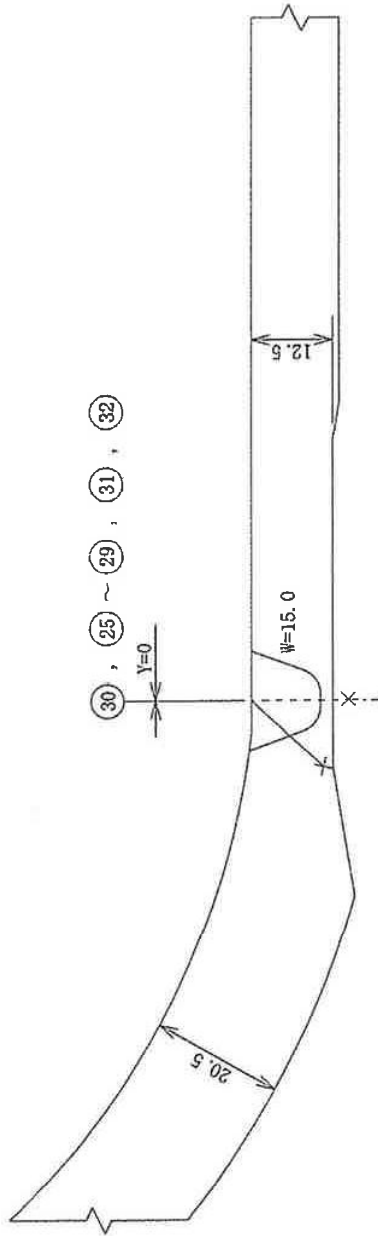
縮尺：1/1

単位：mm

配管系統及びライン名 加圧器スプレイン (Dループ)



溶接線番号 SW-5(H2-3911015)

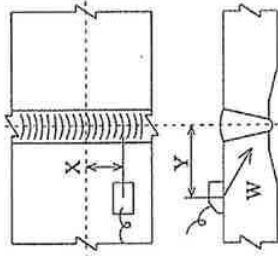


上流側 (エルボ)

下流側 (パイプ)

--- : 破線の様に進んだと思われる。

超音波探傷データシート a (配管インデケーションの記録)



配管系統及びライン名 加圧器スプレインライン (Dループ) 溶接線番号 SW-5(H2-3911015) 探傷角度 45° (小型探触子) (直角)

上流側 エルボ 下流側 パイプ

| 探傷サイド | ピーク指示部 | | | DAC 20% | | DAC 100% | | 備考 |
|--------|----------|--------|--------|---------|---------|-------------------|-----------|-----------|
| | X (mm) | Y (mm) | W (mm) | CRT (%) | DAC (%) | 指示長さ (mm) | 指示長さ (mm) | |
| 1 ○ | 120° +15 | 12 | 19.0 | 41 | 29 | 120° ~ 240° +0 | 120 | 裏波部* |
| 2 ○ | 180° -6 | 13 | 21.0 | 39 | 31 | 120° ~ 240° +0 | 120 | 裏波部* |
| 3 ○ | 210° -7 | 12 | 20.0 | 82 | 61 | 120° ~ 240° +0 | 120 | 裏波部* |
| 4 ○ | 240° -7 | 12 | 20.0 | 68 | 51 | 120° ~ 240° +0 | 120 | 裏波部* |
| 5 ○ | 180° -14 | 24 | 36.0 | 110 | 118 | 120° ~ 240° +0 | 120 | 外表面部 |
| 6 ○ | 120° +12 | 1 | 15.0 | 110 | 66 | 120° ~ 240° +0 | 120 | 柱状晶伝搬エコー* |
| 7 ○ | 180° -15 | 1 | 15.0 | 104 | 62 | 120° ~ 240° +0 | 120 | 柱状晶伝搬エコー* |
| 8 ○ | 210° -3 | 1 | 16.0 | 148 | 92 | 120° ~ 240° +0 | 120 | 柱状晶伝搬エコー* |
| 9 ○ | 240° -6 | 1 | 16.0 | 172 | 107 | 120° ~ 240° +0 | 120 | 柱状晶伝搬エコー* |
| | | | | 以下 | 余白 | | | |
| | | | | | | | | |

備考 * : 30° 毎の記録点間の最大エコー (ピーク) が前後の記録点のエコー高さを超える反射波を示す。

超音波探傷データシートb (配管インデケーションの記録)

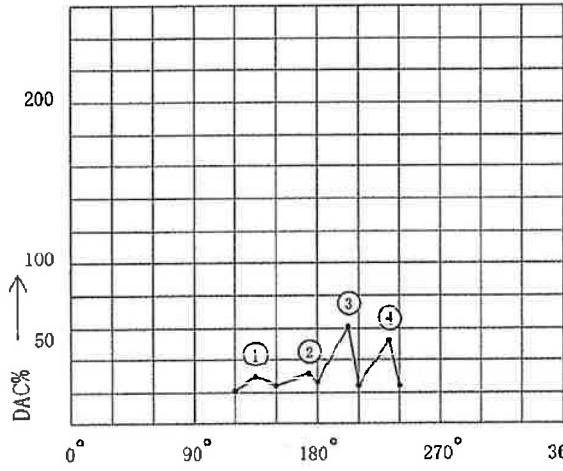
配管系統及びライン名 加圧器スプレイレイン (Dループ) 溶接線番号 SW-5 (H2-3911015) 探傷角度 45° (小型探触子) (直角)

| X位置 | 流 (エルボ) | | | | | | | | | | | | 流 (パイプ) | | | | | | | | | | | |
|--------|-----------|---------|---------|----------|--------|---------|---------|--------|--------|----------|---------|--------|-----------|---------|---------|----------|--------|---------|---------|--------|--------|----------|---------|--|
| | 上 | | | | | | 下 | | | | | | 上 | | | | | | 下 | | | | | |
| | 裏波部 | | | 柱状晶伝搬エコー | | | 裏波部 | | | 柱状晶伝搬エコー | | | 裏波部 | | | 柱状晶伝搬エコー | | | 裏波部 | | | 柱状晶伝搬エコー | | |
| Y (mm) | W (mm) | CRT (%) | DAC (%) | Y (mm) | W (mm) | CRT (%) | DAC (%) | Y (mm) | W (mm) | CRT (%) | DAC (%) | Y (mm) | W (mm) | CRT (%) | DAC (%) | Y (mm) | W (mm) | CRT (%) | DAC (%) | Y (mm) | W (mm) | CRT (%) | DAC (%) | |
| 0° | | | | | | | | | | | | | | | | | | | | | | | | |
| 30° | | | | | | | | | | | | | | | | | | | | | | | | |
| 60° | | | | | | | | | | | | | | | | | | | | | | | | |
| 90° | | | | | | | | | | | | | | | | | | | | | | | | |
| 120° | 13 | 20.0 | 28 | 21 | 1 | 16.0 | 82 | 51 | | | | | | | | | | | | | | | | |
| 150° | 12 | 20.0 | 32 | 24 | 0 | 15.0 | 82 | 49 | | | | | | | | | | | | | | | | |
| 180° | 12 | 20.0 | 35 | 26 | 1 | 16.0 | 78 | 49 | | | | | | | | | | | | | | | | |
| 210° | 12 | 20.0 | 32 | 24 | 1 | 16.0 | 130 | 81 | | | | | | | | | | | | | | | | |
| 240° | 13 | 20.0 | 32 | 24 | 1 | 16.0 | 108 | 67 | | | | | | | | | | | | | | | | |
| 270° | | | | | | | | | | | | | | | | | | | | | | | | |
| 300° | | | | | | | | | | | | | | | | | | | | | | | | |
| 330° | | | | | | | | | | | | | | | | | | | | | | | | |

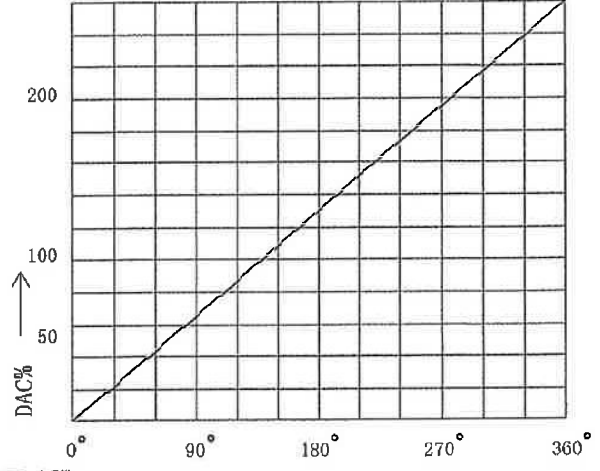
超音波探傷データシートc (配管-インディケーションのマップ)

配管系統及びライン名 加圧器スプレイライン (Dループ)

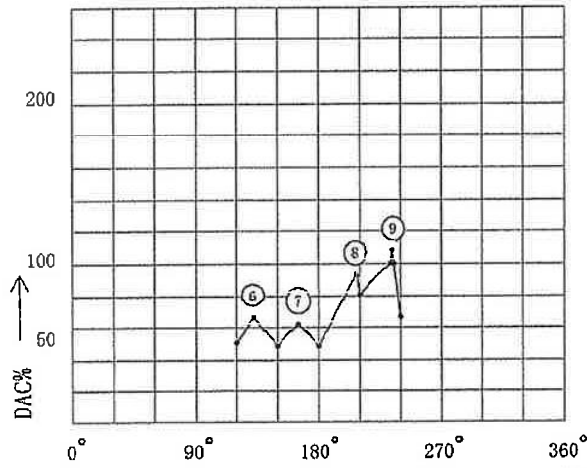
溶接線番号 SW-5 (H2-3911015) (小型探触子)



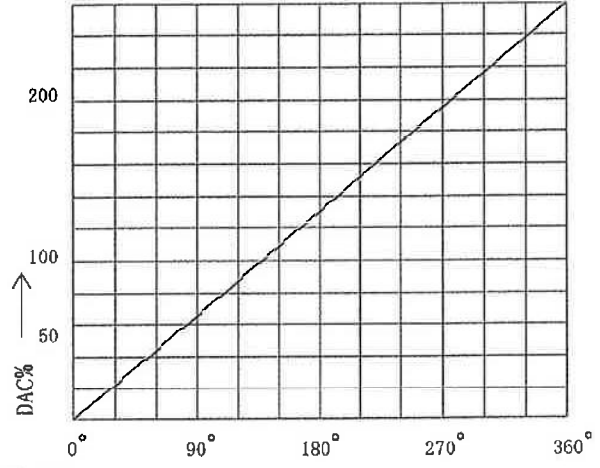
裏波部 45° 上流側



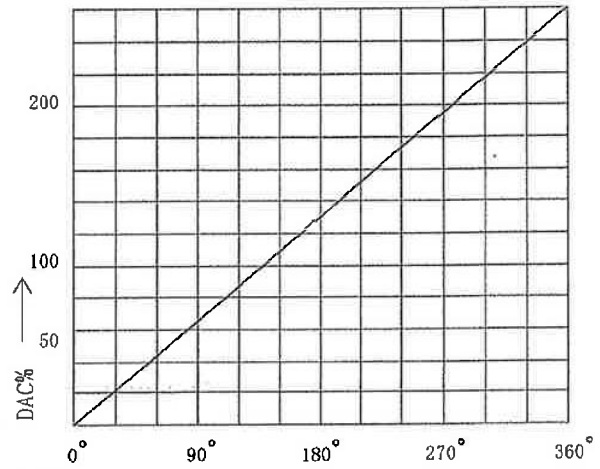
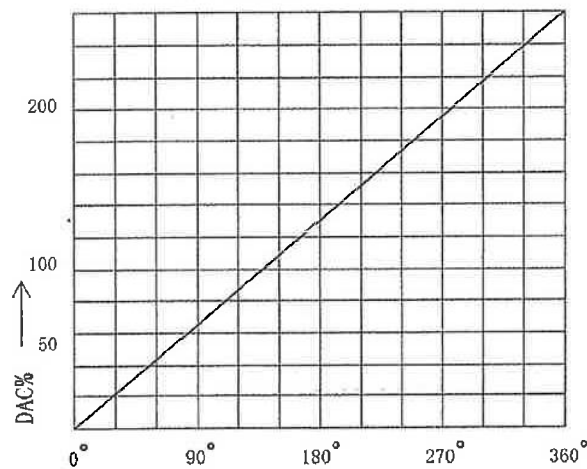
裏波部 45° 下流側



柱状晶伝搬エコー 45° 上流側



柱状晶伝搬エコー 45° 下流側



インデイクエーションの位置

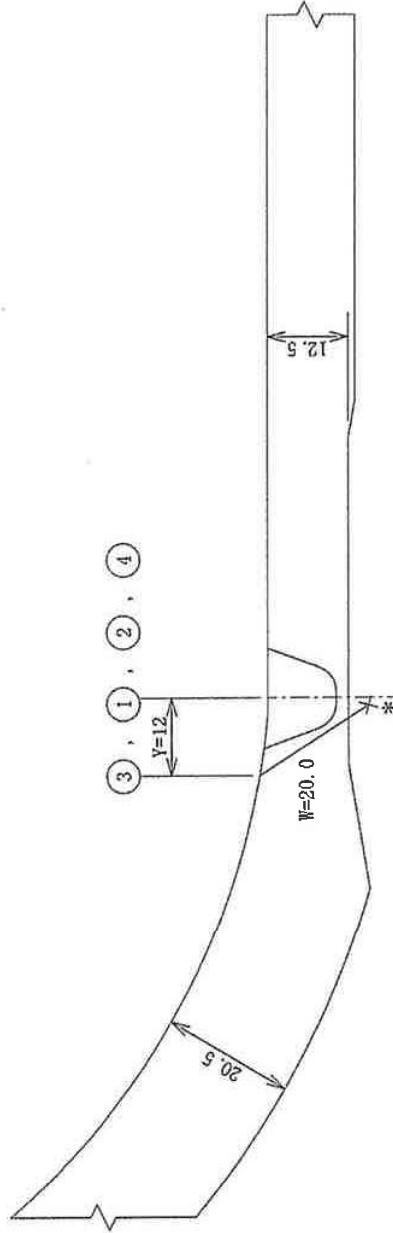
縮尺: 1/1

単位: mm

配管系統及びライン名 加圧器スプレイライン (Dループ)



溶接線番号 SW-5(H2-3911015)



上流側 (エルボ)

下流側 (パイプ)

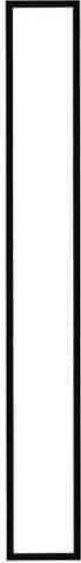
* : ビーム路程、Y距離を計測し作図した結果、裏波部に位置する。

インデイクエーションの位置

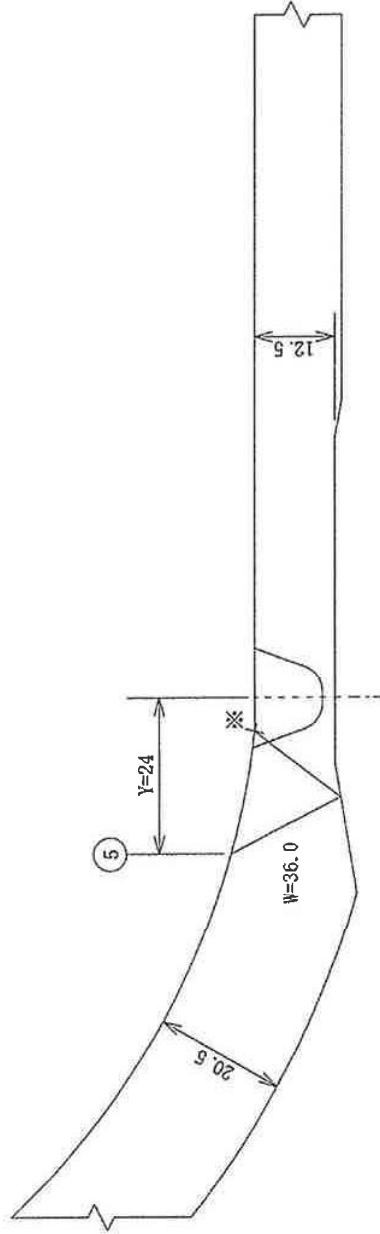
縮尺：1/1

単位：mm

配管系統及びライン名 加圧器スプレイン (Dループ)



溶接線番号 SN-5(H2-3911015)



上流側 (エルボ)

下流側 (パイプ)

※：ビームの到達点の波形の変化を指で確認。

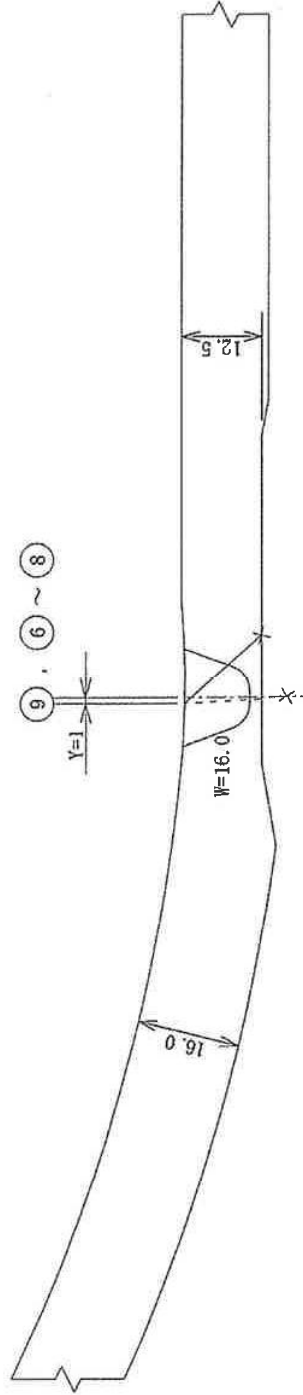
インデイクエーションの位置

縮尺：1/1
単位：mm

配管系統及びライン名 加圧器スプレイトライン (Dループ)



溶接線番号 SW-5 (H2-3911015)

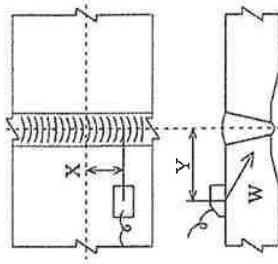


上流側 (エルボ)

下流側 (パイプ)

---: 破線の様に進んだと思われる。

超音波探傷データシート a (配管-インデクセションの記録)



配管系統及びライン名 加圧器スプレイレイン (Dループ) _____ 溶接線番号 SW-5(H2-3911015) _____
 上流側 エルボ _____ 下流側 パイプ _____ 探傷角度 60° (小型探触子) (直角)

| 探傷サイド | ピーク指示部 | | | DAC20% | | | DAC100% | | | 備考 |
|-------|------------|-----|---------|-------------------------|-----------|-----------|-----------|-----------|-----------|-----------|
| | 上流側 | 下流側 | CRT (%) | 指示範囲 (mm) | 指示長さ (mm) | 指示長さ (mm) | 指示範囲 (mm) | 指示長さ (mm) | 指示長さ (mm) | |
| 1 | 240° -3 | 18 | 56 | 210° +0 ~ 240° +0 | 30 | | | | | 裏波部* |
| 2 | 210° +9 | 0 | 170 | 210° +0 ~ 240° +0 | 30 | | | | | 柱状晶伝搬エコー* |
| | | | 以下 | | | | | | | |
| | | | | | | | | | | |
| | | | | | | | | | | |
| | | | | | | | | | | |
| | | | | | | | | | | |
| | | | | | | | | | | |
| | | | | | | | | | | |
| | | | | | | | | | | |
| | | | | | | | | | | |
| | | | | | | | | | | |
| | | | | | | | | | | |
| | | | | | | | | | | |
| | | | | | | | | | | |
| | | | | | | | | | | |
| | | | | | | | | | | |

備考 *: 30° 毎の記録点間の最大エコー (ピーク) が前後の記録点のエコー高さを超える反射波を示す。

超音波探傷データシートb (配管インデケーションの記録)

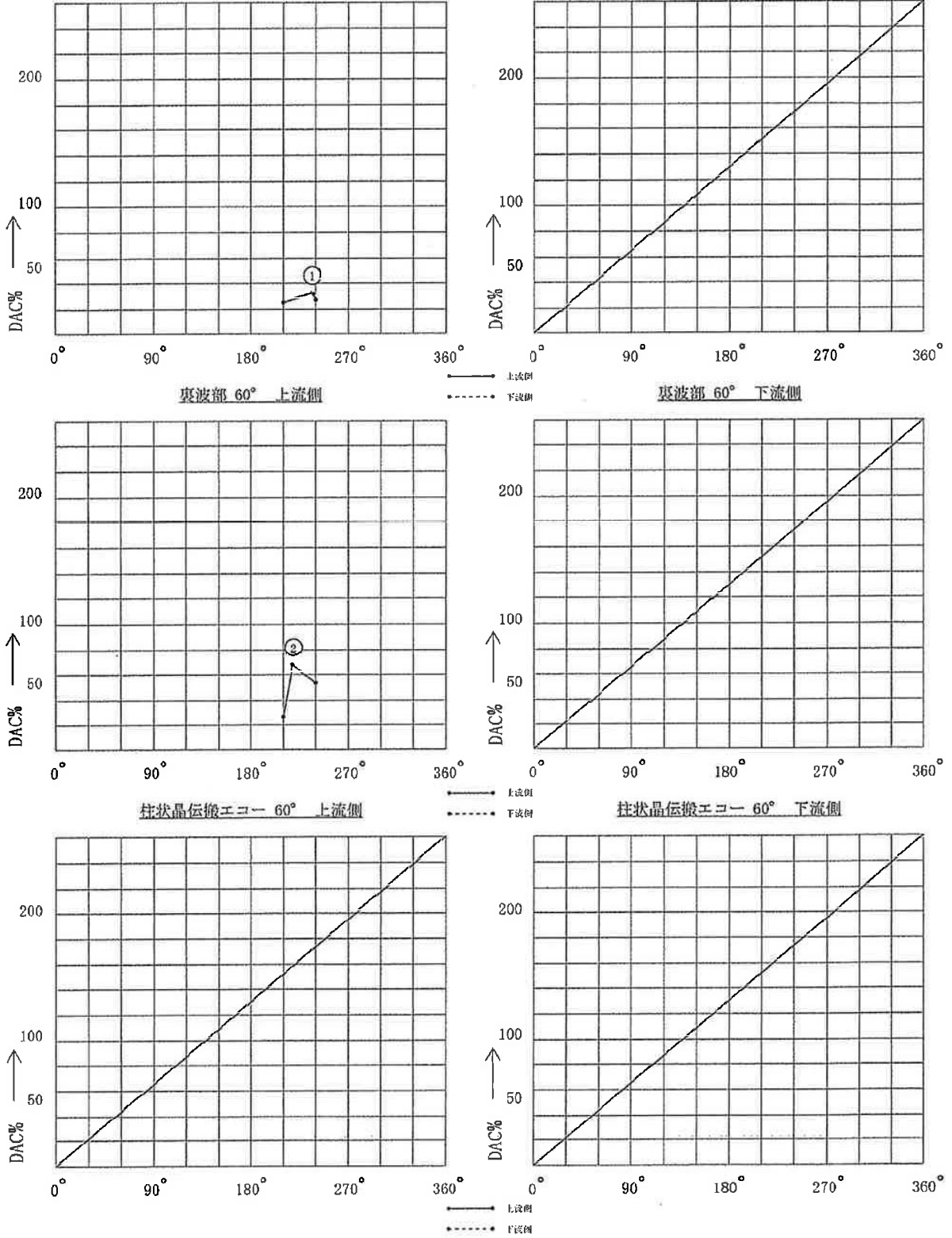
配管系統及びライン名 加圧器スプレイルライン (Dループ) 溶接線番号 SW-5 (H2-3911015) 探傷角度 60° (小型探触子) (直角)

| X位置 | 流 (エルボ) | | | | | | | | | | | | 流 (パイプ) | | | | | | | | | | | | |
|------|-----------|--------|---------|----------|--------|--------|---------|---------|--------|----------|---------|---------|-----------|--------|---------|----------|--------|--------|---------|---------|--------|----------|---------|---------|--|
| | 上 | | | | | | 下 | | | | | | 上 | | | | | | 下 | | | | | | |
| | 裏波部 | | | 柱状晶伝播エコー | | | 裏波部 | | | 柱状晶伝播エコー | | | 裏波部 | | | 柱状晶伝播エコー | | | 裏波部 | | | 柱状晶伝播エコー | | | |
| | Y (mm) | W (mm) | CRT (%) | DAC (%) | Y (mm) | W (mm) | CRT (%) | DAC (%) | Y (mm) | W (mm) | CRT (%) | DAC (%) | Y (mm) | W (mm) | CRT (%) | DAC (%) | Y (mm) | W (mm) | CRT (%) | DAC (%) | Y (mm) | W (mm) | CRT (%) | DAC (%) | |
| 0° | | | | | | | | | | | | | | | | | | | | | | | | | |
| 30° | | | | | | | | | | | | | | | | | | | | | | | | | |
| 60° | | | | | | | | | | | | | | | | | | | | | | | | | |
| 90° | | | | | | | | | | | | | | | | | | | | | | | | | |
| 120° | | | | | | | | | | | | | | | | | | | | | | | | | |
| 150° | | | | | | | | | | | | | | | | | | | | | | | | | |
| 180° | | | | | | | | | | | | | | | | | | | | | | | | | |
| 210° | 18 | 24.0 | 42 | 25 | 0 | 16.0 | 69 | 27 | | | | | | | | | | | | | | | | | |
| 240° | 18 | 23.0 | 48 | 27 | 0 | 15.0 | 144 | 54 | | | | | | | | | | | | | | | | | |
| 270° | | | | | | | | | | | | | | | | | | | | | | | | | |
| 300° | | | | | | | | | | | | | | | | | | | | | | | | | |
| 330° | | | | | | | | | | | | | | | | | | | | | | | | | |

超音波探傷データシート c (配管-インディケーションのマップ)

配管系統及びライン名 加圧器スプレイライン (Dループ)

溶接線番号 SW-5(H2-3911015) (小型探触子)



インデイクエーションの位置

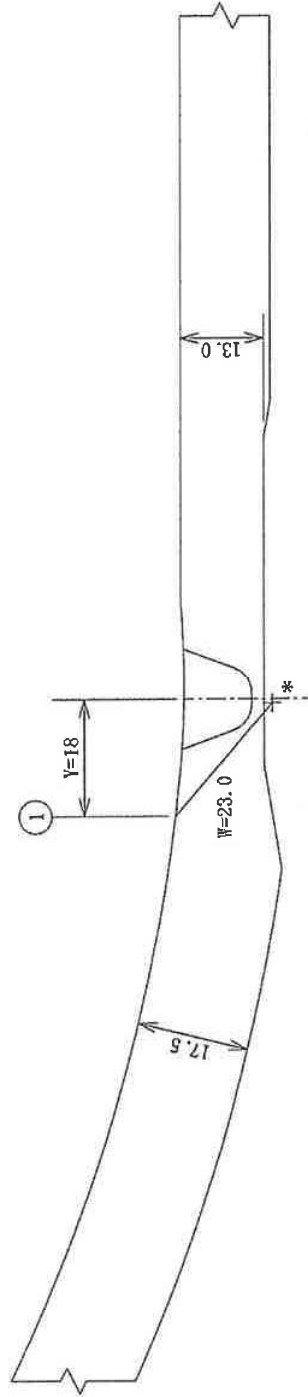
縮尺：1/1

単位：mm

配管系統及びライン名 加圧器スプレライン (D.ループ)



溶接線番号 SW-5 (H2-3911015)



上流側 (エルボ)

下流側 (パイプ)

* : ビーム路程、Y距離を計測し作図した結果、裏波部に位置する。

インデイクエーションの位置

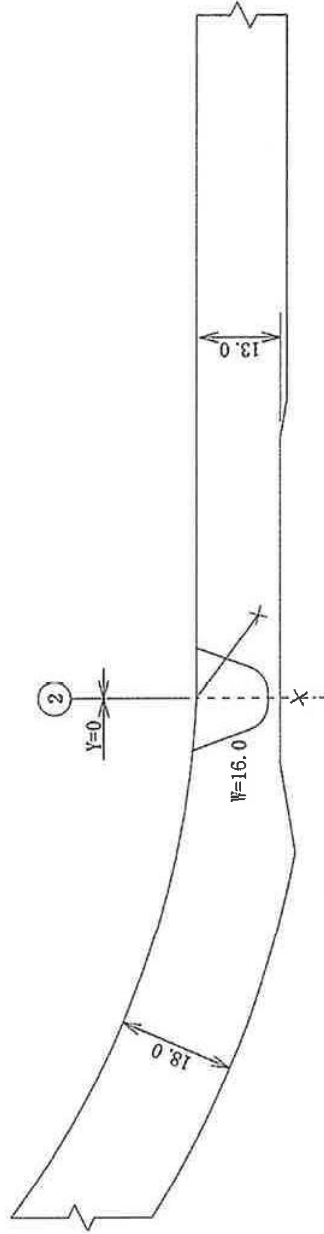
縮尺：1/1

単位：mm

配管系統及びライン名 加圧器スプレイレイン (Dループ)



溶接線番号 SW-5(H2-3911015)



上流側 (エルボ)

下流側 (パイプ)

--- : 破線の様に進んだと思われる。